Laboratory Study of Hygroscopic Properties of Secondary Organic Aerosols Produced From Isoprene and Terpenes

Naeem Ahmad Lodhi

A dissertation submitted to the to the Faculty of Graduate Studies in Partial fulfillment of the requirements for the degree of

Doctor of Philosophy

Graduate Programme in Chemistry
York University
Toronto, Canada

November 2012

Abstract

The hygroscopic properties of secondary organic aerosol formed by the OH-initiated oxidation of isoprene and several terpenes were investigated in the York University smog chamber facility. Pure organic particles were formed in nucleation experiments using either individual hydrocarbons or sequential oxidation of multiple hydrocarbons. In addition, to examine the interaction of organic and inorganic phases, monodisperse ammonium sulfate seed particles were allowed to undergo condensational growth due to partitioning of oxidation products from the gas phase. Humidograms (plots of the hygroscopic growth factor as function of relative humidity [RH]) were measured using a humidified tandem differential mobility analyzer (HTDMA).

The humidograms of pure organic particles formed in nucleation experiments do not show any deliquescence. As RH is raised from 10% to 90%, particles formed from β-pinene pick up water smoothly and particles formed from isoprene showed apparent diameter decrease up to 5% as RH is raised to 40% then showed similar behavior to the β-pinene SOA. The particles formed from Δ^3carene also showed apparent diameter decrease up to 1% as RH is raised to 60% then showed similar behavior to the β-pinene SOA. Particles formed by oxidation of α-pinene, limonene, and Δ^3carene exhibit very little or no water uptake. The results were fitted with an empirical equation and give hygroscopicity parameters (± one standard error) of 0.0154 ± 0.0014 for β-pinene, 0.0042 ± 0.0005 for Δ^3carene, 0.0031 ± 0.0002 for α-pinene, 0.0077 ± 0.0002 for limonene and 0.0401 ± 0.0011 for isoprene. These correspond to diameter growth factors of 1.031, 1.009, 1.006, 1.016 and 1.076 at 85% RH. Water uptake by multi-component secondary organic aerosols obeys the volume additivity rule.

Humidograms of mixed (inorganic/organic) aerosol particles show both smooth hygroscopic growth and deliquescence. These experimental results were fitted with a numerical model that accounts for water uptake by both phases and for the gradual dissolution of ammonium sulfate. The results show that volume additivity is a reasonable approximation for this system and that HTDMA results can be inverted to obtain the organic hygroscopicity parameter and the relative amounts of organic and inorganic material within the experimental uncertainty.

Acknowledgement

The completion of my research work and writing my dissertation is the outcome of support, help and guidance of many individuals.

First and foremost I feel great pleasure in expressing my deep heartiest and sincere gratitude to my honorable learned, reverend and distinguished research supervisor Prof. Dr. Michael Mozurkewich. In fact it is his keen interest, inspiring guidance, blended with affectionate behavior and encouraging attitude which enabled me to successfully complete this task. It was really pleasure to work under his guidance and it was great learning experience. I would like to especially mention his support and guidance to polish my writing skills.

I am highly grateful to my supervisory committee Dr. Donald Hastie and Dr. Geoffrey Harris for their guidance and polite dealings throughout my research. Their suggestion contributed a lot to this work.

I will never forget the unique help and encouragement of my wife Sadia Lodhi in completion of thesis and research. Here I will owe my special regards to my siblings (Naheed, Nadeem, Wasim, Uzma, Saeed and Nazia) and children (Sohaib, Esha, Zoha and Shawaiz) who always prayed for my betterment and success. With respect and honor I feel gratitude for my group members Dr. Yayne Aklilue, Dr. Tak Wai Chan, Jin Zhang, Dr. Kristina Zeromeskiene, Dr. Abdul Qadir, Shervin Sarmad, Aisha Sandhoo, Dr. Abdus Salam and Altin Elezi without whom my research work might remain incomplete.

I would also like to mention all the friends at York who helped me one way or another includes: Yayne, Tak, Kristina, Jin, Shervin. AbdulQadir, Salam, Aisha, Altin, Janeen, Julie, Satoshi, Anna, Marina, Ibrahim, Jamie, Sophie, Rosalyne,Xueping, Richard, Zoya, Zena, Nikolay, Kristin, Octavian, Jeremy, Corinne, Ian, Patryk, Pei, and Mehrnaz.

I want extend my especial thanks to Carol Weldon, Mary Mamais and Magy Baket for their help.

Table of Contents

List of Figures

List of Tables

1 Introduction

1.1 Atmospheric Aerosols

The earth's atmosphere is a complex and dynamic mixture of aerosol particles and gases. The physical state of atmospheric aerosol particles can be solid [Mikhailov et al., 2009; Bones et al., 2012], liquid [Varutbangkul et al., 2006] or a combination of both with varying composition. Aerosol particles affect regional and global climate in a variety of ways through various atmospheric processes that include interference in the radiation budget of the earth, visibility degradation, air quality, smog and acid rain [Kanakidou et al., 2005; Baltensperger et al., 2005; Salma et al., 2008].

Aerosol response to changing relative humidity (*RH*) is important for understanding aerosols' residence time in the atmosphere, optical properties, cloud condensation nuclei (CCN) activity and chemical reactivity. The knowledge of aerosol particles' hygroscopicity is vital for future directions needed to predict and prevent negative impacts of aerosols on our environment and human health.

1.2 Aerosol source, composition, size distribution and lifetime

Aerosol particles have natural and anthropogenic sources in the atmosphere. Natural sources include forest fires, sea spray, volcanic eruptions, windblown dust and emissions from plants. Anthropogenic sources of aerosol include fossil fuel burning, cooking, metal smelting, industrial emissions and secondary activities.

Atmospheric aerosol particles can be classified as coming from primary and secondary sources. Primary sources include all processes that directly introduce particles in the atmosphere. Secondary sources include all processes of particle formation as a result of oxidation of atmospheric precursor gases. Atmospheric gases, e.g., sulfur dioxide (SO_2), ammonia, and oxides of nitrogen are from anthropogenic sources, while volatile organic compounds (VOCs) such as isoprene, terpenes, and toluene are from biogenic sources. Forests or vegetation are the sources of isoprene and terpenes [Holzinger et al., 2005].

Atmospheric particles usually consist of sulfate, ammonium, nitrate, elemental carbon, organic material, trace metals, crustal elements and water. Water contributes most of the aerosol mass in the atmosphere [Seinfeld, J. H. and Pandis,

S.N., 2006]. Water uptake properties of the aerosol particles depend on their physical state and chemical composition and on meteorological conditions. Hygroscopic properties of the particles are associated with many physical and chemical parameters of the particles.

Atmospheric aerosol particles are divided into four groups on the basis of particle size range, with small overlapping regions, namely, nucleation, Aitken, accumulation and coarse (cloud and fog droplets) particles [Finlayson-Pitts, B.J. and Pitts, J.N., 2000b] as shown in figure 1.1. Particles possessing a diameter less than 0.02 μm are referred to as the nucleation mode, while Aitken mode comprises the particles that fall into the particle size range between 0.02 and 0.1 μm. Accumulation mode particles are bigger than 0.1 μm and smaller than 1.0 μm, while particles that exceed 1.0 μm in diameter fall into the coarse mode [Whitby et al., 1972; Whitby, 1978].

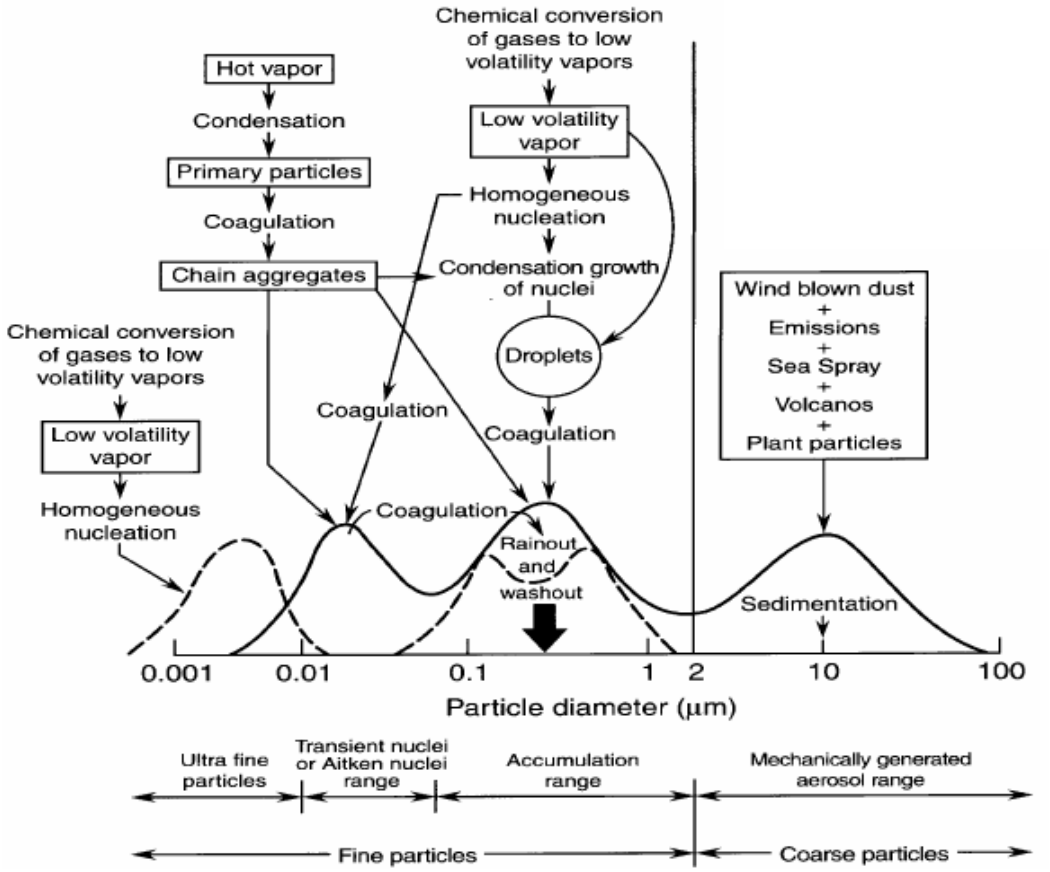

Figure 1.1: Schematic of an atmospheric aerosol size distribution showing four modes. The solid trimodal curves are original hypothesis of Whitby and co-workers and the fourth (dashed lines) represents ultrafine particle mode along with two peaks occasionally observed in accumulation mode (adopted from Whitby and Sverdrup, 1980). [Finlayson-Pitts, B.J. and Pitts, J.N., 2000b]

Nucleation, Aitken and accumulation mode particles are also called fine particles. The nucleation mode particles are often the greatest in number

concentration as compared to those of other modes. These particles are formed by the conversion of gases to particulate material. The low volatility gaseous products partitions from gas phase to particle phase on saturation. Coagulation of nucleation mode particles condensation growth and direct vehicle exhaust produces Aitken mode particles. Accumulation mode particles are produced via direct emission from diesel engines, coagulation of nucleation mode particles and condensation growth of Aitken mode particles. Coarse particles are usually present in arid geographical areas or in the vicinity of mechanical activities.

The lifetime of aerosol particles in the atmosphere varies from hours to weeks depending on particle size, chemistry, height in the atmosphere and the processes involved at the regional scale. Accumulation mode particles (0.1-1.0 μm) have the longest lifetime in the atmosphere compared to other three modes. Nucleation mode particles (<0.02 μm) are removed due higher rate of collision and coagulation. Coarse mode particles (>1 μm) particles have a short lifetime because of sedimentation.

Aerosol particles have many important properties such as size, chemical composition, hygroscopicity, density and shape. Particle size distribution can easily be measured and used to calculate number, mass, volume or surface areas. Size is

normally used to classify aerosol because inferences about the other properties can be drawn from size information. Nucleation and Aitken particles dominate in numbers while Accumulation mode particles contribute more than others to aerosols' surface area however coarse particles contribute a large fraction of aerosol volume. To understand aerosol particles role to human health and climate we need to understand their various properties and atmospheric process involved as discussed above.

1.3 Atmospheric processes

Physical and chemical processes occur in the atmosphere and are interrelated in complicated ways. Physical processes can be classified as transport by winds, formation of clouds and precipitation, while chemical processes consist of chemical reactions that lead to the formation of compounds in the gas phase and in particulate matter.

Volatile organic compounds (VOC) have anthropogenic and biogenic sources. VOCs are oxidized in the atmosphere through atmospheric oxidants. The main atmospheric oxidants are hydroxyl radical (OH), ozone (O_3) and nitrate (NO_3). VOCs on oxidation produce low volatility oxidation products. These low

volatility oxidation products on saturation may partition from gas phase to form new particles via homogeneous nucleation in clean atmosphere and these products may also condense onto pre-existing particles. Above mentioned process is the main source of fine particulate matter. Homogeneous nucleation occurs in the absence of a foreign substrate. In this process solid, liquid and mixed particles are formed from supersaturated vapors. Nucleation needs some basic ingredients to happen: relatively clean particle-free atmosphere and low vapor pressure species or oxidation products of VOCs e.g., terpenes. Nucleation is most commonly observed during spring and summer [Woo et al., 2001; Stanier et al., 2004].

Researchers have observed nucleation in semi-rural areas [Verheggen and Mozurkewich, 2002; Mozurkewich et al., 2004], forested areas [Kavouras et al., 1998; Leaitch et al., 1999; Dal et al., 2000; Aalto et al., 2001; Holzinger et al., 2005], coastal areas [C. O'Dowd et al., 1999], continental areas [Birmili and Wiedensohler, 2000], marine boundary layers [Berg et al., 1998], urban areas [Hameri et al., 1996; Shi et al., 1999; Hämeri and Väkevä, 2000], mountain areas, areas near clouds [Clarke et al., 1999] and the Arctic.

Particle coagulation is the process in which small particles collide with each other because of their random motions and coalesce to form larger particles. Van

der Waals and Coulomb forces (very minor) between the small aerosol particles facilitate the process.

Condensation is the process by which mass transfer from the gas phase to the particle phase takes place. Gas phase molecules that collide with a particle may stick to it, thus causing condensational growth of the particle.

Hygroscopic compounds such as salts absorb water from moist atmosphere at their deliquescence relative humidity *(DRH)* while mixed state (organic + inorganic) particles pick up water even at sub-saturated conditions. Condensation and evaporation from the particles happen continually. Atmospheric conditions are the driving force that determines dominance of one process over the other. If condensation of vapors dominates, particles start to grow, while if evaporation of particles dominates, they start to shrink. The concentration of vapors of condensable material and the temperature play important roles in this regard. At equilibrium, the rates of evaporation and condensation become equal, leaving no change in the net diameter of the particle. A particle with bigger diameter possesses low vapor pressure near its surface compared to small diameter particles. This phenomenon makes condensation more effective on large particles compared to small particles [Kulmala et al., 2004]. Condensation is the most common

atmospheric process for particle growth. There is no room for particle formation via nucleation in the presence of high concentration of particles.

Particles can be removed from the atmosphere via dry and wet deposition. The driving force behind dry deposition is the size of the particle. Dry deposition for particles with diameter between 0.05 and 2 μm is less important, though not negligible. Gravitational settling velocity increases with the square of the particle diameter and is the dominant factor removal of particle with diameter greater than 20 μm. Through turbulent mixing, particles reach the quasi-laminar layer. Inertial impaction through the quasi-laminar layer for the moderate size of particles (2–20 μm) is the main transportation factor. Small particles with diameter less than 0.05 μm can pass easily through the quasi-laminar layer by Brownian diffusion. Particles with diameter 0.05 to 2 μm are removed from the atmosphere mainly by wet deposition. Dry deposition is the dominant removal mechanism for ultrafine and coarse particles [J. H. Seinfeld and Pandis, 1998]. The wet deposition encompasses the deposition pathway that involves water and categorized into rainout, washout and sweepout.

1.4 Aerosol particles' effect on the radiation budget of the earth and visibility

Aerosol particles can affect the radiation budget of the earth and climate. The impacts of aerosols can be categorized into direct and indirect effects.

1.4.1 Direct effects

The direct effect involves interaction of aerosol particles with incoming sunlight, which aerosol either scatter or absorb radiation depending on their chemical composition. The aerosol particles if scatter high amount of sunlight it would cause a cooling effect; on other hand if a high amount of radiation is absorbed it would cause a warming effect [R. J. Charlson and Heintzenberg, 1995; Alfarra et al., 2004; IPCC, 2007; Pierce et al., 2011].

The scattering efficiency of the particles has a direct relationship to the particle sizes, number concentration and refractive index. The scattering efficiency of the aerosols is enhanced when the wavelength of the incoming solar radiation matches the particle size. Aerosol particles are usually abundant in the submicrometer size range and their hygroscopic behavior is of great importance for model calculations used for predicting their impact on climate. Response of these

particles to the changing *RH* is important with regard to the scattering coefficient of the particles [Yu et al., 2012].

Elemental carbon (soot) shows almost non-hygroscopic behavior and is considered having a unique high light absorption [Ackerman and Toon, 1981; Horvath, 1993; Forster, 2007; Alexander et al., 2008; Titos et al., 2012]. The agglomerate form of these particles results in a high-optical-absorption cross-section that is atmospherically of great importance for its known direct effect on global climate change [Waggoner et al., 1981; Heintzenberg, 1982; Haywood et al., 2001; Dinar et al., 2007]. A mixture of elemental carbon and soluble compounds results in a complex system of aerosols with a variety of optical properties. We have limited knowledge of hygroscopic behavior of these particles and need to characterize these properties [Hämeri et al., 1992; Andrews and Larson, 1993].

1.4.2 Indirect effects

The indirect effect of aerosol particles on global climate involves the interaction of clouds with solar and terrestrial radiation. Clouds can reflect or absorb sunlight and infrared radiation emitted from the earth's surface. Aerosols particles are indirectly related to the process by which aerosols influence the

radiation balance of the earth's atmosphere by affecting cloud albedo, cloud amount, cloud formation and precipitation efficiency. The ability of aerosol particles to act as cloud condensation nuclei (CCN) depends on particles' hygroscopicity. Hygroscopicity of the particles as a function of chemical composition influences the microphysical properties of clouds and the droplet number size distribution [Twomey, 1974]. Cloud albedo depends on microphysical properties and has a direct relation to the fraction of sunlight to be reflected [Ackerman and Toon, 1981; Haag and Kärcher, 2004; Yu et al., 2012; Pandithurai et al., 2012].

Parameterization of the hygroscopicity of these particles is necessary to understand their role as CCN. The soluble mass fraction in the particle determines the supersaturation needed for cloud droplets to form. An excess of the soluble mass fraction in the particle over the insoluble mass fraction increases the probability of cloud droplet formation [Kulmala et al., 1996]. We have limited knowledge concerning CCN active particles at the submicrometer particle size range. We can bridge this gap by parameterizing particle hygroscopicity.

The direct and indirect effects in combination are known to affect the regional atmospheric temperature; however, the effect is uncertain at the global level.

1.5 Aerosol effects on human health

In addition to effects on radiation transfer and possibly on global climate, aerosol particles also have been implicated as being detrimental to human health [Peters, Wichmann et al., 1997; Peters, Dockery et al., 1997; Cooney, 1998; Davidson et al., 2005; Pope III and Dockery, 2006; Pope III et al., 2009]. Our respiratory system is efficient in removing particles, but particles in a certain size range (PM 2.5) penetrate deep into the lungs. If they are highly concentrated and toxic they can cause adverse health effects [C. A. Pope III et al., 2002]. Particles that are soluble can be absorbed through the skin and eyes and may cause irritation that could lead to more toxic effects.

Particle sizes and number concentration are important in connection to asthma and lung cancer; however, the mechanism is not fully understood. An epidemiological study found that there was strong dependency of the total mass of

particles with diameters smaller than 10 μm and mortality in American cities [Dockery et al., 1993; C. A. Pope III., 2000a; C. A. Pope III., 2000b; C. A. Pope III et al., 2001; Pope III et al., 2009]. Toxic substances were also found in chemical analysis of these particles but the composition seems to have little effect on the health impacts so it seems something other than toxic components is involved [Nriagu and Pacyna, 1988; Pepper and Dowd, 2009; Andersson et al., 2010].

Aerosol particles' hygroscopicity is very important especially when they enter the humid human respiratory system. The *RH* deep in the lungs was estimated to be approximately 99.0% to 99.5% [Ferron et al., 1993]. When exposed to high humidity in the lungs, aerosols might increase in their diameter upon picking up water and can also undergo heterogeneous reactions [Klimova et al., 2011; Curjuric et al., 2012; Gamble et al., 2012; Plummer et al., 2012].

Bioaerosols include pollen, viruses, bacteria, and proteins; they have a strong connection with human health as well [Dutkiewicz et al., 2011; Chakrabarti et al., 2012; P. Hong et al., 2012; T. Hong and Gurian, 2012; Jung et al., 2012]. Bioaerosols proteins can undergo nitration when exposed to traces of nitrogen dioxide [Franze et al., 2005]; that may be important as a trigger for adverse immune reactions, such as allergies and asthma in humans [Prather et al., 2008].

1.6 Aerosol effect on visibility

Aerosol particles have a great effect on visibility along with their influence on climate and health. The degradation of visibility is a well-known impact of air pollution [Murray and Farber, 1988; Hyslop, 2008; W. Huang et al., 2009; C. Lu et al., 2010; Wen and Yeh, 2010; Deng et al., 2011]. Degraded visibility is well correlated with an increase of aerosol number concentration [Noll et al., 1968; Stjern et al., 2011; Han et al., 2012]. Visibility ranges from 150 to 250 km in unpolluted areas of North and South America while it is 40 to 50 km in rural Europe because of the high density of sources of anthropogenic aerosols [Horvath, 1995a; Horvath, 1995b].

The response of aerosol particles to changing *RH* has a direct link to visibility. Increasing *RH* decreases visibility continuously in the area of high concentration of aerosol [Tsay.S.C et al., 1991; Horvath, 1995a].

1.7 Water and aerosol particles in the atmosphere, thermodynamics, and previous laboratory studies

Water is present on earth in all three phases: solid, liquid and vapor. The varying amount of water vapor present in the atmosphere depends on regional and

global conditions. Average *RH* in atmosphere also has seasonal variations. The percent relative humidity (*RH*) is defined as the water vapor pressure, *P*, at a given temperature, divided by saturation water vapor pressure, P_s, multiplied by a factor of one hundred. Following equation 1.1 gives the relationship of *RH* with vapor pressure and saturation water vapor pressure. Equation 1.2 relates water activity (a_w) with water vapor pressure and saturation vapor pressure.

$$RH = \frac{P}{P_s} \times 100 \tag{1.1}$$

$$a_w = \frac{P}{P_s} \tag{1.2}$$

As the ambient temperature increases, the *RH* decreases because of a strong dependency between the saturation water vapor pressure and the ambient temperature [Lawrence, 2005].

At low *RH* an aerosol particle can be dry and solid. A particle can go into solution when exposed to *RH* equal to or greater than its deliquescence *RH*. Particle hygroscopicity depends on chemical composition, which can be divided into two major groups: inorganic and organic. Inorganics are the more soluble part of the particle and mainly consist of salts such as ammonium sulfate (AS), ammonium

nitrate, ammonium bisulfate and sodium chloride. The hygroscopicity of inorganic aerosols has been investigated by numerous researchers [C. K. Chan et al., 1992; I. N. Tang and Munkelwitz, 1994]. These researchers thoroughly explain hydration and dehydration patterns of various inorganic salts and summarize information about the solute mass fraction and the density of a particle at various *RHs* along with crystallization and deliquescence points [I. N. Tang, 1980; I. N. Tang and Munkelwitz, 1994]. We can use this information to calculate the hygroscopic growth factor (HGF) of pure inorganic salts at various *RHs*.

Pure AS particles are solid and in the crystalline state at 10% *RH*, and they remain solid until *RH* reaches its deliquescence relative humidity (*DRH*). A sudden change in diameter takes place as a particle reaches *DRH* and forms a saturated aqueous solution. The *DRH* is specific for each deliquescent compound at specific temperature. As *RH* is increased beyond *DRH*, particle size keeps increasing smoothly until the thermodynamic equilibrium is reached, i.e., equilibrium of water between the gaseous and aqueous phase. As *RH* decreases, water from the particle evaporates to maintain the vapor equilibrium, so the crystallization *RH* is therefore much lower than the *DRH* [Cohen et al., 1987; I. N. Tang and Munkelwitz, 1994].

Following figure 1.2 shows the hydration and dehydration curves of AS along with deliquescence and crystallization *RHs*.

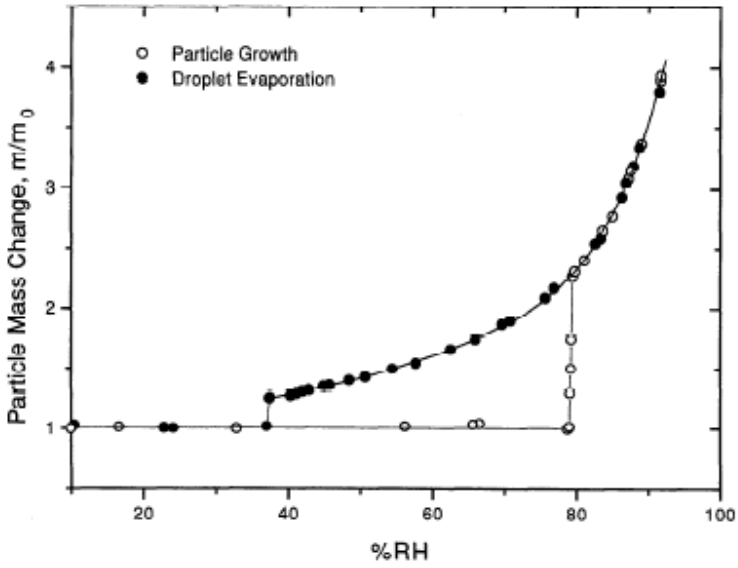

Figure 1.2: Ammonium sulfate particle growth and evaporation pattern as a function of relative humidity at room temperature (from Tang and Munkelwitz 1996). [I. N. Tang, 1996]

Multicomponent aerosol particles show different behavior on hydration and dehydration than do single-component particles. When multicomponent particles are hydrated, they can show deliquescence in multiple steps, and dehydration may involve more than one step for crystallization to take place. A mixture of sodium

chloride and potassium chloride, for example, shows deliquescence at 72.7% *RH*, i.e., different from the pure individual salts' *DRH* as given in table 1.1. Hydration and dehydration curves depend solely on the composition of the aerosol particles and become more complex with increasing composition complexity.

Table 1.1: Atmospherically important inorganic salts with their deliquescence relative humidity *(DRH)*, crystallization relative humidity *(CRH)*, and density. [I. N. Tang, 1996]

Inorganic Salts	**DRH (%)**	**CRH (%)**	ρ_{dry} **(g cm^{-3})**
Na_2SO_4	84.2	59–57	2.7
$(NH_4)_2SO_4$	79.9	40–37	1.77
NaCl	75.3	48–46	2.17
$NaNO_3$	74.3	30–0.05	2.26
NH_4NO_3	61.8	32–25	1.73
NH_4HSO_4	40	22–0.05	1.78

In addition to the inorganic fraction of atmospheric particles, the other main part is carbonaceous material, which often presents more than half of the mass of submicron particles [Jimenez et al., 2009] and adds further complexity to the hydration and dehydration pattern of the particles. Carbonaceous materials can be classified into elemental carbon (EC) and organic carbon (OC). EC and

hydrocarbons are nonhygroscopic under atmospheric conditions, while oxygenated organics, usually composed of thousands of individual species such as oxalic acid, are hygroscopic [Saxena and Hildemann, 1996].

Atmospheric particles are very complex in composition, with contributions from numerous classes of individual organic species [Goldstein and Galbally, 2007]. Hygroscopic properties of a few species out of thousands of individual species have been investigated [Duplissy et al., 2011]. Various approaches were used to determine the influence of these species on the overall hygroscopicity of ambient aerosols under various *RH* conditions. The initial laboratory studies were done to investigate a simple system of internally mixed aerosol particles of single inorganic and single organic species [F. D. Pope et al., 2010] such as carboxylic acid or dicarboxylic acids and multifunctional organic acids or their salts [Choi and Chan, 2002a] and also their mixture with inorganic salts [Cruz and Pandis, 2000a; Hämeri et al., 2002; Choi and Chan, 2002b].

The presence of organics alters the hygroscopicity of internally mixed inorganic components, as organics are less hygroscopic than pure individual inorganic species. Internally mixed aerosol particles (inorganic + organic) pick up water at a range of *RH*s less than the *DRH* of the individual inorganic component of

the particle because of the organics [Dick et al., 2000; M. N. Chan and Chan, 2003; Braban and Abbatt, 2004; Pant et al., 2004; Badger et al., 2006], while pure inorganics remain solid or gradually start dissolving at these *RH*s. Organics can alter the *DRH* of inorganics as observed by Brooks et al 2002 [Brooks et al., 2002] and also observed from the study of internally mixed particles of carboxylic acid and AS [Braban and Abbatt, 2004; Pant et al., 2004]. The change in *DRH* was considered to be due to physical reasons instead of chemical change. The factors behind the change in *DRH* are the amount and number of organic species along with the type of species. An organic mole fraction of 0.1 to 0.35 in the particle [Braban and Abbatt, 2004; Pant et al., 2004] does not shift *DRH* substantially; however, on increasing the mole fraction to more than 0.35 in the particle decreased *DRH* of AS when a single-component system of particle composition (inorganic + organic) was studied. The hydration and dehydration patterns of internally mixed aerosols are more complex in multicomponent atmospheric particles than in a simple system of single-component aerosol particles [Marcolli et al., 2004].

Hygroscopic properties of mixed particles have been studied by several research teams [Cruz and Pandis, 2000a; Peng et al., 2001; Brooks et al., 2002;

Choi and Chan, 2002b; Prenni et al., 2003; Wise et al., 2003; Braban and Abbatt, 2004; Marcolli and Krieger, 2006; Varutbangkul et al., 2006]. More complex systems such as humic acids also drew the attention of researchers [M. N. Chan and Chan, 2003; Gysel et al., 2004; Pant et al., 2004; Parsons et al., 2004]. Recent research has shown that the hygroscopicity of organic particles is low without a clear phase transition [Prenni et al., 2001; Choi and Chan, 2002b; M. N. Chan and Chan, 2003; Gysel et al., 2003] and that some organics are non-hygroscopic below 85% RH [Cruz and Pandis, 2000b; Peng et al., 2001; Prenni et al., 2001].

Aerosols can be classified as internal or external mixtures [Winkler and Junge, 1972; Lesins et al., 2002; J. Lu and Bowman, 2010] depending on their chemical composition. Aerosols individually consisting of mixtures of different components are referred to as internally mixed, while mixtures of aerosols each comprising a different single component are referred to as externally mixed. There are varieties of intermediate states of internally and externally mixed aerosol particles present at ambient conditions [J. Lu and Bowman, 2010]. The hygroscopicity of particles belonging to internally or externally mixed shows different patterns [Peckhaus et al., 2012]. Externally mixed particles can show different hygroscopic groups, while one hygroscopic mode could belong to

internally mixed particles. Hygroscopic properties provide information about the mixing state of particles and are important in connection with direct and indirect climate effects, visibility [Andreae and Rosenfeld, 2008; J. Wang et al., 2008; Heintzenberg and Charlson, 2009] and human health [Davidson et al., 2005; Pope III et al., 2009].

1.8 Relevant prior work

Many researchers used isoprene and selected monoterpenes to produce secondary organic aerosols (SOA) to parameterize the hygroscopicity and CCN activity. Following are previous studies in chronological order with some resemblance however experimental conditions were different compared to ours.

The hygroscopic properties of ozonolysis products of α-pinene [Virkkula et al., 1999; Cocker et al., 2001; Saathoff et al., 2003], β-pinene and limonene [Virkkula et al., 1999] were studied. Pure organic aerosols and mixed (AS/SOA) SOA were produced. Experimental results show that inorganic and organic pick up water independently which is consistent to our finding. Our experimental results of pure organic SOA growth factor (GF) at 85% RH were within 7% to Virkkula's [Virkkula et al., 1999] finding for nucleated SOA. Cocker [Cocker et al., 2001] and

Saathoff [Saathoff et al., 2003] found that depositing less hygroscopic ozonolysis products on ammonium sulfate seed reduces GF of ammonium sulfate. GF of seed aerosol decreases with increase in organic volume fraction in the particle. Saathoff [Saathoff et al., 2003] found that nucleated SOA do not show any deliquescence on increasing RH however seeded SOA shows deliquescence at 80% RH. Huff Hartz [Huff Hartz et al., 2005] and VanReken [VanReken et al., 2005] studied ozonolysis products of α-pinene, β-pinene, Δ^3carene and limonene for their property if these SOA can act as cloud condensation nuclei (CCN). According to VanReken [VanReken et al., 2005] limonene SOA were most CCN active however SOA becomes less CCN active with time. According to Huff [Huff Hartz et al., 2005] findings monoterpenes SOA's are CCN active and activate like highly water soluble organics at high RH. Varutbangkul [Varutbangkul et al., 2006] produced SOA in humid chamber (~50% RH) by ozonolysis of monoterpenes. According to experimental results SOA's are slightly hygroscopic compared to inorganic aerosol substances. He also found that pure organic aerosol humidogram shows smooth water uptake (consistent to our finding without deliquescence and efflorescence). Our experimental results of growth factor were within 7% to Varutbangkul [Varutbangkul et al., 2006].

Meyer [N. K. Meyer, Duplissy, Gysel, Metzger, Dommen, Weingartner, Alfarra, Prevot, Fletcher, Good, McFiggans, Jonsson et al., 2009a] studied ozonolysis products of α-pinene and monitored GF changes at 75% and 85% RH. He found that on increasing soluble organic volume fraction at 75% RH to seeded aerosol particle partially help in dissolution of ammonium sulfate (AS) however at higher RH (85%) GF of ammonium sulfate seed decreases with increase in organic volume fraction. Satoshi [Takahama et al., 2007] found that adding dark ozonolysis oxidation products of limonene or α-pinene to seed aerosol (AS) may have negligible effect on efflorescence transition of AS. Petters [Petters et al., 2009] produced SOA by ozonolysis of α-pinene and found that SOA were slightly hygroscopic at or below 98% RH. Smith [M. L. Smith et al., 2011] produced mixed (AS/SOA) aerosol particles by dark ozonolysis of α-pinene. Smith's experimental results shows shift in DRH of ammonium sulfate with condensation of oxidation products of α-pinene. Bertram [Bertram et al., 2011] studied oxidation products of α-pinene and its effect on efflorescence RH and deliquescence RH of the particles and found that the oxidation products affected the efflorescence RH and deliquescence RH of the mixed (AS/SOA) aerosol particles. Tritscher [Tritscher et al., 2011] produced SOA by ozonolysis of α-pinene and followed by aging with OH radicals. He found that hygroscopicity of particles initially increased during O_3

induced condensation but during later stages even after exposing to OH radicals remained unchanged. Mostly researchers used ozonolysis to produce SOA under humid conditions. We produced SOA under dry conditions by OH radical photooxidation to parameterize the hygroscopic growth factor of pure organic SOA and mixed (AS/SOA) SOA.

1.9 Objective of this study

Atmospheric particles contain significant amount of both organic and inorganic material. The inorganic portion consists largely of AS, while the organic portion contains many individual, and largely unidentified, compounds [Hallquist et al., 2009]. The water uptake properties of atmospherically important inorganic salts are well known [I. N. Tang and Munkelwitz, 1994]. Although it is known that organics can alter the hygroscopic growth factor of inorganic particles, these effects are still not fully characterized [Swietlicki et al., 2008]. Oxidation products of VOCs form a significant fraction of the secondary organic aerosol (SOA) mass, biogenic terpenes being especially important in rural and forested areas [Hallquist et al., 2009].

Because of the different hygroscopic behavior of the inorganic and organic components, field measurements of particles' hygroscopicity have been used to infer the relative amounts of these two components in atmospheric particles [Y. Aklilu and Mozurkewich, 2004; M. N. Chan et al., 2005; Zelenyuk et al., 2008]. These inferences are based on the volume additivity (or ZSR) rule; this assumes that the different components take up water independently. The same assumption is used to estimate the hygroscopic properties of particles from measurements of chemical composition. Although this assumption has been verified for particles consisting of AS or sodium chloride and various organic components [Y. Aklilu and Mozurkewich, 2004; Swietlicki et al., 2008], a number of tests have also been done using actual oxidation products [N. K. Meyer, Duplissy, Gysel, Metzger, Dommen, Weingartner, Alfarra, Prevot, Fletcher, Good, McFiggans, Jonsson et al., 2009b].

Mixed (inorganic/organic) particles typically show gradual deliquescence at relative humidities below the deliquescence point of the salt. Although this is widely understood as being due to the partial dissolution of the salt, there has been no readily applied method of analyzing this phenomenon or of applying the volume additivity rule to this situation. We (Mozurkewich group) tested such a method for

particles consisting of AS and condensable products of isoprene and selected terpenes (α-pinene, β-pinene, Δ^3carene and limonene). Initially we applied the test for the simple system where an individual hydrocarbon was oxidized to produce mixed particles (inorganic/organic). Further we applied this method to more complex situations where two or three hydrocarbons were oxidized to produce condensable oxidation products that sequentially coated the surface of seed aerosols to produce mixed particles.

Isoprene and terpenes are globally abundant reactive organic gases with the formulas C_5H_8 and $C_{10}H_{16}$ respectively. They are emitted into the atmosphere by a variety of plants [Guenther et al., 1995]. Terpenes are very reactive and form particulate matter with high mass yields [T. Hoffmann et al., 1997; Bonn and Moortgat, 2002; Hallquist et al., 2009; Jimenez et al., 2009]. To investigate water uptake by secondary organic aerosol (SOA) formed by the oxidation of isoprene and selected terpenes (α-pinene, β-pinene, Δ^3carene and limonene), nucleation experiments (pure SOA) and seeded experiments (mixed organic and inorganic) were performed in the York University Smog Chamber.

2 Instrumentation

2.1 Historical background of HTDMA

A tandem differential mobility analyzer (TDMA) technique was first introduced by Liu [B. Y. H. Liu et al., 1978] to study the changes in particle size as a result of an imposed aerosol processing [Swietlicki et al., 2008]. Rader and McMurray [Rader and McMurry, 1986] showed that TDMA data can be inverted to find out the size changes and proved that diameter changes can be measured with a precision of about 0.3%.

The TDMA technique is classified depending on the type of processing, as humidification (HTDMA), volatility (VTDMA), chemical reaction (RTDMA) and uptake of organic vapor (OTDMA). We used the HTDMA technique [Sekigawa, ; Stolzenberg, M.R. and McMurray, P.H., 1988] to study the hygroscopicity of aerosol particles. An HTDMA system consists of two DMAs, a condensation particle counter (CPC) and a humidification system. A simplified flow diagram of the HTDMA instrument is shown in figure 2.1.

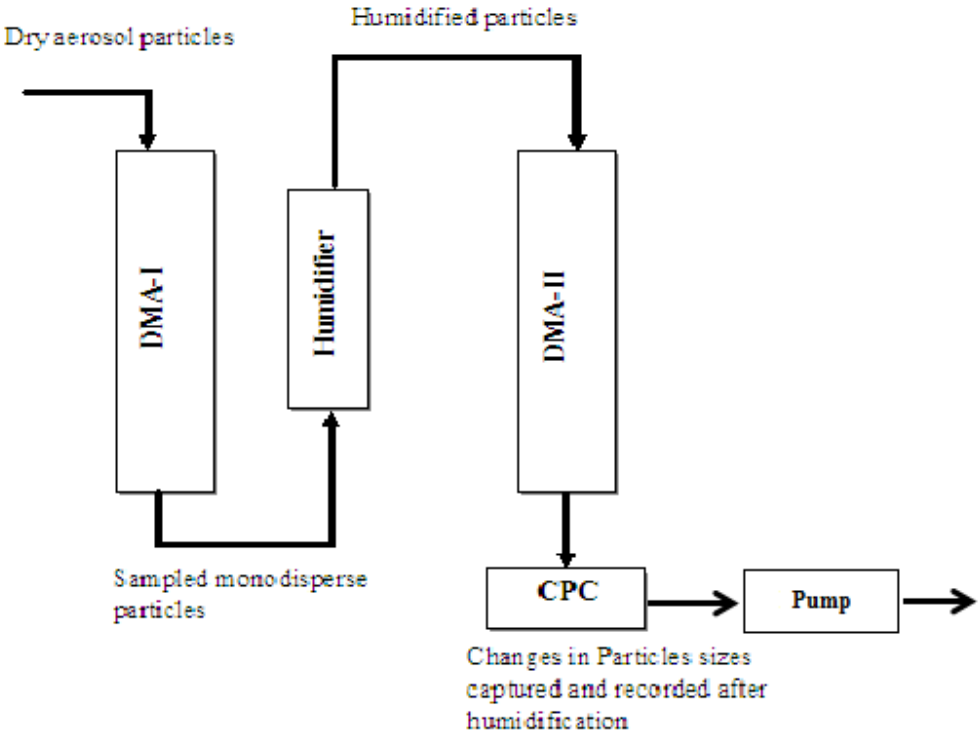

Figure 2.1: Simplified diagram of the HTDMA system to investigate hygroscopic properties of particles (modified from Aklilu PhD thesis 2005) [Y. Aklilu, 2005b]

The dry polydisperse aerosol sample flow was drawn to DMA1 using a Gast diaphragm pump, which selects a narrow range of particle sizes. Further selected dry particles passed through a humidification system and were scanned by the second DMA to measure changes in particle size due to particle processing by the humidification system. HTDMA measurements are presented as a growth

factor, i.e., the ratio of humidified to dry diameter of the particle as a function of relative humidity (RH).

2.2 Design and principle of the DMA

The differential mobility analyzer (DMA) is the core of the HTDMA system. It can be used to select a narrow range of monodisperse particles from the charged population of polydisperse particles. The selected narrow range of monodisperse particle sizes depend on the fixed voltage applied to the DMA, charge on the particle and ratio of sample to sheath flow. The particle sizes can be sorted to determine the particle size distribution if the DMA voltage is scanned in conjunction with a suitable detector.

Figure 2.2 provides a detailed cross sectional view of the DMA, TSI model 3071 [Kinney et al., 1991]. It consists of an electrically grounded outer housing, an inner rod with negative DC voltage applied to it, and two inlet and two outlet flow openings.

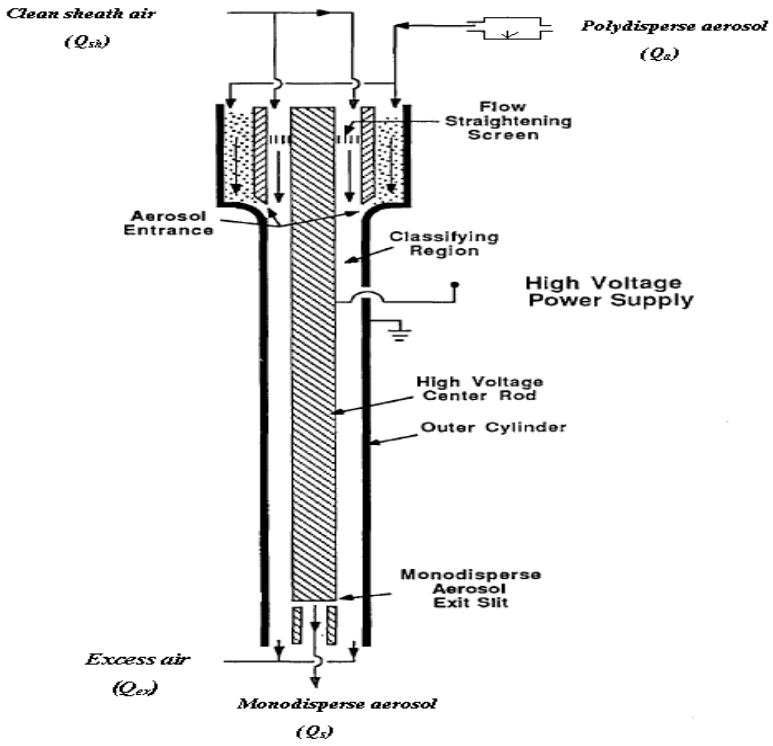

Figure 2.2: Schematic diagram of differential mobility analyzer (TSI Model 3071) (modified from Kinney et al., 1991 [Kinney et al., 1991].

Inlet openings carry polydisperse aerosol (Q_a) and sheath flow (Q_{sh}) to the DMA while outlet openings are for the exiting sampled monodisperse aerosol (Q_s) and excess air (Q_{ex}). In our HTDMA system, the sheath flow was approximately 10 times the aerosol flow. Polydisperse aerosol flow carries charged particles into the

DMA while sheath flow (Q_{sh}) flows axially down the central rod and pushes a thin layer of aerosol to move along the outer wall of the DMA. Positively charged aerosol particles migrate into the clean sheath air because of the electrical field. Particles under the influence of electrostatic and drag forces in the classifying region gain radial velocity proportional to their electrical mobility (Z_p). Positively charged particles with specific mobility are selected by the DMA when a fixed voltage is applied on the central rod. Particles with a larger diameter and lower mobility are lost along with the sheath flow or are deposited below the exit slit, while particles smaller than the selected diameter would move toward the central rod above the exit slit because of high mobility and would be deposited there. The electrical mobility (Z_p) of spherical particles is associated with diameter (D_p) and charge (e) as given in equation 2.1[Kinney et al., 1991]. Particle size that is selected by the above procedure is associated with a specific electrical mobility that can be calculated using equation 2.1 if we know the slip correction. Equation 2.2 can be used to calculate the slip correction factor.

$$Z_p = \frac{Q_{sh+}\, Q_{ex}}{4\pi VL}\; ln\left(\frac{r_2}{r_1}\right)\frac{enC(D_p)}{D_p} \qquad (2.1)$$

Here

Q_{sh}= sheath air flow rate (175 cm^3 sec^{-1})

Q_{ex}= excess air flow rate (175 cm^3 sec^{-1})

r_1 = outer radius of the centre rod (0.937 cm)

r_2 = inner radius of outer cylinder (1.958 cm)

e = elementary charge (1.6×10^{-19} C)

n = number of elementary charges on the particle

L = axial distance between the aerosol inlet and the exit slit (44.44 cm)

V = voltage applied to the centre rod (volts)

D_{p} = particle diameter (cm)

$$C_{(D_p)} = 1 + K_n[1.155 + 0.471\, exp(-\frac{0.596}{K_n})] \quad (2.2)$$

$C_{(D_P)}$ = slip correction [Allen and Raabe, 1982], diameter dependent

Here K_n is the Knudsen number, which is related defined by

$$K_n = \frac{2\lambda}{D_p} \quad (2.3)$$

Here λ = mean free path of air molecules at a given temperature and pressure; the mean free path was corrected for operating conditions of the DMA as given in equation 2.4 [Kinney et al., 1991].

$$\lambda = \lambda_0 \left(\frac{T}{T_0}\right)\left(\frac{P_0}{P}\right)\left(\frac{1+110.4/T_0}{1+110.4/T}\right) \quad (2.4)$$

Here λ_0 is the mean free path and has the value of 6.73×10^{-6} cm; at pressure P_0 (1.01×10^5 Pa) and temperature T_0 (296.15 K).

The main function of the DMA is to separate charged particles based on their different electrical mobility. Before entering the DMA, particles were charged by passing through a bipolar charger. ^{85}Kr or ^{210}Po are bipolar charging materials used in TDMA technology. ^{85}Kr is an inert radioactive gas that emits β-particles, while ^{210}Po is a solid substance that emits α-particles. α or β particles continuously ionize the gas molecules inside the bipolar charger. On passing through the bipolar charger, aerosol particles attain a negative or positive charge when they collide with negative or positive ions. The aerosol particles can attain single, double or multiple positive or negative charges. The major portion of charged aerosols attains a single charge; however, 5% of aerosols may attain multiple charges. For simplification of data analysis it was assumed that all particles were singly charged.

In the HTDMA system a ^{210}Po bipolar charger was used to charge particles. The charged particles carrying a positive charge move radially toward the central rod of the DMA under the influence of the electric field, while particles with a negative charge were deposited on the inner surface of the outer cylinder.

Selection of any specific particle size from a polydisperse population depends on the electrode voltage and electrical mobility. At any specific central rod voltage, the radial speed of the particle depends on its electrical mobility for given flow rates, which in turn depends on the applied voltage, the flows and the geometry of the DMA. Particles having the same electrical mobility that are sampled by the DMA are not truly monodisperse because they don't follow a single path to the exit slit at a given (fixed) voltage (V_o) at the central rod. Positively charged particles possessing electrical mobility in the range of $Z_p \pm \frac{1}{2}\Delta Z_p$ are capable of passing through the exit slit at the base of the inner rod. Some particles may follow a shorter or longer path to the exit slit (see figure 2.3); thus some particles will exit at a lower or higher voltage than V_o, as shown in figure 2.3. Sampled aerosols will fall into a narrow range of particle size. An upper and lower limit of particle sizes with electrical mobility Z_p and the transfer function together governs their probability of passing through the exit slit for the given sample and

sheath flow. The appearance of sampled particles as a function of the voltage can be explained by the transfer function (Ω) as "the probability that an aerosol particle which enters the mobility analyzer via the aerosol inlet will leave via the sampling flow, given that its mobility is Z_p" [Knutson and Whitby, 1975].

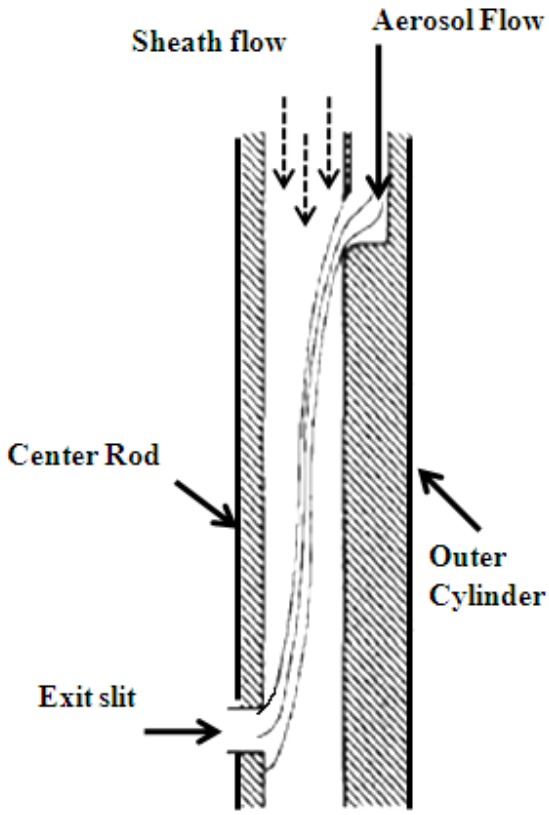

Figure 2.3: Schematic presentation of possible particle path within the DMA (modified from Knutson and Whitby, 1975) [Knutson and Whitby, 1975].

Several important features of the transfer function are apparent from figure 2.4. DMA flows are important in connection with the transfer function. A ratio of the sample flow to the sheath flow (β) determines the size range of sampled particles. β is defined as the ratio of aerosol flow to sheath flow, so larger excess flow (Q_{ex}) and sheath flow (Q_{sh}) mean a smaller β and a narrow size range of particles as given by equation 2.5,

$$\beta = \frac{Q_a + Q_s}{Q_{ex} + Q_{sh}} \qquad 2.5$$

Q_{sh} and Q_{ex} are explained above, while Q_a and Q_s are aerosol and sample flow respectively, ranging from 1.0 to 1.4 L min^{-1}.

If the aerosol inlet flow (Q_a) and monodisperse sampling flow (Q_s) are equal, $Q_a = Q_s$, and the transfer function has a triangular shape with a sharp peak corresponding to a probability Ω of 1. This is the optimum condition for obtaining an accurate particle size [Kinney et al., 1991]. If $Q_a \neq Q_s$, then the transfer function gains a trapezoidal shape because there will be a range of voltages by the central rod for which all the inlet aerosol particles with mobility Z_p will be sampled by the monodisperse outlet. This fact implies that the transfer function is unity for a range

of voltages, which in turn leads to a flat-topped rather than triangular peak (figure 2.4) [Kinney et al., 1991].

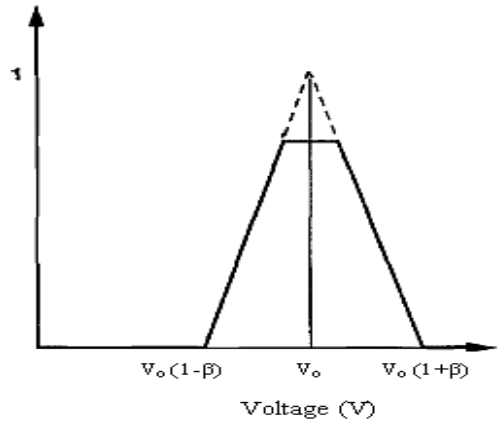

Figure 2.4: The differential mobility analyzer transfer function. It determines for any given voltage (Vo) the probability that a charged particle can exit the DMA (modified from Kinney 1991) [Kinney et al., 1991].

2.3 The condensation particle counter (CPC)

Atmospheric particles can be detected and measured using a condensation particle counter (CPC). In our HTDMA and scanning mobility particle sizer (SMPS), we used two CPCs, TSI models 7610 and 3010 respectively, to determine particle concentration. A CPC is a single-particle counter that uses light scattering to detect particles. The technique is sophisticated enough to measure the

concentration of particles with a diameter from a few nanometers to submicrometers depending on the model of the counter.

The chronological historical development was explained by McMurray [McMurry, 2000]. Figure 2.5 shows the cross-section of the CPC (TSI model 3010). The working principle of TSI models 3010 and 7610 is the same. Before passing through a detector, the particles must be enlarged into droplets to make them detectable, a process achieved by condensing butanol vapors on them.

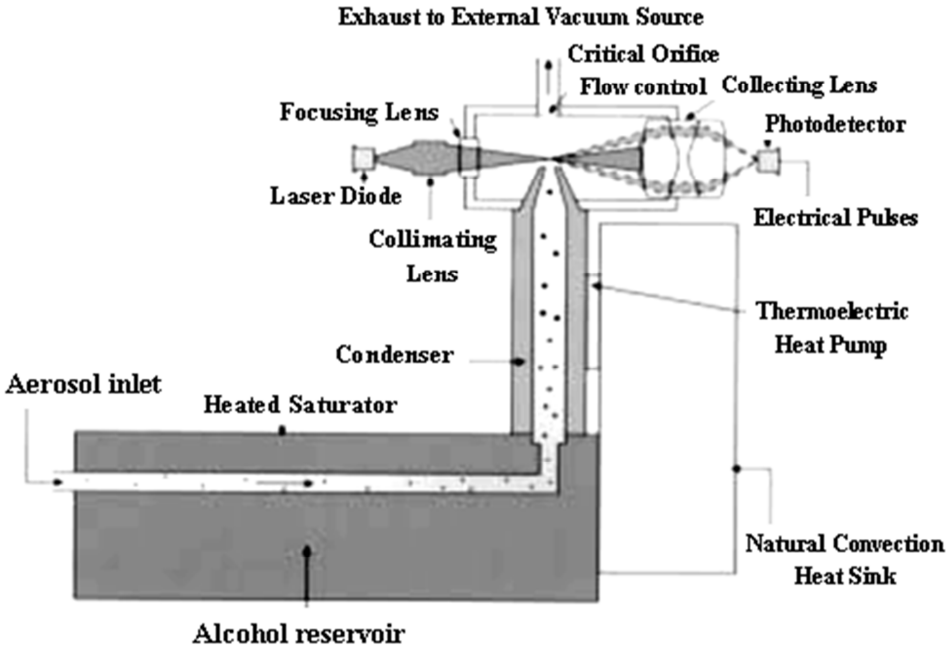

Figure 2.5: Schematic diagram of condensation particle counter (modified from TSI Model 3010 manual, figure 1-2).

The CPC sample flow of 1.4 Lm^{-1} was maintained by flow through a critical orifice sustained by a Gast diaphragm pump (Model DOA-P104-AA) at the exit of the CPC. The aerosol particles enter through the aerosol inlet into the saturator, located at the entrance of the CPC. The saturator contains a butanol reservoir that is kept above room temperature. The butanol has a relatively low saturation vapor pressure, so the gas flow is saturated with butanol within the compartment before entering the cooled condensing chamber downstream from the saturator. The flow of heat toward the walls of the cooled condenser is much faster than the flow of alcohol vapor, because air molecules are much lighter than the alcohol. This creates supersaturation within the cooled condenser. The supersaturated alcohol vapors condense on the surface of the incoming particles, allowing them to grow to more than a micrometer in diameter before they reach the exit of the cooled condenser.

The grown particles pass through the exit nozzle. A laser beam is set up horizontally above the aerosol nozzle. The grown particles scatter the laser beam on passing through it. The scattered laser light is collected on a photoreceptor. The photoreceptor produces an electrical pulse for each particle. Those are counted and

transmitted to the computer, which performs the incident counting. Incidents were counted for 0.2 seconds for every reading. If the particle concentration is higher than 10^4 particles cm^{-3}, there are chances that the signals of two particles may overlap and count as one, so a coincidence correction to the counting should be applied; however, particle concentrations during laboratory measurements were lower than the threshold, so a coincidence correction was not required.

Using the information of flow rate and CPC counting time, the concentration of particles can be computed from the detected signal. Buzorius [Buzorius, 2001] shows a characteristic efficiency function for the CPC (TSI model 3010) which provides the probability of detection at a given particle diameter. Each CPC model varies in its efficiency and threshold diameter. The technique is considered 100% efficient above a particle diameter of 25 nm and at a certain level of particle concentration, i.e., 10^4 particles cm^{-3}. During our smog chamber study the sampled diameter of the particle was always above 50 nm so issues related to efficiency of detection were negligible.

2.4 Conditioning system (humidification system)

Figure 2.6 shows a simplified diagram of the HTDMA humidification system, which lies upstream from the second DMA and has two main components: a saturator and an equilibrator. These are used in combination to regulate the humidity of the sheath flow of the second DMA and the sampled aerosol. A saturator adds water to the sheath flow while the equilibrator makes sure that the RH is the same in the aerosol and sheath flows before these enter the second DMA.

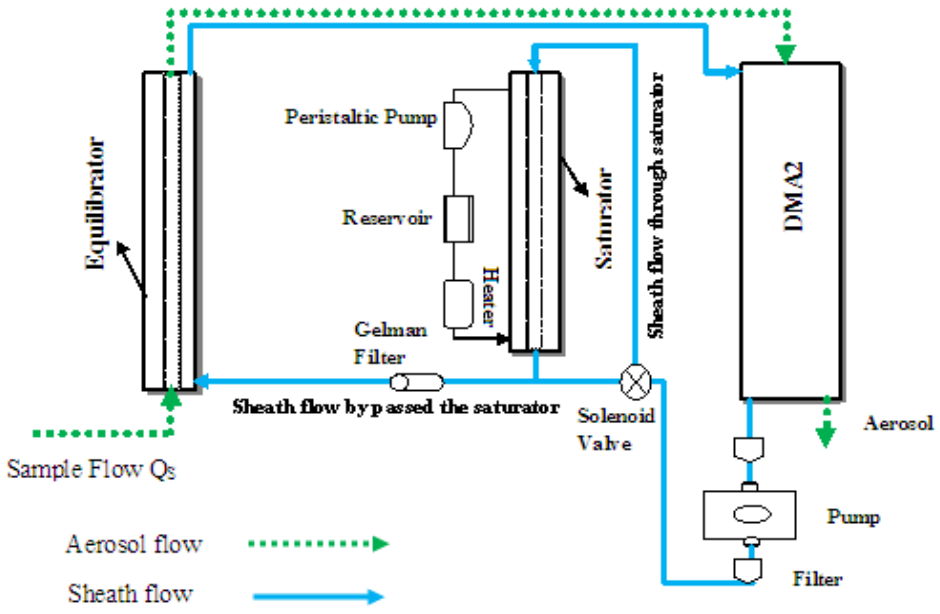

Figure 2.6: Sample humidification system.

The saturator consists of nafion tubing encased in a polypropylene shell (Perma Pure model MH-070-24P), and the equilibrator consists of an outer shell of fluorocarbon (Perma Pure model MD-110-24F) and inner nafion tubing. Both nafion tubings (in the saturator and equilibrator) are 58 cm long with an outer diameter of 0.18 cm.

A saturator is a shell-and-tube moisture exchanger that allows the transfer of water vapor between a liquid water supply and a flowing gas stream. The sheath flow was passed through the inner shell of the saturator (nafion tubing) while distilled water was circulated through the outer shell counter-current to the sheath flow. Circulation of water was regulated using a peristaltic pump. The sheath flow of the second DMA was 10 lpm. The sheath flow was recirculated repeatedly in a closed loop through the inner shell of the saturator to achieve the required high level of steady state RH. Water is absorbed into the walls of the nafion tube and transferred to the dry gas stream. The transfer is driven by the difference in partial pressure of water vapor on opposite sides (Perma Pure manual). Water diffusion from the outer shell to the inner side of the nafion tubing resulted in evaporative cooling; to compensate for this effect, the circulation water was heated a few

degrees above room temperature, using a heater between the peristaltic pump and the saturator.

RH of the aerosol sample and DMA2 sheath flows were equilibrated before the flows entered the second DMA. The humidified sheath flow passes through the outer shell of the equilibrator while the aerosol sample passes through the inner nafion tubing. The water concentration differential between the two gas streams (sheath and aerosol flow) drives the process. Because of the difference of partial pressures, water diffuses across the membrane to humidify the aerosol particles. The water concentration differential between the two gas streams (sheath and aerosol flow) cause the moisture to passe quickly to the aerosol flow from the sheath flow across the membrane. The process of moisture exchange across the nafion tube wall equilibrates the RH in the sample and sheath flows. The RHs of the sample and sheath flows were measured after passing through the equilibrator and agreed within 2% [Y. Aklilu, 2005a]. The RH of the sheath flow was regularly monitored just before the flow entered DMA2.

2.5 DMA2 relative humidity regulation

RH is the most important parameter in the HTDMA. Accurate RH is necessary for accurate hygroscopic growth factor (HGF) measurements because inconsistent RH could result in uncertainty in determining the water interaction of particles, which would lead in turn to uncertainty in finding the HGF. For accurate HGF measurements, accuracy of determining the RH is particularly important above an RH of 80%.

To study the particle interaction with water at various humidities, the RH of the DMA2 flow had to change over time. To increase the RH, the sheath flow was passed through the saturator, while to decrease the RH, the sheath flow was passed around the saturator using a solenoid valve. The HTDMA humidification system allows us to gradually scan through various RHs. Equation 2.6 provides a relationship of water vapor mass balance while the sheath flow passes through or around the saturator.

$$RH_{DMA2}(Q_{Sh} + Q_S) = RH_{sat}Q_{Sh} + RH_sQ_s \quad (2.6)$$

Q_{sh} and Q_s are sheath and sample flow respectively. RH_{DMA2} is the RH of DMA2; RH_{sat} is the RH of the sheath flow that exits the saturator after passing through it and is assumed to be saturated. RH_s is the RH of sample before humidification.

Equation 2.6 can be rearranged to equation 2.7, which can be used to calculate the RH of the DMA2 sheath flow.

$$RH_{DMA2} = \frac{(RH_{sat}Q_{Sh}) + (RH_S Q_S)}{(Q_{Sh} + Q_S)} \quad (2.7)$$

RH_s was almost 5%; however, RH_{sat} = 100% on exiting the saturator. Sample flow (Q_s) is 1.0 lpm, so alternating the sheath flow (10 lpm) through the saturator and around it provided steady state RHs. Ideally the set-up should allow us to scan RH values ranging between 1% and 92% in the HTDMA. The initial RH of the sample was not exactly 5% in our experiment, and RH_{sat} was less than 100% with the given sheath flows. Because of the above-mentioned discrepancies in RHs, the obtained steady state RH was not quite as indicated above. The re-circulation of sheath flow (10 alpm) through the saturator could provide a maximum RH of 74% on exiting the saturator without heating. The tubing and DMA were insulated to minimize the loss of heat. With the help of the above-mentioned changes in the set-up we could achieve steady state RH within DMA2 ranging from 80% to 86%. All lab

experiments were performed under a controlled conditioning system, so there were no temperature fluctuations and we achieved fairly consistent steady state RH within the HTDMA.

To achieve the upper level of RH takes 10 to 15 minutes, while decreasing the RH takes a much longer time, i.e., 90 to 105 minutes. RH data was collected and recorded every 0.2 seconds. The average of the 10^{th} and 90^{th} percentiles of RH measurements was calculated and recorded. The data was to be rejected if the spread between the 10^{th} and 90^{th} percentiles exceeded 3%. In our system the RH measurement difference between the 10^{th} and 90^{th} percentiles exceeded 3% when RH was ramped up, so a few initial scans were rejected. A scan was 1 minute in duration, so a complete cycle of RH ramping produces almost 160 scans. A typical RH cycle takes 150 to 165 minutes to complete.

2.6 The working principle of the humidification tandem differential mobility analyzer (HTDMA)

The HTDMA system was designed to measure the HGF of the particles. A simplified schematic diagram of the system is shown in figure 2.7. The system consists of a ^{210}Po bipolar charger, two DMAs, a conditioning system and a CPC. To measure the HGF of the particles, the dry sample flow (1.2 lpm) was first

passed through a ^{210}Po bipolar charger before entering DMA1. The ^{210}Po bipolar charger introduces a distribution of positive and negative charges on the particles. DMA1 was used to select charged monodisperse particles when a fixed voltage was applied on the central rod. The fixed voltage on the central rod of DMA1 produces a narrow range of sampled particle sizes for the typical DMA sample-to-sheath-flow ratio of 0.12, as discussed in section 2.2. The major portion of sampled particles is single-charged; however, a minor portion may have multiple charges. The probability of multiple charged particles contribution at sampled particle sizes depends on number of particles present at higher diameter. For example if sampled particles diameter is 200 nm it may have contribution from doubly charged particles of 320 nm because the doubly charged particles with 320 nm would have the same electrical mobility as 200 nm sampled particles. In our experiments number of particles at higher diameter that may contribute to sampled particle sizes or very few in numbers so their contribution to sampled particle is negligible so we assume that all particles are singly charged; however, a minority that contains multiple charges would appear smaller than the size calculated by assuming a single charge. The dry condition for sheath flow of DMA1 was maintained in order to maintain a dry sample during size selection; this was accomplished by recirculating the sheath flow. The recirculation of the sheath flow was maintained

using a mass flow controller (MKS model 1259C) and a diaphragm pump (Gast model DOA-P10A-AA); the set-up was comparable to the Jokinen and Mäkelä (1997) [Jokinen and Mäkelä, 1997]. In our HTDMA, equilibrium between the sample and sheath flows was achieved in almost half an hour.

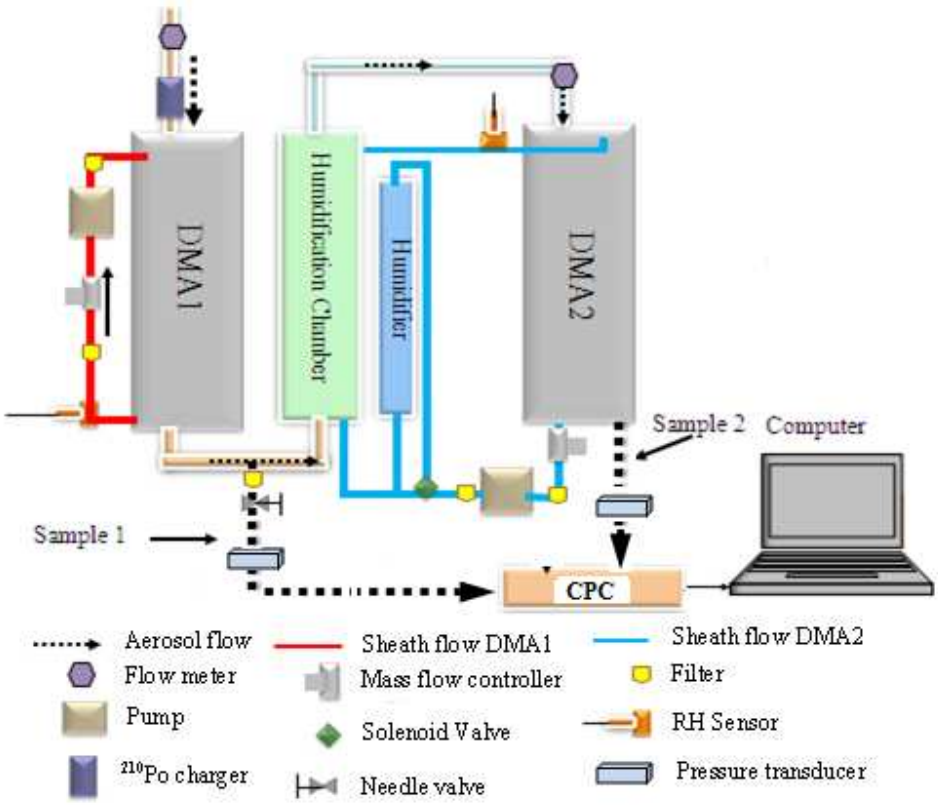

Figure 2.7: Schematic diagram of humidification tandem differential mobility analyzer (HTDMA).

A fraction (0.3 lpm) of the sampled flow from DMA1 was sent through the filter or it may be bypassed the filter before sending it to the CPC. Fraction of the sampled flow was bypassed the filter to determine the particle size distribution if SMPS is unavailable. The remainder of the sampled flow (1.1 lpm) passed through the humidification system, where it was equilibrated at a certain RH. On leaving the equilibrator, the sample flow entered the second DMA. DMA2 captured changes in particle sizes due to humidification. The total flow from both DMAs to the CPC was 1.4 lpm, almost 20% from DMA1 and the rest from DMA2.

DMA1 voltage (V_{DMA1}) was cycled through two to three voltages from experiment to experiment, which means two or three initial diameters were sampled. DMA2 voltage (V_{DMA2}) was a multiple of V_{DMA1} and was scanned exponentially through a range of voltages during one sample period.

$$V_{DMA2} = (f_0 \times V_{DMA1}) exp\left(\frac{t}{\tau}\right) \quad (2.8)$$

Here f_0 was equal to 0.5 and τ was 90 seconds. If flows in both DMAs are equal and particle size remains unchanged, then the peak of the size distribution would occur when V_{DMA2} is equal to V_{DMA1}. The full particle size distribution can be

captured if we set the f_0 value less than unity because monodisperse particles that exit DMA1 have a narrow size range. The upper limit of voltage was set to about 2.5 to 3.5 times V_{DMA1}. The range of the voltages applied was adequate to capture the complete distribution of pure ammonium sulfate (AS) humidified from 80% to 90% RH. Figure 2.8 represents the voltage settings during three sample periods. To determine the particle size distribution, DMA1 was set to scan mode (1 V–10,000 V) while the second DMA was adjusted to $V_{DMA2} = 0$.

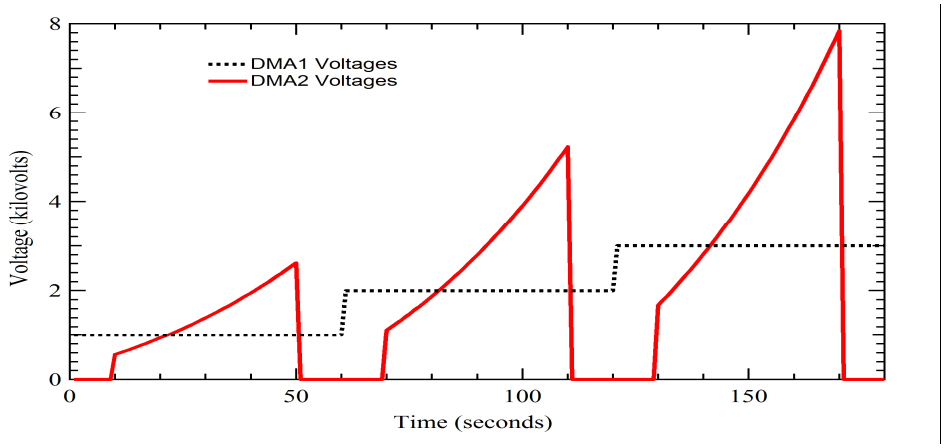

Figure 2.8: Voltages applied to first and second DMAs.

The aerosol sample flows into both DMAs were measured using the pressure drop across laminar flow elements and monitored using Magnehilic

gauges (Dwyer series 2000-0 C). The reading from the gauges for the sampled aerosol flows in a typical sample day was fairly constant. The relative standard deviation of fluctuation of sample flow was not more than 2%. Flows from both DMAs to the CPC were more critical for HGF calculations, so they were measured using laminar flow elements and monitored using a differential pressure transducer (Omega transducer (model XP277)). Readings of sample flows from both DMAs were recorded using the computer data acquisition system; the sample flow average for a sample period was used for data processing. The sheath flow of both DMAs was measured and monitored using mass flow controllers. The computer data acquisition system was set to read and record the electrical signal from the mass flow controller and convert it to the calibrated volume. The volumetric flows from DMAs were used in calculating particle size. The temperature and pressure inside the laboratory was well controlled, so calibration and sample flows were matched fairly well from experiment to experiment. Because the HTDMA results involve a comparison of particle size at both DMAs, any fluctuation due to use of a mass flow controller at both DMAs would be similar, so its use didn't affect the results. The mass flow controllers were calibrated using a bubble flow meter (Gilian Gilibrator) and were set to read the flow at the calibration conditions. Vaisala Humitter 50Y sensors were used to monitor and record the temperature and RH of

the sheath flows of both DMAs. The sensors were calibrated against an EG&G dew point sensor (model 911 DEW-ALL) and were set to read and record at calibration conditions.

In our smog chamber experiments the concentrations of aerosols for HTDMA sampling remained relatively constant and generated fairly consistent data, so there were no complications for data processing such as could occur during ambient sampling.

2.7 Calibration and standardization of the HTDMA system

The performance of the HTDMA instrument can be verified using inorganic salts. For this purpose experiments were run using various inorganic salts, and their growth factors were measured at various RHs and compared with the calculated growth factors. To perform tests with inorganic salts, solutions were prepared using analytical grade reagents (around 99% purity) and deionized water. Particles were atomized using single jet collision nebulizer [BGI,] using pressurized air from a pure air generator (AADCO-737-12). The particles were dried using a multi-tube nafion dryer before they entered the first DMA. Dry monodisperse particles were selected by the first DMA and equilibrated at a variable RH, and the resulting size

distribution was measured by the second DMA. The variability of RH during one sample period was 3% or less.

HTDMA measurements results are reported as a growth factor. The growth factor GF at a certain RH is defined as the ratio of the diameter of the humidified particle, $D_{p,wet}$, to that of the dry classified particle, $D_{p,dry}$.

$$GF = \frac{D_{p,wet}}{D_{p,dry}} \quad (2.9)$$

The literature values of water activity and density of salt solutions [I. N. Tang and Munkelwitz, 1994] were used to calculate the expected growth factor for the inorganic salts used to test the HTDMA performance. The growth factor cubed is proportional to the volume ratio of the humidified particle to the dry. The volume of the particle can be calculated as mass divided by its density, so the growth factor can be calculated as follows.

$$GF_{inorg} = \left(\frac{m_{sol}\rho_{dry}}{m_{dry}\rho_{sol}}\right)^{1/3} \quad (2.10)$$

GF_{inorg} is the growth factor of pure inorganic salt, ρ_{dry} is the density of the dry particle, while ρ_{sol} is the density of the solution, and $m_{\mathrm{dry}}/m_{\mathrm{sol}}$ is the solute

mass fraction (m_{f}). ρ_{sol} for various water activities (a_{w}) and mass fractions (m_{f}) was calculated using a polynomial relationship determined by Tang (1997)[I. N. Tang, 1997] and Tang and Munkelwitz (1994)[I. N. Tang and Munkelwitz, 1994]:

$$\rho_{sol} = 0.997 + \sum_i D_i m_f^i \quad (2.11)$$

$$a_w = 1 - \sum_i A_i m_f^i \quad (2.12)$$

The Köhler theory established the relationship of ambient RH with the HGF of a spherical droplet as given in equation 2.13 [Seinfeld, J. H. and Pandis, S.N., 2006; Rose et al., 2008; Mikhailov et al., 2009; S. Metzger et al., 2011] RH has a direct relation with water activity and Kelvin curvature correction factor (K_e). The Kelvin effect relates the equilibrium vapor pressure over the curved surface of an aqueous droplet to the corresponding vapor pressure over the same solution with a flat surface; the former is always larger. The relative vapor pressure increase over an aqueous droplet of diameter *D* is given in equation 2.13[Gysel et al., 2002; Gysel et al., 2004].

$$RH = a_w \times K_e = a_w \times exp\left(\frac{4M_w\sigma_{sol}}{RT\rho_w D}\right) \quad (2.13)$$

Here M_{w} and ρ_{w} are the molar mass and density of water respectively, σ_{sol} is the surface tension of the solution, R is the ideal gas constant and T is the temperature.

Thus using equations 2.9 through 2.13, expected growth factors were calculated for various RHs. The deliquescence RH and crystallization RH can be found from Tang (1997)[I. N. Tang, 1997] and Tang and Munkelwitz (1994) [I. N. Tang and Munkelwitz, 1994], to which readers are directed for further detail of how to calculate the growth curves of inorganic salts. Densities can be obtained from CRC (2003) [CRC, 2003].

The growth factors were obtained from the HTDMA data using TDMA-Fit [Stolzenberg, M.R. and McMurray, P.H., 1988]. Ammonium sulfate ($(NH_4)_2SO_4$) and Sodium chloride (NaCl) were used to evaluate the instrument performance; good agreement with known curves was obtained, as shown in figures 2.9 and 2.10; for NaCl, the dry particles were assumed to be cubic, so dynamic shape factor for a cube (1.08) was used to correct the HGF result, where the expected growth factor was reduced by the factor of 1.08.

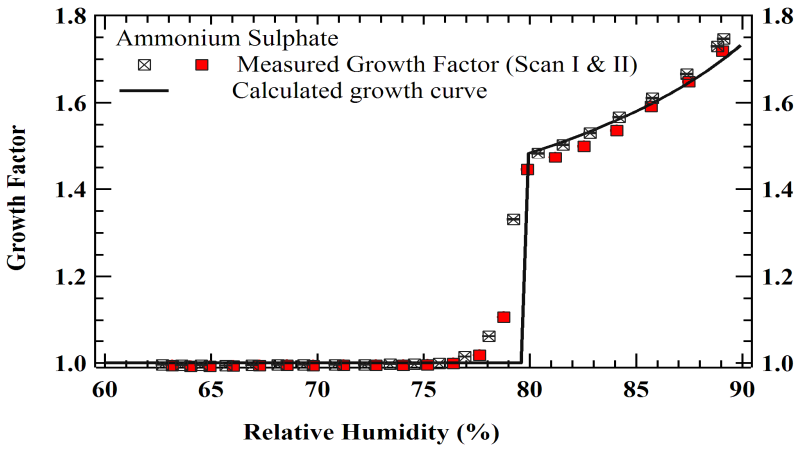

Figure 2.9: Comparison of measured growth factor of ammonium sulfate to the calculated factor (based on Tang and Munkelwitz, 1994) [I. N. Tang and Munkelwitz, 1994].

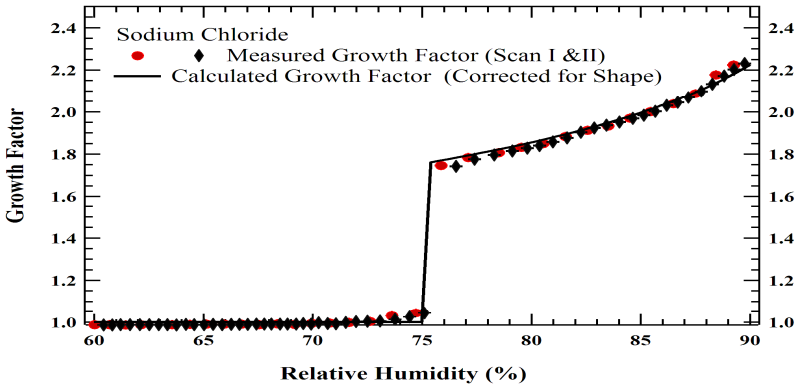

Figure 2.10: Comparison of measured growth factor of sodium chloride to the calculated value (based on Tang and Munkelwitz, 1994) [I. N. Tang and Munkelwitz, 1994]. The calculated growth factor was corrected for shape.

2.8 Scanning mobility particle sizer (SMPS)

A scanning mobility particle sizer (SMPS) is used to monitor the particle size distribution during nucleation and polydisperse seeded experiments. The instrument consists of a DMA (TSI model 3071); a CPC (TSI model 3010); and a system for data acquisition, reading and recording.

The DMA structure and detailed working principle are discussed in section 2.1. In short, before entering the DMA, particles were charged in the SMPS using ^{85}Kr as a radioactive source. The polydisperse sample flow and sheath flow were drawn into the system by a diaphragm pump (Model DOA-P104-AA). The scanning voltage ranged from 10 to 10,000 V, which corresponds to a diameter between 8 and 600 nm. The aerosol flow (Q_{a}, i.e., 1.0 alpm) and sheath flow (Q_{sh}, i.e., 5.0 alpm) were balanced by sample flow (Q_{s}) and excess flow (Q_{ex}) respectively to achieve equilibrium in the system. Balanced input and output flows provided optimum operating conditions for the SMPS and reliable data on particle size changes during the experiments.

The instrument was controlled by the programme written by Prof. Michael Mozurkewich (Centre for Atmospheric Chemistry, York University) in software Igor Pro. 6.0 WaveMatrics. The programme sends a signal to scan voltages on the central rod of the DMA. It takes 5 minutes to complete one scan. First of all it scans down exponentially from 10,000 to 10 V in 10 seconds, and then stays at 10 V for 10 seconds before it starts to scan exponentially up to 10,000 V within 4.5 minutes. Between two consecutive scans it stays at 10,000 V for 10 seconds. During the scanning process the CPC counts every 0.1 seconds to collect raw data. The raw data were summed up after every 2 seconds and further converted to a frequency reading for every 5 minutes' scan. Frequency readings were converted to a mobility distribution during data processing. To calculate the mobility distribution, important corrections were applied to the SMPS data. The data were corrected for the system time delay, particle counting efficiency of the CPC, charging efficiency of the radioactive source and estimation of the number concentration with the transfer function. The programme accounts for all necessary corrections before recording and displaying the data for mobility distribution and particle size distribution. Details of corrections are discussed in Chan's thesis [2005] [T. W. Chan, 2005].

The mobility distribution on applying all applicable corrections is converted to a particle size distribution and described as $dN/dlnD_p$ with 32 size bins. The total number concentration of particles can be estimated by integrating the entire measured size distribution. Figure 2.11 provides a typical particle size distribution obtained during a sequential nucleation experiment. The SMPS data on particle size distribution can be used to calculate mass per bin and overall mass of the particles at a given diameter.

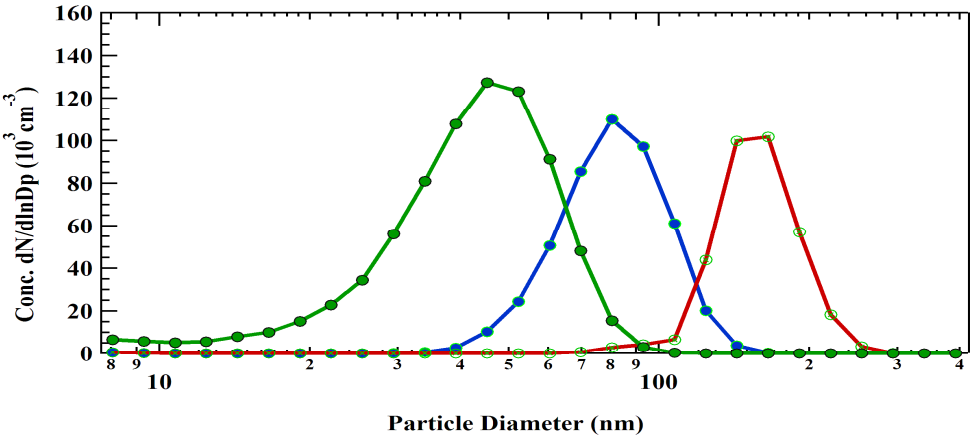

Figure 2.11: Typical particle size distributions measured by the DMA-CPC system during a sequential nucleation experiment. Here hydrocarbons (isoprene, β-pinene and Δ^3carene) were sequentially introduced and oxidized to produce pure organic particles in the chamber.

2.9 Production of monodisperse seed aerosol

In our monodisperse seeded experiments, the oxidation products of selected hydrocarbons were deposited on monodisperse seed aerosol to produce mixed (AS/SOA) particles. The mixed particles (AS/SOA) were sampled to parameterize the hygroscopicity of these particles. The volume fraction of inorganic and organic material in the particle can be determined from the sampled particle size and initial seed aerosol size. The determination was made to understand the relationship of hygroscopicity with the composition of the particles.

To produce mixed (AS/SOA) particles, we first introduced monodisperse seed aerosol in the clean, dry and particle-free chamber using the DMA, and then selected hydrocarbons were oxidized to deposit oxidation products of hydrocarbons on the surface of seed aerosols. To introduce a sufficient number of monodisperse seed aerosol particles in an 8 m^3 chamber was very challenging. The first limitation or challenge was DMA sample input flow (1.0 alpm), which can't be increased.

To introduce monodisperse seed aerosols initially we used a similar set-up to that to generate polydisperse seed aerosol particles. To generate polydisperse seed aerosols, the double jet atomizer (BGI, 2001) with 0.5% AS solution, 10 alpm

(Aadco) air flows was used to atomize the seed aerosols. Primarily we used the same parameters to generate seed aerosol as discussed above except for the Aadco air flow. The Aadco air flow was reduced to 1.0 alpm to match the DMA input for the sample flow. The effort to introduce adequate concentration of monodisperse seed aerosol particles in the chamber to perform seeded experiments was unsuccessful. Later we worked out that a 2.0% AS solution in a double jet atomizer (BGI, 2001) [BGI,] with 10 alpm clean (Aadco) air flow can produce a sufficient concentration of seed aerosol. Due to the limitations of the DMA intake of the sample flow, 9.0 alpm was bypassed and 1.0 alpm was directed toward the DMA. The monodisperse seed aerosols were selected by applying a fixed voltage on the DMA. Before entering the chamber, the selected monodisperse seed aerosols were neutralized using a ^{210}Po neutralizer. The neutralization was necessary to prevent them from being lost on the teflon surface of the chamber because its surface can quickly absorb charged particles. For the above-explained reason, stainless steel tubing was used for the transportation of seed aerosols to the DMA and from the DMA to the chamber.

The detailed layout of monodisperse seeded experiments is given in Figure 2.12. The double jet atomizer produces small droplets, the major portion of which

impacted on the internal wall of its container and washed back to the solution, leaving only less than 1% to survive out of the container with the air flow [May, 1973]. The particles generated by the process were dried using a silica drier before they were passed through a ^{210}Po source for charging. The charged particles enter the DMA, which selects narrow quasi-monodisperse seed particles. The selected monodisperse seed particles were neutralized before entering the chamber. The process of filling the chamber with monodisperse seed aerosol particles takes almost 2.5 hours.

The set up used to select narrow size range of monodisperse seed aerosols. The median diameter of the monodisperse seed aerosols was 100 nm. HTDMA was used to measure size distribution because SMPS was not available. A Typical particle size distribution of monodisperse seed aerosols introduced in the chamber is given figure 2.13.

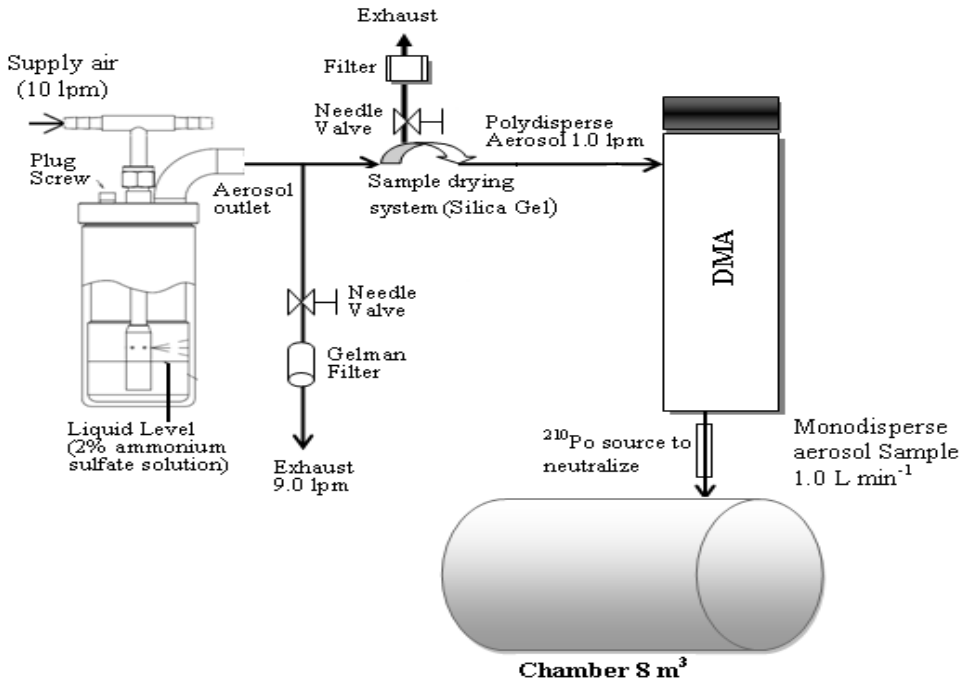

Figure 2.12: Schematic of sorting of monodisperse seed aerosol (via DMA) to fill the chamber to perform monodisperse seeded experiments. The collision nebulizer is modified from that in the BGI manual 2001

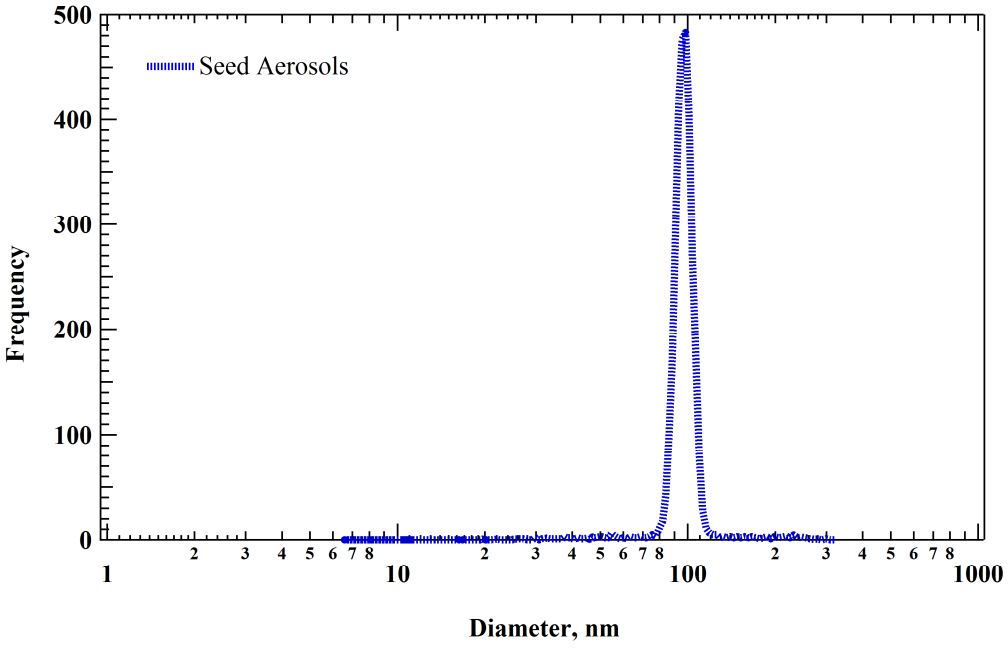

Figure 2.13: A Typical particle size distribution of monodisperse seed aerosols introduced in the chamber measured using HTDMA. Y-axis labeled with frequency because SMPS was not available for size distribution measurements.

2.10 The smog chamber

The York University Smog Chamber was used to perform the experiments. The chamber consists of a tube of teflon film mounted between teflon coated end plates, with a volume of 8 m^3. Between experiments, the chamber was flushed with dry, clean, particle-free air from an AADCO 737 Pure Air Generator. The air was

not humidified, so the RH was less than 5%. The chamber is surrounded by twelve UV lamps (Philips F40 BL, 40 Watt) used to initiate photochemical reactions; it is enclosed so that when the lights are off, no photochemistry occurs. Temperature and RH were measured and monitored using an Omegaette HH311 humidity temperature meter. All the reactants were introduced and sampled through the inlet and outlet openings at the end plates of the cylindrical chamber on either side.

3 Fully Organic Particles

3.1 General Overview of Nucleation Experiments

The main purpose of nucleation experiments was to produce pure organic particles rather than to study nucleation. Nucleation experiments are categorized into three main groups: simple, mixed and sequential. In simple nucleation experiments an individual hydrocarbon (isoprene, β-pinene, limonene, Δ^3carene or α-pinene) is oxidized, while several combinations of these hydrocarbons were used to produce SOA in the mixed and sequential nucleation experiments. Two or three hydrocarbons are oxidized either at the same time or sequentially to produce SOA in mixed hydrocarbon or sequential nucleation experiments respectively.

All of our experiments were performed in a dry, clean (i.e., particle-free) chamber, so the resulting aerosols produced by nucleation were purely organic. To perform nucleation experiments, measured volumes of selected hydrocarbons, isopropyl nitrite (IPN) and nitric oxide (NO) were introduced into the chamber. The hydrocarbons and reactants were given sufficient time for mixing and evaporation before photooxidation was initiated by turning on UV light. IPN photooxidation in the presence of NO produced OH radicals, which oxidize the hydrocarbons. To ensure that hydrocarbon photooxidation was governed solely by OH radicals, an

excess of NO was introduced to scavenge any ozone produced during the photooxidation of hydrocarbons.

The main challenge in performing nucleation experiments successfully was to keep particle sizes within the HTDMA sampling range. In this regard, the simple and mixed hydrocarbon nucleation experiments were easier than the sequential nucleation experiments.

To overcome the challenge, rapid oxidation that consumes all of the hydrocarbon was performed. For this, a high concentration of OH radicals was needed, so IPN was introduced at five to ten times the hydrocarbon mixing ratio. The rapid oxidation of the hydrocarbons produced a high concentration of low-volatility oxidation products in a short span of time. The low-volatility oxidation products saturated quickly and partitioned from the gas phase (nucleated) to produce SOA, with limited condensational growth due to limited supply of the oxidation products. The limited supply of the products was controlled using brief UV exposures and hydrocarbon at the threshold concentration, which is the minimum amount needed to produce SOA on oxidation.

The HTDMA was set to sample two or three sizes from across the particle size distribution. Sampling of particles was done mostly while the chamber was dark, except for some experiments where UV was kept on. Further, relative humidity (RH) was cycled by the HTDMA to capture water uptake properties of aerosols; a full cycle took 2.5 hours. The RH was cycled one to three times at each stage, sometimes with additional periods of UV illumination between the cycles. This was done to investigate whether aging or oxidation of the particles altered the aerosol's hygroscopic properties. The particle size distributions remained nearly constant during the dark portions of the experiments except for a slow concentration decrease due to dilution, coagulation and wall loss.

Table 3.1 provides an overview of the experiments combinations in each category of nucleation experiments.

Table 3.1: Overview of hydrocarbons used in nucleation experiments.

Hydrocarbon-I	Hydrocarbon-II	Hydrocarbon-III	Comments
β-pinene	-	-	Simple
α-pinene	-	-	Simple
Δ^3carene	-	-	Simple
Limonene	-	-	Simple
Isoprene	-	-	Simple
β-pinene	Limonene	-	Mixed HC
α-pinene	β-pinene	Δ^3carene	Mixed HC
β-pinene	Δ^3carene	-	Sequential
Isoprene	β-pinene	-	Sequential
Isoprene	Δ^3carene	β-pinene	Sequential
Isoprene	β-pinene	Δ^3carene	Sequential

3.1.1 Hygroscopic growth factor of pure organic material

A humidogram of the pure organic aerosols was used to parameterize the hygroscopic growth factor (HGF). A two-parameter function to describe the HGF of pure organic aerosols was developed and this derivation follows Aklilu and Mozurkewich [Y. Aklilu and Mozurkewich, 2004]. The humidified particle volume was determined on the basis of partial molar volumes [Atkins, 1994] assuming additive volumes as given in equation 3.1.

$$\frac{\pi D_{pwet}^3}{6} = n_s V_s + n_w V_w \qquad (3.1)$$

Here $D_{p_{wet}}$ is wet diameter of the particle, V_s and V_w are molar volume of solute and water, and n_s and n_w are the number of moles of solute and water respectively.

The dry particle volume is

$$\frac{\pi D_{p_{dry}}^3}{6} = n_s V_s \tag{3.2}$$

and $D_{p_{dry}}$ is dry diameter of the particle. Assuming that molar volumes of the solute remain the same in dry and humidified particles, the HGF of the particles is as follows in equation 3.3:

$$GF_{org} = \frac{D_{p_{wet}}}{D_{p_{dry}}} = \left[\frac{n_s V_s + n_w V_w}{n_s V_s}\right]^{1/3} \tag{3.3}$$

Simplified, this yields equation 3.4,

$$GF_{org} = \frac{D_{p_{wet}}}{D_{p_{dry}}} = \left[1 + \left(\frac{n_w V_w}{n_s V_s}\right)\right]^{1/3} \tag{3.4}$$

The ratio of solute to solvent is related to the a_w by the osmotic coefficient [Mortimer, 2000],

$$-ln(a_w) = \frac{i \emptyset n_s}{n_w} \tag{3.5}$$

Here i is the van't Hoff factor, which for nonionizing solute is unity, and $\emptyset$ is the osmotic coefficient. The ratio of solvent to solute in equation 3.4 is replaced using equation 3.5, yielding equation 3.6:

$$GF_{org=}\frac{D_{p_{wet}}}{D_{p_{dry}}} = \left[1 - \left(\frac{i\emptyset V_w}{V_s\ ln(a_w)}\right)\right]^{1/3} = \left[1 - \left(\frac{b}{ln(a_w)}\right)\right]^{1/3} \quad (3.6)$$

The term $\frac{i\emptyset V_w}{V_s}$ is equated to the fitted parameter b. We also assumed that the components that make up the fitted parameter are constant and are independent of the composition of the solution. The variation in components that make up the fitted parameter may have a second-order effect in determining the change in size of the particle. If the osmotic coefficient and solute-to-water density ratio $\frac{i\emptyset\rho_s}{\rho_w}$ are near unity then the hygroscopicity parameter should be comparable to the ratio of the molar volume of water to the molar volume of the solute; it might be much smaller than that ratio if a significant portion of the organic material does not dissolve.

Equation 3.6, given by Aklilu and Mozurkewich [Y. Aklilu and Mozurkewich, 2004] was modified to equation 3.7 (which was used to parameterize the HGF):

$$GF_{org} = g * \left[1 - \left(\frac{b}{ln(a_w)}\right)\right]^{1/3} \quad (3.7)$$

Here g allows for the offset between the two DMAs (section 2.2). The offset parameter g was not directly applied to the data however it was included in the fits.

Equation 3.7 is similar to the expression used by Petters and Kreidenweis [Koehler et al., 2006; Petters and Kreidenweis, 2007] and becomes identical to it at RH near 100%. The difference is that the equation of Petters and Kreidenweis uses dilute solution standard states while equation 3.7 uses pure liquid standard states. As a result, equation 3.7 gives good fits to empirical data over a wider range of RH; this gives values of b that are somewhat smaller than the κ values of Petters and Kreidenweis.

3.2 Simple Nucleation Experiments

In these experiments only single hydrocarbon is oxidized.

3.2.1 β-pinene Nucleation Experiments

Table 3.2 summarizes the experimental conditions for the β-pinene nucleation experiments. The UV durations given in table 3.2 were for exposures

prior to each scan except for the second scan in experiments 8 and 9, during which the UV was left on.

Table 3.2: Experimental conditions of β-pinene nucleation experiments.

Experiment number	β-pinene (ppbv)	IPN (ppbv)	No. of Scans	UV Duration (minutes)
1	160	458	1	10
2	160	458	1	10
3	160	458	1	9
4	160	458	2	15, 0
5	160	458	3	15, 13, 0
6	240	458	3	10, 0, 0
7	240	458	3	8, 5, 0
8	64	436	2	9, continuous
9	64	220	2	9, continuous
10	32	1100	1	9
11	32	1100	3	4, 0, 0

Figure 3.1 shows a typical particle size distribution obtained in a β-pinene nucleation experiment. The distributions remained nearly constant during dark portions of the experiment except for slow concentration decreases due to dilution and wall loss. The HTDMA was set to sample three sizes from across the distribution.

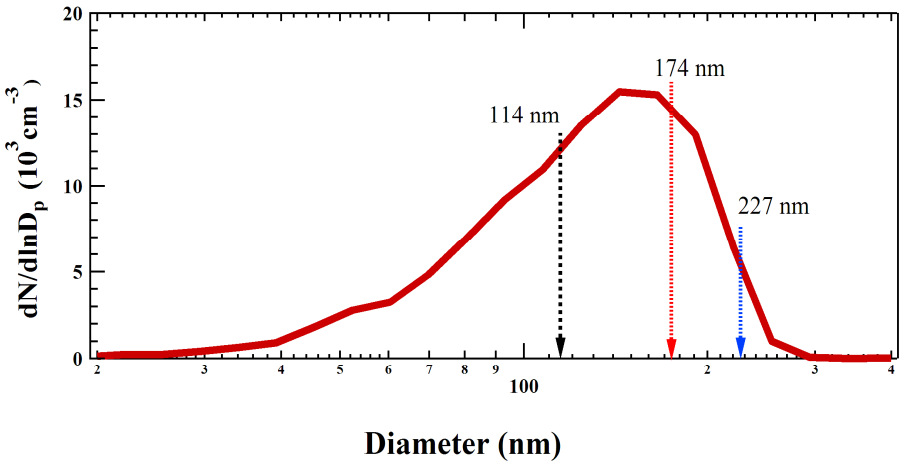

Figure 3.1: Particle size distribution of a typical β-pinene simple nucleation experiment. The particle sizes sampled by the HTDMA are indicated.

Figure 3.2 shows the humidogram of the sampled particles during a nucleation experiment. All dry sizes behaved on the same qualitative manner. The particles were found to be slightly hygroscopic and picked up water smoothly, with no indication of deliquescence, as RH increased from 20% to 90%. This suggests that no phase transition is needed to allow for water uptake; in other words, it suggests that a significant portion of the organic material is either liquid or an amorphous solid [Mikhailov et al., 2009] even at the very low RH inside the chamber.

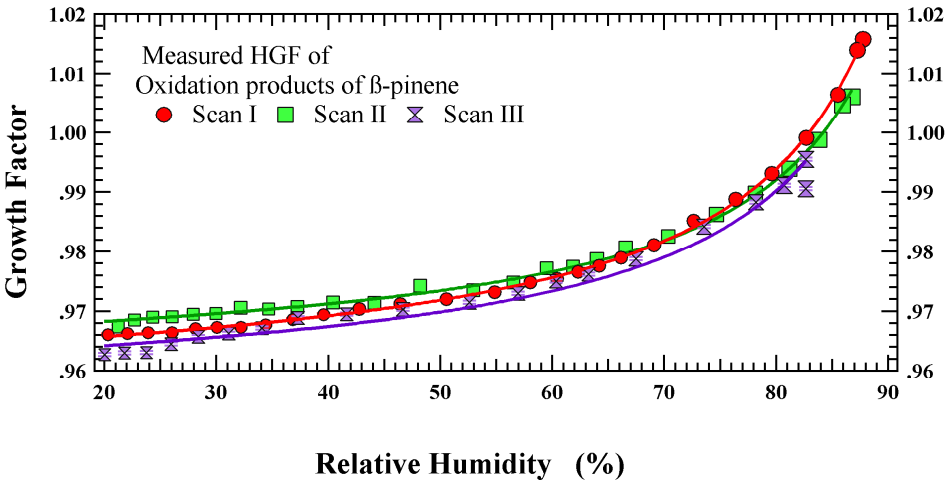

Figure 3.2: Humidograms of 174 nm dry diameter particles for the same nucleation experiment as in Figure 1. Results are shown for three successive humidity scans. The solid lines (red, green and purple) are fitted (for scan-I, -II and -III respectively) to the data using equation 3.7.

Equation 3.7 was used to fit (non-weighted) the humidograms. Each experiment yielded multiple humidograms, since one to three scans were taken at each of several particle sizes; a total of 69 humidograms were collected and analyzed.

Table 3.3: Results of humidogram fits for the particles produced by oxidation of β-pinene. When multiple scans were done, the offset parameter, *g*, was the same for all scans.

Dry Diameter	*b* Scan-I	*b* Scan-II	*b* Scan-III	*g*
Experiment 1				
72 nm	0.0215 ± 0.0027	-	-	1.005 ± 0.0024
114 nm	0.0172 ± 0.0009	-	-	1.005 ± 0.0010
179 nm	0.0237 ± 0.0012	-	-	0.995 ± 0.0010
201 nm	0.0230 ± 0.0006	-	-	1.001 ± 0.0005
Experiment 2				
146 nm	0.0108 ± 0.0002	-	-	0.998 ± 0.0002
240 nm	0.0125 ± 0.0005	-	-	1.008 ± 0.0003
188 nm	0.0112 ± 0.0004	-	-	1.001 ± 0.0003
215 nm	0.0109 ± 0.0005	-	-	1.011 ± 0.0004
240 nm	0.0107 ± 0.0005	-	-	1.012 ± 0.0003
Experiment 3				
188 nm	0.0223 ± 0.0005	-	-	0.998 ± 0.0006
214 nm	0.0258 ± 0.0006	-	-	1.011 ± 0.0005
240 nm	0.0260 ± 0.0005	-	-	1.014 ± 0.0005
Experiment 4				
188 nm	0.0092 ± 0.0003	0.0098 ± 0.0004	-	0.978 ± 0.0003
215 nm	0.0093 ± 0.0002	0.0101 ± 0.0002	-	0.989 ± 0.0002
240 nm	0.0091 ± 0.0002	0.0104 ± 0.0004	-	0.986 ± 0.0002
Experiment 5				
218 nm	0.0116 ± 0.0003	0.0107 ± 0.0002	0.0157 ± 0.0009	0.983 ± 0.0002
215 nm	0.0115 ± 0.0003	0.0110 ± 0.0002	0.0143 ± 0.0010	0.989 ± 0.0002
218 nm	0.0118 ± 0.0005	0.0109 ± 0.0003	0.0166 ± 0.0012	0.992 ± 0.0002
Experiment 6				
188 nm	0.0133 ± 0.0005	0.0083 ± 0.0002	0.0102 ± 0.0003	0.971 ± 0.0003
215 nm	0.0127 ± 0.0005	0.0093 ± 0.0001	0.0105 ± 0.0002	0.973 ± 0.0006
240 nm	0.0134 ± 0.0005	0.0092 ± 0.0002	0.0110 ± 0.0005	0.974 ± 0.0004
Experiment 7				
188 nm	0.0218 ± 0.0005	0.0113 ± 0.0002	0.0120 ± 0.0002	0.963 ± 0.0003
215 nm	0.0206 ± 0.0008	0.0127 ± 0.0003	0.0119 ± 0.0003	0.973 ± 0.0004
240 nm	0.0221 ± 0.0005	0.0121 ± 0.0002	0.0119 ± 0.0002	0.976 ± 0.0006
Experiment 8				
188 nm	0.0100 ± 0.0002	0.0100 ± 0.0004	-	0.970 ± 0.0003
215 nm	0.0110 ± 0.0003	0.0100 ± 0.0003	-	0.980 ± 0.0004
240 nm	0.0120 ± 0.0003	0.0100 ± 0.0003	-	0.980 ± 0.0002
Experiment 9				
188 nm	0.0200 ± 0.0006	0.0200 ± 0.0007	-	0.970 ± 0.0003
215 nm	0.0200 ± 0.0005	0.0190 ± 0.0006	-	0.980 ± 0.0004
240 nm	0.0210 ± 0.0009	0.0200 ± 0.0006	-	0.970 ± 0.0002
Experiment 10				
114 nm	0.0220 ± 0.0003	-	-	0.970 ± 0.0003
160 nm	0.0230 ± 0.0003	-	-	0.960 ± 0.0003
240 nm	0.0250 ± 0.0004	-	-	0.980 ± 0.0003
Experiment 11				
114 nm	0.0224 ± 0.0003	0.0177 ± 0.0003	0.0210 ± 0.0007	0.968 ± 0.0003
174 nm	0.0236 ± 0.0001	0.0198 ± 0.0002	0.0218 ± 0.0009	0.964 ± 0.0003
227 nm	0.0252 ± 0.0004	0.0220 ± 0.0003	0.0236 ± 0.0008	0.972 ± 0.0005

The error estimates for individual values of *b* are based on the scatter about the fitted lines; these estimates were much smaller than the scatter between among values of *b* from a different humidogram. Otherwise, these experiments gave consistent results, with an average hygroscopicity parameter (± one standard error) of 0.0154 ± 0.0014 for β-pinene. Here the uncertainty is twice the standard error based on the scatter between the humidogram. Particle aging, with or without additional illumination, did not affect hygroscopicity.

The hygroscopicity parameter, *b*, can be used to estimate the molecular weight of the organic molecules in the particle phase if it is assumed that all the organic material is in the liquid phase and that activity coefficients are of the order of unity. For an ideal solution, *b* equals the molar volume ratio of water to solute; if the organic material has a density of 1.2 g cm^{-3} [Kostenidou et al., 2007], this implies a molecular weight of about 1400 for β-pinene oxidation products. The estimation of large molecular weight may be due to formation of dimers, trimers, oligomers or polymers that is close to the findings of Kalberer [Kalberer et al., 2004; Kalberer et al., 2006; Reinhardt et al., 2007] . The other reason of large estimation of molecular weight might be due to a large portion of the organic material being in the solid phase (amorphous, semisolid, crystalline, rubber or

glass) [Angell, 1995; Zobrist et al., 2008; Mikhailov et al., 2009; Virtanen et al., 2010; Bones et al., 2012].

We observed a sampling artifact in the dry particle size that was described by the offset parameter, g, in equation 3.7. The dry diameter measured by the second DMA was typically offset by 1% to 3% from that selected by the first DMA. This offset was in the direction of the mode maximum and was likely due to the slope of the size distribution biasing the selected size.

3.2.2 Δ^3carene Nucleation Experiments

The procedure of performing Δ^3carene nucleation experiments was the same as for β-pinene nucleation experiments, and conditions for the experiments are summarized in table 3.4. Briefly, the IPN mixing ratio was kept almost five to ten times higher than the Δ^3carene mixing ratio. In experiments 1 and 2, UV exposures were kept brief while experiments 3 and 4 used continuous UV exposure during their second stage.

Table 3.4: Overview of Δ^3carene simple nucleation experiments.

Experiment number	Δ^3carene (ppbv)	IPN (ppbv)	No. of Scans	UV Duration (minutes)
1	178	1840	2	20
2	266	1226	2	17
3	178	1595	3	22, continuous
4	142	1595	4	25, continuous

Figure 3.3 shows the particle size distribution of experiment 3, a nucleation experiment using Δ^3carene as precursor. Here red and dotted blue lines indicate the particle size distribution after first and continuous UV exposure, respectively. The particle size distribution stayed nearly constant during the dark portion of the experiments except for minor changes due to wall loss and dilution. During the continuous, second UV exposure, particles were grown to bigger sizes due either to further partitioning of oxidation products of unconsumed Δ^3carene from the gas phase to the particle phase or due to the secondary reactions in the gas phase. Figure 3.4 shows the time series of the volume changes after first and continuous UV exposure. First UV exposure was given at 10:58 am and it was around 22 minutes and continuous UV exposure was given at 3:14 pm. The figure shows increase in volume of particulate matter at each UV exposure. Particulate matter

volume increase points toward the photoxidation of unreacted Δ^3carene. Three sampled particle sizes are indicated across the distribution.

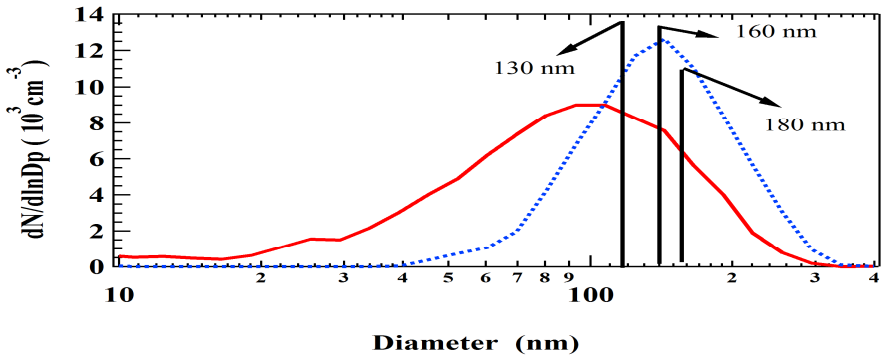

Figure 3.3: Particle size distributions in experiment 3, a Δ^3carene simple nucleation experiment. The red line represents particle size distribution after the first UV exposure; the blue line, during the second, continuous UV exposure. The particle sizes sampled by the HTDMA are indicated at both stages of the experiment.

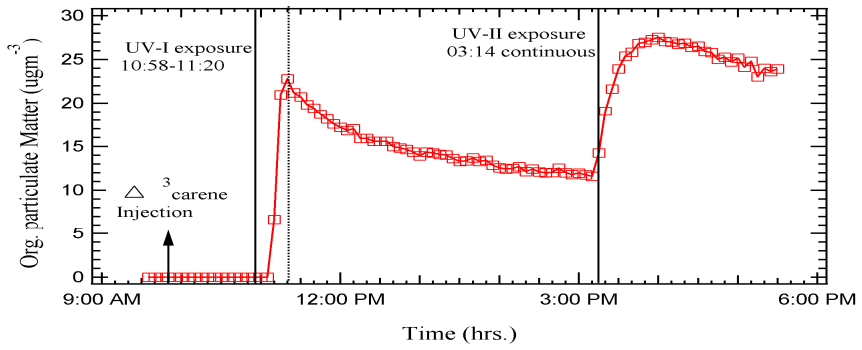

Figure 3.4: Time series of organic particulate matter volume changes in experiment 3. The vertical black solid lines represent time of UV initiation and dotted black vertical lines indicate the time when UV was turned off.

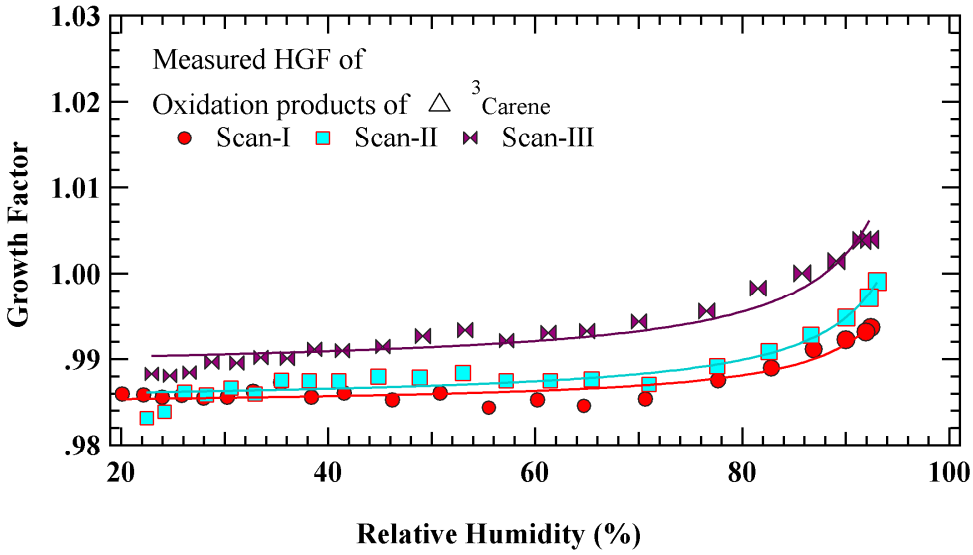

Figure 3.5: Humidogram of 160 nm dry diameter particles for the same nucleation experiment 3 as in Figure 3.3. Results are shown for three successive humidity scans at two stages of the experiment. The data solid lines (red, cyan and maroon) are fitted (scan-I, II and -III respectively) to the data using equation 3.7.

Figure 3.5 shows the humidograms from experiment 3. The first two humidogram scans were taken during the dark phase in the chamber after the first UV exposure. The third humidogram scan was taken during continuous UV exposure. The humidograms showed an offset between the two DMAs, an offset resulting in HGFs less than unity at lower RH. Only the first of the humidograms scan showed shrinking behavior in diameter until RH reached 60%. At higher RH,

particles started picking up water smoothly without any indication of deliquescence. The shrinking behavior of the particles may be due to rearrangements of the oxidation products [N. K. Meyer, Duplissy, Gysel, Metzger, Dommen, Weingartner, Alfarra, Prevot, Fletcher, Good, McFiggans, Jonsson et al., 2009b; Tritscher et al., 2011], to compaction of void volume in the particle, or to oligomerization.

The fitted results are presented in table 3.5. Experimental results were fitted using equation 3.7.

Table 3.5: Result of humidogram fits (non-weighted) for the particles produced by oxidation of Δ^3carene. When multiple scans were done, the offset parameter, g, was the same in experiment 1 and 2 for all scans however in experiment 3 and 4 it slightly changed with the slope of the particle size distribution biasing selected size.

Dry Diameter	b Scan-I	b Scan-II	b Scan-III	b Scan-IV	g
Experiment 1					
220 nm	**0.0011 ± 0.0003**	**0.0027 ± 0.0005**	-	-	**1.02 ± 0.0004**
227 nm	**0.0011 ± 0.0002**	**0.0025 ± 0.0004**	-	-	**1.02 ± 0.0004**
240 nm	**0.0018 ± 0.0003**	**0.0026 ± 0.0004**	-	-	**1.02 ± 0.0004**
Experiment 2					
227 nm	**0.0015 ± 0.0003**	**0.0017 ± 0.0002**	-	-	**0.99 ± 0.0002**
240 nm	**0.0015 ± 0.0002**	**0.0016 ± 0.0002**	-	-	**0.99 ± 0.0002**
Experiment 3*					
130 nm	**0.0022 ± 0.0002**	**0.0031 ± 0.0002**	**0.0042 ± 0.0003**	-	**0.99 ± 0.0002**
160 nm	**0.0022 ± 0.0002**	**0.0032 ± 0.0003**	**0.0047 ± 0.0004**	-	**0.99 ± 0.0003**
180 nm	**0.0022 ± 0.0002**	**0.0035 ± 0.0002**	**0.0045 ± 0.0004**	-	**0.98 ± 0.0004**
Experiment 4*					
160 nm	**0.0042 ± 0.0002**	**0.0047 ± 0.0003**	**0.0084 ± 0.0003**	**0.0091 ± 0.0003**	**0.98 ± 0.0003**
180 nm	**0.0043 ± 0.0002**	**0.0046 ± 0.0003**	**0.0087 ± 0.0003**	**0.0101 ± 0.0005**	**0.98 ± 0.0003**
180 nm	**0.0048 ± 0.0002**	**0.0047 ± 0.0003**	**0.0084 ± 0.0004**	**0.0095 ± 0.0004**	**0.99 ± 0.0004**

*The data of scans III and IV was collected during additional UV exposure. The fitted results of humidograms show that particles hygroscopicity slightly increased.

Our experimental fit (non-weighted) results showed that the particles were slightly hygroscopic. Δ^3carene oxidation products may be composed of two phases, liquid and solid-like similar as β-pinene SOA. Most likely the liquid phase interacts with water, resulting in slightly hygroscopic behavior of the particles. The pure organic aerosols show a slight increase in their hygroscopicity during continuous UV exposure as in experiments 3 and 4. The aerosols may further oxidize during

extended and continuous UV exposure. Oxidation at the particle level may enhance the uptake of water.

As in the case of β-pinene, each experiment gave multiple humidograms since several scans were taken at each of several particle sizes. The fitted results gave an average of all *b* values (± one standard error) of 0.0042 ± 0.0005 for Δ^3carene.

Molecular weight was estimated by using hygroscopicity parameter as discussed in section 3.2.1. The estimated molecular weight of Δ^3carene oxidation products was 5000. As with β-pinene, the estimate was large, this suggested that a large portion of the organic material was in the solid and hydrophobic phase. The solid and hydrophobic phase may contain sticky, rubbery, plastic, gelatinous and gooey material. The physical character of the particles would make them very resistive toward uptake of water. This would lead to low hygroscopicity parameter and a high approximation of the molecular weight. The additional UV exposure increased the water uptake capabilities of the particles. Oxidation at particle level might be the reason behind improved hygroscopic behavior as in experiment 3 and 4.

3.2.3 α-pinene Nucleation Experiments

Table 3.6 summarizes experimental conditions for the α-pinene experiments. These experiments were also performed in a clean, dry and particle-free chamber. The procedure for generating aerosols was the same as discussed in section 3.2.1.

Table 3.6: Overview of α-pinene nucleation experiments.

Experiment number	α-pinene (ppbv)	IPN (ppbv)	No. of Scans	UV Duration (minutes)
1	130	1227	2	7
2	120	859	3	8
3	120	613	2	6
4	120	490	2	6

Figure 3.6 shows a typical particle size distribution obtained by photooxidation of α-pinene. UV exposures were kept brief during these experiments to keep particle size distribution within the HTDMA sampling range. During the dark portion of all experiments, the particle size distribution remained constant except for wall loss and dilution. In α-pinene nucleation experiments we couldn't study the effect of extended or additional UV exposures on particle hygroscopicity because of difficulty in keeping particle sizes within the HTDMA sampling range.

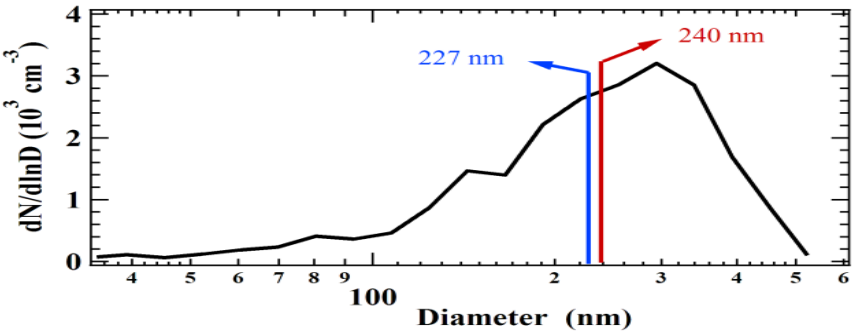

Figure 3.6: Particle size distributions in a typical α-pinene simple nucleation experiment 1. UV was turned off after particle formation. The two particle sizes were sampled by the HTDMA while the chamber was dark.

Figure 3.7 shows typical humidograms of oxidation products of α-pinene. Experimental results were fitted (non-weighted) using equation 3.7.

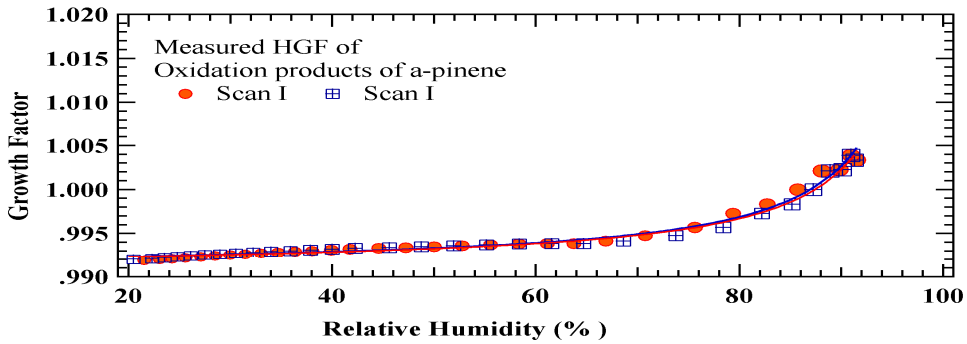

Figure 3.7: Humidogram of 227 nm dry diameter particles for the same nucleation experiment as in Figure 3.5. Results are shown for humidity scans. The solid lines (red and blue) are fitted (scan-I and II respectively) to the data using equation 3.7.

Table 3.7 summarizes these fit results.

Table 3.7: **Result of humidogram fits for the particles produced by oxidation of *α* pinene. When multiple scans were done, the offset parameter, *g*, was the same for all scans.**

Dry Diameter	b Scan-I	b Scan-II	b Scan-III	*g*
Experiment 1				
227 nm	0.0018 ± 0.0003	0.0019 ± 0.0003	-	0.98 ± 0.0003
240 nm	0.0017 ± 0.0003	0.0018 ± 0.0003	-	0.98 ± 0.0004
Experiment 2				
227 nm	0.0038 ± 0.0005	0.0039 ± 0.0003	0.0038 ± 0.0005	0.98 ± 0.0005
240 nm	0.0039 ± 0.0004	0.0038 ± 0.0003	0.0038 ± 0.0004	0.98 ± 0.0004
Experiment 3				
227 nm	0.0031 ± 0.0003	0.0032 ± 0.0002	-	0.98 ± 0.0004
240 nm	0.0031 ± 0.0002	0.0032 ± 0.0003	-	0.98 ± 0.0004
Experiment 4				
227 nm	0.0041 ± 0.0003	0.0042 ± 0.0002	-	0.95 ± 0.0003
240 nm	0.0043 ± 0.0003	0.0041 ± 0.0003	-	0.95 ± 0.0003

The fitted gave an average hygroscopicity parameter (± one standard error) of 0.0031 ± 0.0002 for α-pinene. The estimated molecular weight (section 3.2.1) of α-pinene oxidation products was around 7000. The large estimation of molecular weight might be due to the same reasons discussed in section 3.2.1. The hygroscopicity parameter was consistent within an experiment; however, it showed some inconsistencies in consecutive experiments as given in table 3.7.

Hygroscopicity parameters show that α-pinene SOA was slightly hygroscopic. Aging did not alter the water interaction of the particles as shown by the fit results in table 3.7.

3.2.4 Limonene Nucleation Experiments

The procedure for generating pure organic aerosol during limonene nucleation experiments was same as discussed earlier section 3.2.1; Table 3.8 summarizes reactant concentrations and duration of UV spans in these experiments.

Table 3.8: Overview of limonene nucleation experiments.

Experiment number	Limonene (ppbv)	IPN (ppbv)	No. of Scans	UV Duration (minutes)
1	186	1840	1	6
2	167	1840	2	6
3	167	1840	2	6

Figure 3.8 shows RH dependence of pure organic aerosols generated in limonene nucleation experiments. To parameterize the HGF of the particles experimental results were fitted (non-weighted) using an empirical equation 3.7.

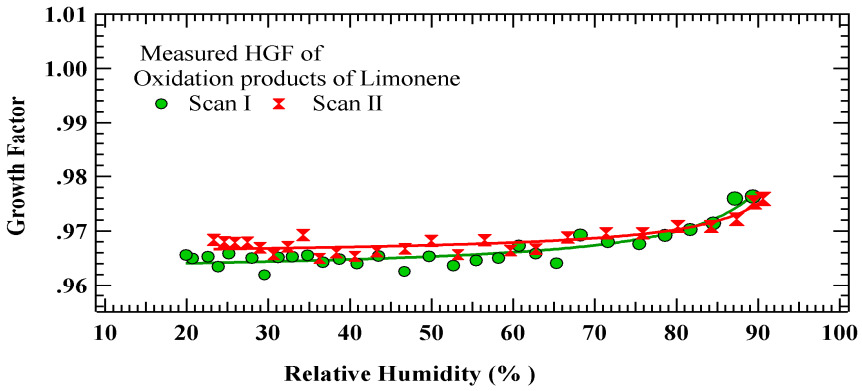

Figure 3.8: Humidogram of 253 nm dry diameter particles for the simple nucleation experiment 3. The data solid lines (green and red) are fitted (scan-I and II respectively) to the data using equation 3.7.

Table 3.9 summarizes these fit results.

Table 3.9: Result of humidogram fits for the particles produced by oxidation of limonene. When two scans were done for each sampled particle size except experiment 1, the offset parameter, g, was the same for all scans.

Dry Diameter	b Scan-I	b Scan-II	g
Experiment 1			
253 nm	0.0071 ± 0.0004	-	0.97 ± 0.0005
277 nm	0.0068 ± 0.0003	-	0.96 ± 0.0005
Experiment 2			
265 nm	0.0079 ± 0.0004	0.0075 ± 0.0003	0.97 ± 0.0005
277 nm	0.0078 ± 0.0004	0.0072 ± 0.0003	0.97 ± 0.0004
Experiment 3			
253 nm	0.0081 ± 0.0005	0.0082 ± 0.0003	0.97 ± 0.0004
277 nm	0.0082 ± 0.0004	0.0083 ± 0.0004	0.97 ± 0.0004

The fitted results gave an average hygroscopicity parameter (± one standard error) of 0.0077 ± 0.0002 for limonene SOA. We found the limonene SOA are 50% less hygroscopic than the SOA of β-pinene, almost 80% and 150% more hygroscopic than the Δ^3carene and α-pinene SOA respectively. We also found that aging didn't alter the hygroscopicity of the particles.

The average hygroscopicity parameter, *b*, was used to estimate the molecular weight of the organic molecules in the particle phase, as discussed in section 3.2.1. The estimated molecular weight of limonene oxidation products was around 2800. The reason for a high approximation of molecular weight and a low hygroscopicity parameter was most likely the same as discussed earlier in section 3.2.1.

3.2.5 Isoprene Nucleation Experiments

Concentrations of reactants and UV duration used in producing isoprene SOA are given in Table 3.10. We used similar reactants concentration except in experiment 2, here it was 50% more compared to experiment 1 and 3. To produce SOA, UV duration was intentionally varied to investigate its effect on the

hygroscopic behavior of the particles. The SOA were produced to quantify RH dependence of isoprene oxidation products.

Table 3.10: Overview of isoprene nucleation experiments.

Experiment number	Isoprene (ppbv)	IPN (ppbv)	No. of Scans	UV Duration (minutes)
1	210	613	2	40
2	315	920	1	23
3	210	613	4	90

The procedure for isoprene nucleation experiments was the same as discussed in section 3.2.1; however, we faced some additional challenges. The main challenge was that the volatility of isoprene made it very problematic to introduce the exact amount of isoprene into the chamber. To introduce a threshold concentration of isoprene added an additional level of difficulty because it evaporates quickly from the tip of the syringe. If the mixing ratio of isoprene is below the threshold concentration, the substance doesn't generate particles on oxidation. Introducing an exact amount of isoprene is necessary to generate pure organic aerosol by photooxidation. The isoprene container and syringe should be refrigerated and handled in an insulated container to avoid direct hand contact with the bottle during filling of the syringe. Direct hand contact may warm the bottle,

resulting in evaporation of isoprene. As a precautionary measure, a proper mask and gloves should be worn to avoid excessive inhalation and absorption through the skin during handling of isoprene. After the syringe is filled, it should immediately be injected in the chamber to avoid loss due to evaporation.

Figure 3.9 shows a particle size distribution of experiment 3, a nucleation experiment using isoprene as precursor. In this experiment UV was exposed for 90 minutes so photochemical reactions continued and caused condensation growth as shown in figure 3.9 until all of the isoprene was consumed. The isoprene SOA slowly kept growing to bigger sizes due to coagulation even in the dark period of the experiment. The concentration of particulate matter slowly decreased because of wall loss, coagulation and dilution. Two sampled particle sizes are indicated across the distribution.

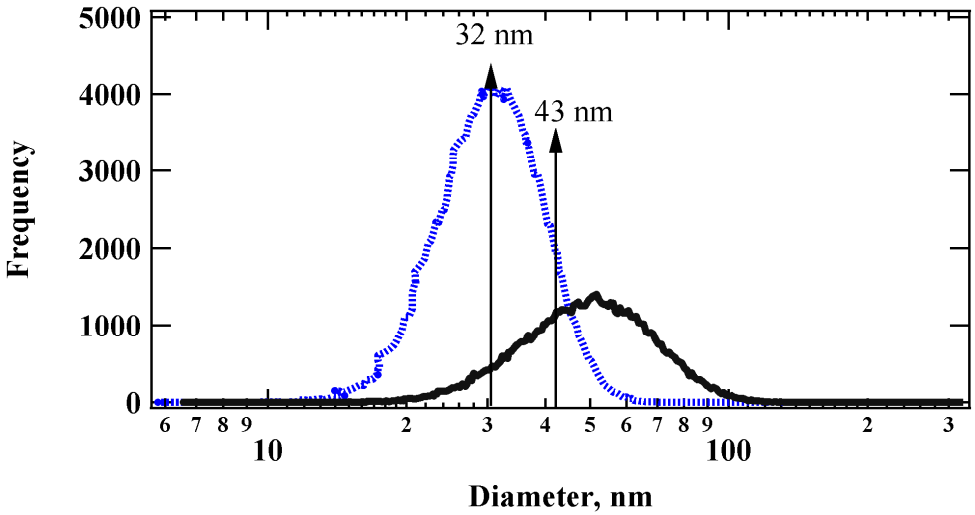

Figure 3.9*: Particles size distributions for experiment 3. The two particle sizes sampled by the HTDMA are indicated. The concentrations of reactants and the UV duration are given in table 3.10. Blue dashed lines indicate particle size distribution at the beginning of the experiment, while black solid lines indicate particle size distribution at the end of the experiment. The reactants were exposed to UV for an extended time. *HTDMA was used to determine particle size distribution due to unavailability of SMPS so y-axis in the graph is labeled with "Frequency" instead of "dN/dlnDp" (gives concentration in each size bins on using SMPS).

Figure 3.10 shows the humidogram of oxidation products of isoprene. The humidograms initially didn't show a positive or negative effect on particle HGF when RH was increased; however, the HGF started to shrink gradually around 30% RH. The particles started to pick up water as they approached 40% RH and, as happens with known pure organic particles, smoothly kept picking up water without any deliquescence behavior [Bahreini et al., 2005; Varutbangkul et al.,

2006]. Humidograms obtained from isoprene nucleation experiments were fitted (non-weighted) with an empirical equation 3.7 to parameterize the hygroscopicity of these particles. We fitted these humidograms above 40% RH because after this RH point the particles pick up water smoothly.

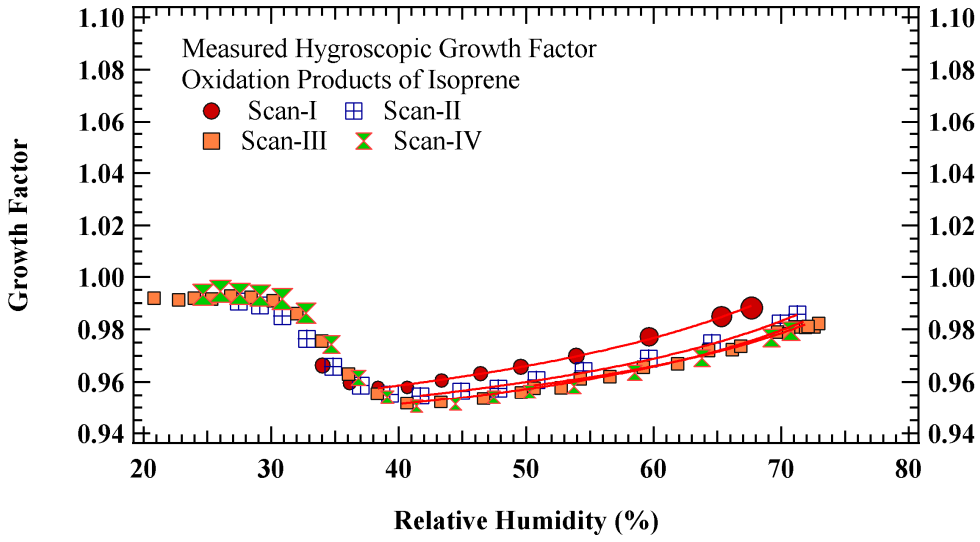

Figure 3.10: Humidogram of 43 nm dry diameter particles for experiment 3, the same nucleation experiment as in Figure 3.8. The data solid lines (red, blue, brown and green) are fitted (scan-I, II, III and IV respectively) to the data using equation 3.7.

Fitted results are summarized in Table 3.11.

Table 3.11: Fitted result of humidogram for the particles produced by the oxidation of isoprene. The offset parameter, ***g***, was in the direction of the mode maximum and was likely due to the slope of the size distribution biasing the selected size and remained consistent for multiple scans during each experiment for the same sampled particle size.

Dry Diameter	b Scan-I	b Scan-II	b Scan-III	b Scan-IV	***g***
Experiment 1					
40 nm	**0.0409 ± 0.0002**	-	-	-	**0.98 ± 0.0002**
52 nm	**0.0358 ± 0.0004**	-	-	-	**0.99 ± 0.0009**
72 nm	**0.0438 ± 0.0009**	**0.0358 ± 0.0004**	-	-	**0.97 ± 0.0004**
96.4 nm	**0.0436 ± 0.0011**	**0.0349 ± 0.0003**	-	-	**0.95 ± 0.0011**
Experiment 2					
58 nm	**0.0329 ± 0.0006**	-	-	-	**0.99 ± 0.0005**
72 nm	**0.0341 ± 0.0007**	-	-	-	**0.96 ± 0.0004**
96 nm	**0.0344 ± 0.0003**	-	-	-	**0.95 ± 0.0005**
130 nm	**0.0338 ± 0.0006**	-	-	-	**0.93 ± 0.0005**
Experiment 3					
32 nm	**0.0441 ± 0.0018**	**0.0446 ± 0.0022**	**0.0445 ± 0.0010**	**0.0468 ± 0.0017**	**0.98 ± 0.0012**
43 nm	**0.0411 ± 0.0016**	**0.0421 ± 0.0012**	**0.0429 ± 0.0023**	**0.0458 ± 0.0045**	**0.94 ± 0.0007**

The fitted results gave an averaged hygroscopicity parameter (± one standard error) of 0.0401±0.0011. We compared the hygroscopicity parameter of oxidation products of isoprene to those of terpenes. We found that isoprene SOA were 60% more hygroscopic than β-pinene and almost up to 90% more than those of the limonene, Δ^3carene and α-pinene SOA. Particle aging did not affect water uptake by these particles.

The molecular weight of the isoprene oxidation products estimated on the basis of its hygroscopicity parameter, *b*, as discussed in section 3.2.1. The estimated molecular weight is almost 600. The large prediction of molecular weight suggests that a) particles (organic material) may be composed of solid and liquid portions and that only the liquid phase was responsible for the interaction with water, or b) there may be an activity coefficient different from unity. Here polymerization is not out of the question and may be the second reason for a high estimate of molecular weight.

3.3 Three-component (Mixed Hydrocarbon) Nucleation Experiments

Table 3.12 summarizes experimental conditions for mixed nucleation experiments.

Table 3.12: Overview of mixed hydrocarbon nucleation experiments.

Experiment Number	α-pinene (ppbv)	β-pinene (ppbv)	Δ^3carene (ppbv)	IPN (ppmv)	No. of Scans	UV Duration (minutes)
1	78	53	48	9.8	1	5
2	78	53	48	9.8	2	5
3	39	27	23	4.9	2	6
4	37	55	34	7.4	3	6

The procedure for oxidation to produce SOA was similar to that discussed in section 3.2.1 for β-pinene. The concentration of hydrocarbon and reactants was

comparable in experiments 1 and 2 and was reduced to half for experiment 3. In experiment 4 the β-pinene concentration was almost doubled compared to that of other hydrocarbons. This was done to find out if it makes any difference to the hygroscopicity of the particles. In these experiments three selected hydrocarbons were oxidized at the same time to produce SOA.

Figure 3.11 shows the humidograms of mixed hydrocarbon (α-pinene, β-pinene and Δ^3carene) oxidation products.

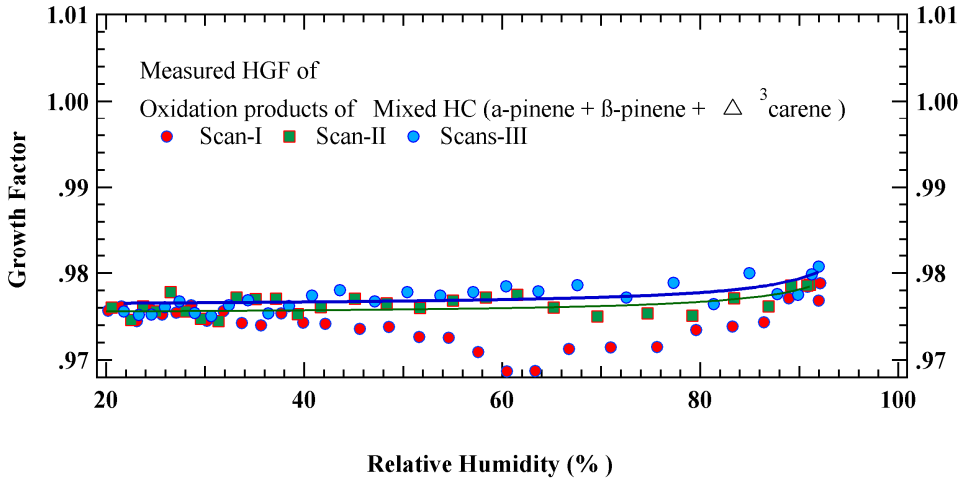

Figure 3.11: Humidogram of 252 nm dry diameter of the particles for experiment 4. The mixed hydrocarbons (α-pinene, β-pinene and Δ3carene) were oxidized to produce pure organic SOA. Results are shown for three successive humidity scans. The solid lines are fitted using equation 3.7.

The first humidogram showed a size decrease on increasing RH that is comparable to the humidogram of Δ^3carene oxidation products as shown in figure 3.5. The humidograms of later scans did not show a particle size decrease on increasing RH.

Table 3.13 summarizes the fitted (non-weighted) results of the humidogram for the mixed hydrocarbon nucleation experiments.

Table 3.13: Result of humidogram fits for the particles produced by oxidation of mixed hydrocarbons. When one to three scans were done for each sampled particle size, the offset parameter, *g*, was the same for all scans.

Dry Diameter	b Scan-I	b Scan-II	b Scan-III	*g*
Experiment 1				
227 nm	0.0013 ± 0.0003	-	-	0.98 ± 0.0004
240 nm	0.0015 ± 0.0004	-	-	0.98 ± 0.0005
Experiment 2				
227 nm	0.0008 ± 0.0002	0.0008 ± 0.0002	-	0.98 ± 0.0002
240 nm	0.0009 ± 0.0002	0.0010 ± 0.0002	-	0.98 ± 0.0003
Experiment 3				
227 nm	0.0015 ± 0.0003	0.0009 ± 0.0005	-	0.98 ± 0.0004
240 nm	0.0016 ± 0.0002	0.0008 ± 0.0005	-	0.98 ± 0.0004
Experiment 4				
227 nm	0.0019 ± 0.0002	0.0016 ± 0.0002	0.0011 ± 0.0002	0.98 ± 0.0003
240 nm	0.0016 ± 0.0003	0.0016 ± 0.0002	0.0011 ± 0.0001	0.98 ± 0.0003

The humidograms collected for all the experiments were fitted using equation 3.7 and gave a hygroscopicity parameter (± one standard error) of 0.0013 ± 0.0004 for mixed SOA of α-pinene + β-pinene + Δ^3carene oxidation products. The results show that SOA are very slightly hygroscopic or almost nonhygroscopic.

We compared the hygroscopicity parameter of mixed (α-pinene + β-pinene + Δ^3carene oxidation products) SOA with individual hydrocarbon (α-pinene, β-pinene and Δ^3carene) SOA and found that the mixed results don't resemble any of the individual SOA results. The individual hydrocarbon SOA gave a hygroscopicity parameter (± one standard error) of 0.0031 ± 0.0002, 0.0154 ± 0.0014 and 0.0042 ± 0.0005 for α-pinene, β-pinene and Δ^3carene respectively. The reason for the low or almost non-hygroscopic behavior of mixed (org/org) SOA could be due to polymerization, co-polymerization or generation of solid, plastic-like material having minimal interaction with water. Aging didn't improve the water interaction of these SOA; however, in experiments 3 and 4 particle hygroscopicity shows a decreasing trend that may be due to compaction with aging. The other possibility is of cross-polymerization among the oxidation products of the mixed hydrocarbon.

The estimated molecular weight (calculation method discussed in section 3.2.1) of mixed SOA by using the hygroscopicity parameter is 15,000, which is

very high and supports the view related to physical state of SOA in the particle as discussed earlier.

3.4 Sequential Nucleation Experiments

3.4.1 Two-Component Sequential Nucleation Experiments

The two-component sequential nucleation experiments were those experiments where we used β-pinene and Δ^3carene sequentially to produce pure secondary organic aerosols (SOA). We used only two terpenes in the sequential nucleation experiments because of the challenges, the main one being to keep the particle sizes within the HTDMA sampling range during the sequential photooxidation stages.

The typical mixing ratios of hydrocarbons, IPN, duration of photooxidation and number of scans at each sequential stage are given in table 3.14. In these experiments the β-pinene concentration was maintained at an almost matching level; however, the Δ^3carene concentration was almost doubled in comparison to that in experiment 1. The IPN mixing ratio was kept very high compared to the ratio for hydrocarbons. The main purpose was to perform rapid oxidation of

hydrocarbons. The IPN was introduced at each time along with hydrocarbons except in experiment 3.

Table 3.14: Overview of two-component sequential nucleation experiments.

Experiment Number	β-pinene (ppbv)	Δ^3carene (ppbv)	IPN (ppbv)	No. of Scans	UV Duration (minutes)
1	71	53	1840, 1226	2, 2	10, 15
2	62	89	2453, 1226	2, 2	6, 6
3	78	89	2453, 0.000	2, 2	11, 10

To produce SOA, UV was turned on briefly to initiate photochemistry, in the course of which the OH radicals rapidly oxidized β-pinene. After the production of SOA, UV was turned off and RH was ramped twice between the values of 20% and 90% to evaluate the hygroscopicity of the SOA. After RH was ramped, Δ^3carene and IPN were introduced while the chamber was still dark. Photochemistry was initiated once more to produce SOA after mixing and evaporation. The oxidation products of Δ^3carene partitioned from the gas phase to the pure organic SOA of β-pinene. The mixed (org/org) pure organic SOA were produced and RH (20% to 90%) was ramped to evaluate the hygroscopic behavior while the chamber was dark.

Figure 3.12 presents a typical particle size distribution generated during experiment 1, a two-component sequential nucleation experiment. In this figure red and blue lines represent particle size distributions after the UV exposure along with particle sizes sampled for HTDMA. According to experimental results, the particle size distributions stayed constant during the dark portion of the experiment; however, wall loss and dilution produced minor changes in particle number concentration.

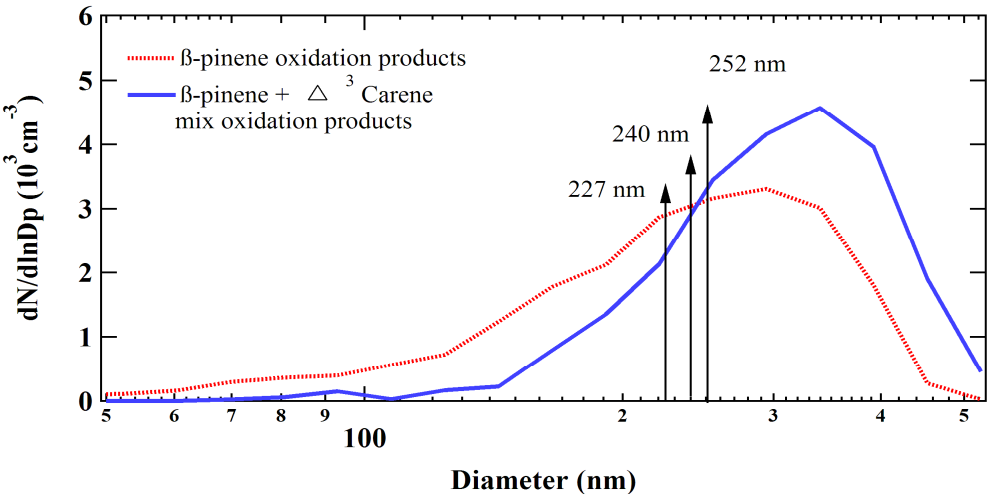

Figure 3.12: Particle size distributions of two-component (ß-pinene and Δ3carene) sequential nucleation experiment 1. The particle sizes sampled by the HTDMA are indicated.

Figure 3.13 presents the humidogram obtained in experiment 1. The mixed (β-pinene + Δ^3carene oxidation products) SOA hygroscopicity may not be

representative of its contributors because of a variety of interactions and due to possibility of complex chemistry. The nature and interactions of the products may lead them to behave like rubbery, gooey, sticky, plastic-like material or hydrophobic solids. The above-discussed factors individually or in combination play an important role in the hygroscopic behavior of the particles. There are chances of changes due to complex chemistry at the particle level too, and oxidation products may undergo oligomerization or polymerization.

Based on the above-mentioned chemical and physical factors, the estimated and experimentally determined hygroscopicity parameter may deviate. The comparison of experimentally determined and estimated hygroscopicity is discussed in detail in section 3.6.

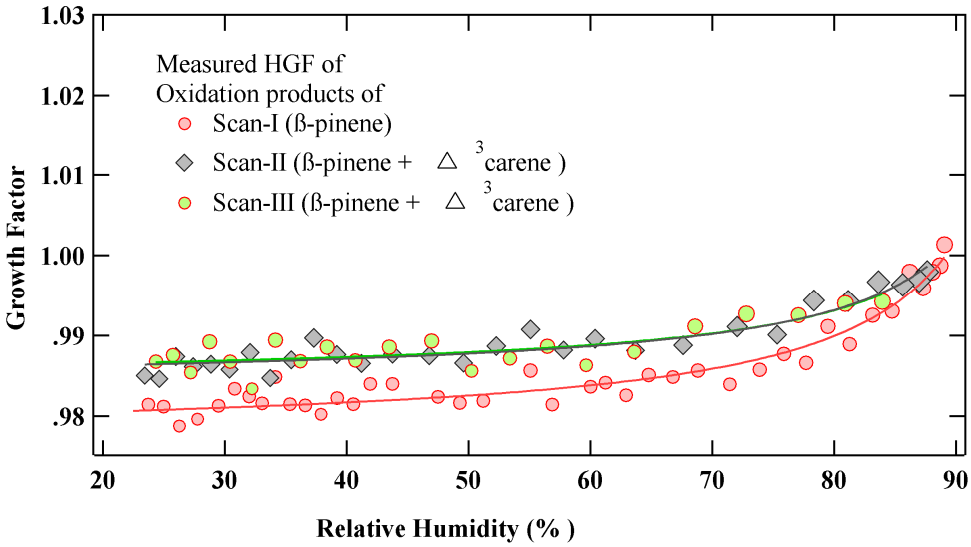

Figure 3.13: Humidograms of 240 nm dry diameter particles for nucleation experiment 1. ß-pinene and Δ^3carene were oxidized sequentially to produce SOA in the chamber. Results are shown for three successive humidity scans. The solid lines are fitted to the data using equation 3.7.

The humidograms were fitted (non-weighted) with an empirical equation 3.7 to determine the hygroscopicity parameter of the particles. Table 3.15 summarizes the fitted results of the humidogram for the two component sequential nucleation experiment, where scan-I and -II were taken after the first photooxidation. Scan-III and -IV were taken after the second photooxidation, in which β-pinene oxidation products were coated with Δ^3carene oxidation products.

Table 3.15: Result of humidogram fits for the particles produced by sequential oxidation hydrocarbons in a two-component sequential nucleation experiment. When one to four scans were done for each sampled particle size, the offset parameter, g, slightly changed however rounded remained the same for all scans.

Dry Diameter	b Scan-I	b Scan-II	b Scan-III	b Scan-IV	g
Experiment 1					
227 nm	**0.0117 ± 0.0003**	**0.0108 ± 0.0005**			**0.98 ± 0.0003**
240 nm	**0.0112 ± 0.0004**	**0.0101 ± 0.0002**	**0.0091 ± 0.0005**	**0.0089 ± 0.0003**	**0.98 ± 0.0003**
254 nm			**0.0086 ± 0.0004**	**0.0085 ± 0.0002**	**0.98 ± 0.0003**
Experiment 2					
227 nm	**0.0118 ± 0.0002**	**0.0117 ± 0.0004**			**0.98 ± 0.0003**
240 nm	**0.0110 ± 0.0002**	**0.0119 ± 0.0005**	**0.0090 ± 0.0004**	**0.0085 ± 0.0005**	**0.98 ± 0.0002**
254 nm			**0.0095 ± 0.0006**	**0.0091 ± 0.0004**	**0.98 ± 0.0004**
Experiment 3					
227 nm	**0.0119 ± 0.0004**	**0.0101 ± 0.0004**			**0.98 ± 0.0003**
240 nm	**0.0109 ± 0.0004**	**0.0102 ± 0.0003**	**0.0080 ± 0.0008**	**0.0080 ± 0.0004**	**0.98 ± 0.0004**
254 nm			**0.0085 ± 0.0004**	**0.0082 ± 0.0008**	**0.98 ± 0.0006**

The fitted results gave an average hygroscopicity parameter (± one standard error) of 0.0111 ± 0.0002 for β-pinene SOA and 0.0087 ± 0.0001 for β-pinene + Δ^3carene SOA. The results correspond to diameter growth factors of 1.022 and 1.018 at 85% RH. The multiple RH scans at each sequential stage served to probe the effect of aging on the particles' hygroscopicity. The fitted results of the humidograms show that there was slight decrease in water uptake properties with age.

The HGF of β-pinene SOA apparently decreased on condensing oxidation products of Δ^3carene. To evaluate the experimental results we applied a volume additivity approach this will be discussed in section 3.5.

The molecular weight of the organic molecules in the particle phase was estimated as discussed in section 3.2.1. The calculated molecular weight was of about 2000 and 2500 for oxidation products of β-pinene and β-pinene + Δ^3carene respectively. The estimate of molecular weights was large and reasons could be similar as discussed in section 3.2.1.

3.4.2 Three-Component Sequential Nucleation Experiments

Atmospheric aerosols are very complex in their chemical composition and physical properties, which are extremely challenging to understand. The physical state and chemical composition determine the particles' hygroscopicity. The physical state of the particles could be solid, liquid or mixed (solid + liquid). In consideration of the complexity of ambient aerosols, we designed our experiments from simple to gradually more complex, with the latter being more relevant to atmospheric conditions. For this purpose we performed sequential nucleation experiments, in which selected hydrocarbons were sequentially introduced into the chamber and oxidized to produce SOA. The experiments provided insight into pure SOA at various sequential evolutionary stages and a convenient way to parameterize the particles' hygroscopicity.

As discussed previously, the sequential nucleation experiments were more challenging than simple nucleation experiments because of the difficulty of keeping particle sizes within the HTDMA sampling range for all sequential stages. This was achieved by performing rapid and brief photooxidation of threshold concentration of hydrocarbons at each sequential stage.

Table 3.16 summarizes information regarding concentrations of hydrocarbons and IPN along with duration of UV exposures and number of scans at each sequential stage of the experiments.

Table 3.16: Overview of three-component sequential nucleation experiments.

Experiment Number	Isoprene (ppbv)	β-pinene (ppbv)	Δ^3carene (ppbv)	IPN (ppbv)	No. of Scans	UV Duration (minutes)
1A	140 (1)	35.5 (2)	89 (3)	613, 613, 613	1, 1, 2	46, 10, 129
2B	140 (1)	35.5 (3)	54 (2)	613, 613, 613	1, 1, 2	65, 20, 41
3B	140 (1)	35.0 (3)	89 (2)	613, 490, 490	1, 1, 2	116, 25, 23

A) Experiment 1A: Hydrocarbons (isoprene, β-pinene and Δ^3carene) were introduced in the chamber according to the number listed in the brackets.

B) Experiments 2B and 3B: The sequence of introducing the hydrocarbons (β-pinene and Δ^3carene) was reversed compared to experiment 1A as listed.

In these experiments, hydrocarbons were sequentially oxidized to produce SOA. At the first oxidation stage, SOA were produced as a result of nucleation, and subsequent sequential oxidations resulted in condensational growth of the nucleated pure organic SOA. The three-component sequential nucleation experiments deployed isoprene as the starting hydrocarbon to produce SOA, which was further coated sequentially with the oxidation products of β-pinene and Δ^3carene. The main reason behind the choice of isoprene as the starting hydrocarbon was its unique

property to produce SOA with a median diameter of 50 nm ± 5 nm on rapid oxidation at its threshold mixing ratio. Particles of this size are ideal for further employment as organic seed aerosols to condense oxidation products of two more hydrocarbons.

Here we discuss experiment 1 as an example of sequential nucleation experiments. In the experiment, isoprene was oxidized to produced SOA at the first sequential stage. There was a gap of almost half an hour between the initiation of photochemistry and emergence of SOA. The delay in particle formation suggests that the second-generation oxidation products might have contributed to the particles' formation.

The UV was turned off after particle formation and RH (20% to 90%) was ramped in our HTDMA in order to evaluate hygroscopicity of the oxidation products of isoprene. After ramping the RH, we introduced β-pinene into the chamber along with excess IPN as measured volumes. At the second sequential stage of the experiment, the reactants were given enough time for mixing and evaporation before we initiated photochemistry to produce oxidation products of β-pinene. The oxidation products of β-pinene partitioned from the gas phase onto the isoprene SOA. Once the mixed SOA (isoprene + β-pinene oxidation products)

were formed, UV was turned off and RH (20% to 90%) was ramped again to evaluate hygroscopicity of the particles (isoprene + β-pinene oxidation products). In the third sequential stage of the experiment, Δ^3carene and IPN were introduced into the system. The reactants were again given sufficient time for mixing and evaporation before we initiated photochemistry. The Δ^3carene oxidation products condensed on the mixed (isoprene + β-pinene oxidation products) SOA. The RH was ramped to evaluate the hygroscopicity of the mixed (isoprene + β-pinene + Δ^3carene oxidation products) SOA.

Figure 3.14 represents typical particle size distributions produced in experiment 1. The particle size distributions stayed nearly constant during the dark portions of the experiments; however, wall loss and dilution produced minor changes in particle number concentrations. Prolonged UV exposure at the third stage didn't show any further condensational growth because all hydrocarbons had already been consumed during the sequential oxidation processes.

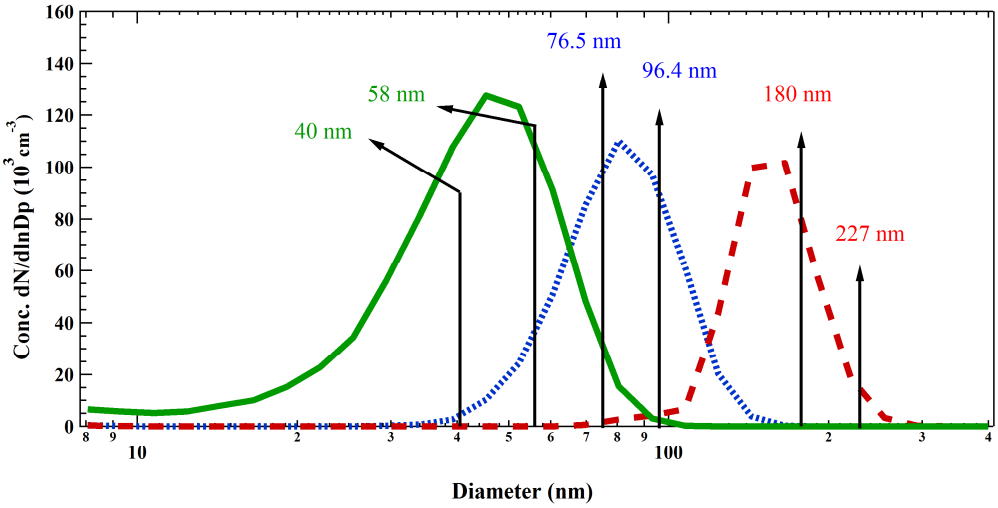

Figure 3.14: Particle size distributions in experiment 1, a typical sequential nucleation experiment (the same as in table 3.16), while isoprene, β-pinene and Δ^3carene were used as precursor hydrocarbons in sequence to produce pure organic aerosols. In figure 3.14 green solid lines, blue dotted lines and red broken lines represent particle size distribution after each UV exposure respectively. The two particle sizes sampled by the HTDMA at each stage are indicated.

Humidograms of sampled particles at three sequential stages are shown in Figure 3.15. The humidogram of isoprene SOA is represented by green spheres, while double blue triangles show the humidogram of isoprene + β-pinene SOA. The humidogram obtained after the third sequential stage, represented by red

squares, is of isoprene + β-pinene and Δ^3carene SOA. Green, blue and red lines are fitted using equation 3.7.

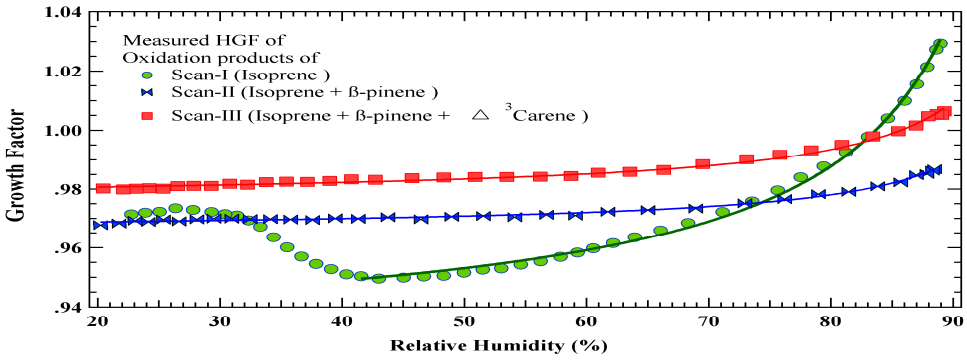

Figure 3.15: Humidogram of 58 nm (SOA of isoprene), 76 nm (SOA of isoprene + β-pinene) and 180 nm (SOA of isoprene + β-pinene and Δ^3carene) dry diameter particles for the same nucleation experiment as in Figure 3.14. Results are shown for one humidity scan of each size at each stage of experiment. The data (solid lines) are fitted (non-weighted) using equation 3.7.

SOA produced from isoprene oxidation products showed an apparent diameter decrease of up to 5% as RH was raised to 40%. The humidogram was fitted above 40% RH because isoprene oxidation products start picking up water smoothly above 40% RH.

Table 3.17 summarizes the fitted results of humidograms after the first, second and third sequential stages of the experiments.

Table 3.17: Result of humidogram fits for the particles produced by sequential oxidation of hydrocarbons. Scan-I and II were taken after the first and second UV exposure, while scan-III and IV were taken after the third UV exposure. When multiple scans were done, the offset parameter, g, was in the direction of the mode maximum and was likely due to the slope of the size distribution biasing the selected size and remained consistent for multiple scans during each experiment for the same particle size.

Dry Diameter	*b* Scan-I	*b* Scan-II	*b* Scan-III	*b* Scan-IV	g
Experiment 1					
40 nm	**0.0356 ± 0.0004**	-	-	-	**0.97 ± 0.0005**
58 nm	**0.0402 ± 0.0005**	-	-	-	**0.96 ± 0.0007**
76 nm	-	**0.0108 ± 0.0002**	-	-	**0.95 ± 0.0002**
96 nm	-	**0.0106 ± 0.0002**	-	-	**0.93 ± 0.0005**
180 nm	-	-	**0.0085 ± 0.0002**	**0.0115 ± 0.0002**	**0.98 ± 0.0002**
227 nm	-	-	**0.0090 ± 0.0002**	**0.0121 ± 0.0004**	**0.97 ± 0.0003**
Experiment 2					
40 nm	**0.0354 ± 0.0005**	-	-	-	**0.98 ± 0.0006**
58 nm	**0.0401 ± 0.0006**	-	-	-	**0.92 ± 0.0005**
96 nm	-	**0.0118 ± 0.0002**	-	-	**0.96 ± 0.0005**
114 nm	-	**0.0119 ± 0.0002**			**0.96 ± 0.0006**
180 nm	-	-	**0.0087 ± 0.0005**	**0.0091 ± 0.0005**	**0.98 ± 0.0005**
227 nm	-	-	**0.0086 ± 0.0006**	**0.0085 ± 0.0006**	**0.97 ± 0.0005**
Experiment 3					
40 nm	**0.0546 ± 0.0005**	-	-	-	**0.97 ± 0.0003**
58 nm	**0.0654 ± 0.0008**	-	-	-	**0.94 ± 0.0002**
76 nm	-	**0.0117 ± 0.0002**	-	-	**0.97 ± 0.0002**
96 nm	-	**0.0116 ± 0.0002**	-	-	**0.98 ± 0.0003**
180 nm	-	-	**0.0085 ± 0.0004**	**0.0087 ± 0.0004**	**0.97 ± 0.0002**
227 nm	-	-	**0.0087 ± 0.0002**	**0.0085 ± 0.0002**	**0.97 ± 0.0002**

The humidograms fitted results of all experiments gave averages of hygroscopicity parameters (± one standard error) of 0.0452 ± 0.0045 for isoprene SOA, 0.0107 ± 0.0001 for isoprene + β-pinene SOA, 0.0118 ± 0.0001 for isoprene + Δ^3carene SOA and 0.0092 ± 0.0004 for isoprene + β-pinene + Δ^3carene SOA. These correspond to diameter growth factors of 1.085, 1.021, 1.024 and 1.019 at 85% RH. The hygroscopicity of these particles depends on the composition and nature of their constituents. Experimental results apparently show that the hygroscopicity of SOA decreased substantially after the second sequential stage of the experiments and slightly after the third.

We performed multiple RH scans in our HTDMA along with an additional period of UV illumination to find out the relationship of hygroscopicity of the particle to aging and potential oxidation at the particle level. In experiments 1A and 3B, SOA were given prolonged UV exposure at the third and first sequential stage of the experiments respectively to find out the potential effect of oxidation and aging. According to our experimental results, the hygroscopicity of the particles was not altered by aging in the dark, it however slightly increased by prolonged UV exposure as in experiment 1A and almost 30% in experiment 3B. We applied a

volume additivity approach to understand the hygroscopicity of the particles at three sequential stages, discussed in section 3.5.

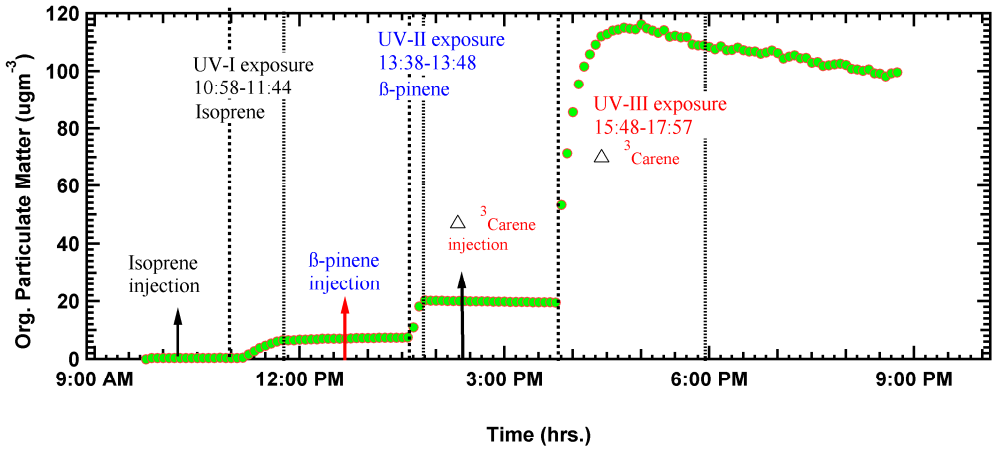

Figure 3.16: Time series of particulate matter formation in a three-component sequential nucleation experiment. Isoprene, ß-pinene and Δ^3carene were used in sequence as precursor hydrocarbons in the chamber to undergo photooxidation. The injection times of hydrocarbons in the chamber to undergo photooxidation. The injection time of hydrocarbons and duration of UV exposures are also shown in the figure.

Figure 3.16 presents experiment 1A, time profile and particulate matter formation at each sequential stage of the experiment. At the first sequential photooxidation, isoprene produced high concentration of fine SOA (average

diameter of 50 nm ± 5 nm). The SOA concentration went down quickly because of coagulation, dilution and wall loss; however, particulate matter remained almost constant because of a small effect of loss. After the second photooxidation, β-pinene oxidation products partitioned from the gas phase to the isoprene SOA. The mixed (isoprene + β-pinene oxidation products) SOA were produced as a result of condensational growth. During the second photooxidation process, particulate matter increased twofold. The third photooxidation stage involved Δ^3carene photooxidation. The oxidation products of Δ^3carene partitioned from the gas phase to mixed (isoprene + β-pinene) SOA, and the particulate matter volume formed up to 118 μgm^{-3}. The final volume fractions of isoprene, β-pinene and Δ^3carene SOA after third sequential oxidation were calculated in the particle and found to be 6%, 12% and 82% respectively. Extended UV exposure was given at the third sequential stage of the experiment to find out its effect on the aging and hygroscopicity of the particles. During the extended UV exposure no further condensational growth of the particles was seen. The observation suggests that hydrocarbons were completely consumed and that no more unreacted hydrocarbon was available for the formation of particulate matter. However, a slow decrease in particulate matter was due to wall loss and dilution as in figure 3.16.

3.5 Hygroscopicity Parameter and Volume Additivity

The hygroscopicity parameter '*b*' of mixed pure organic particles (as in sequential nucleation experiments) can be estimated using the hygroscopicity parameter of the individual components and their respective volume fractions in the particle, by applying the ZSR relation (Stokes and Robinson, 1966); the hygroscopicity parameter can be calculated as in equation 3.9.

$$b_{total} = \sum \frac{b_i V_i}{V_{total}} \quad (3.9)$$

Here b_i is the SOA hygroscopicity of an individual component while V_i is the volume fraction of the individual component that constitutes the mixed particle, and V_{total} is the total volume of the SOA at each sequential stage. Here the V_i of each component can be calculated using SMPS data by knowing that during the dark portion of the experiments the particle size distribution stays nearly constant except for some wall loss and dilution. A relatively stable particle size distribution enabled us to calculate the volume fraction of each component and the total volume produced at each sequential stage.

According to the assumption of the ZSR relationship, which is simplified from that of thermodynamic models, there is no solute-solute interaction; i.e., the

water uptake by individual components in the mixed (org/org) pure organic particle is equal to the sum of the individual water uptakes. We also assumed that particles are spherical and exhibit no volume change on mixing.

The sequential nucleation experiments were performed to probe the effect of sequentially adding oxidation products of selected terpenes (β-pinene and Δ^3carene) on the isoprene oxidation products. Sequentially adding and altering sequence of HC oxidation enabled us to quantify its effect on the hygroscopicity of mixed (org/org) SOA.

Table 3.18 summarizes the hygroscopicity parameter, *b*, of simple nucleation experiments, estimated and experimentally determined at each sequential stage of the sequential nucleation experiments. The estimated hygroscopicity parameter is calculated by using the information of individual volume fractions in the particle and average hygroscopicity of individual HC oxidation products.

Table 3.18: Summary of estimated and experimental values of the hygroscopicity parameter, *b*.

Experiment #	% Volume fraction (V_f)			Simple Nucleation Experiments		Estimated		This Study Pure organic SOA	
SOA'S of				b_{avg}	$\pm\sigma_{SD}$	b_{est}	$\pm\sigma_{SD}$	b_{exp}	$\pm\sigma$
1									
Isoprene	100	-	-	0.0401	0.0048	0.0401	0.0048	0.0379	0.0004
+ β-pinene	35	65	-	0.0154	0.0056	0.0241	0.0053	0.0107	0.0002
+ Δ^3carene	6	12	82	0.0042	0.0036	0.0077	0.0039	0.0103	0.0002
2									
isoprene	100	-	-	0.0401	0.0048	0.0401	0.0048	0.0378	0.0005
+ Δ^3carene	25	75	-	0.0042	0.0036	0.0133	0.0039	0.0118	0.0002
+ β-pinene	4	11	85	0.0154	0.0056	0.0151	0.0054	0.0087	0.0005
3									
isoprene	100	-	-	0.0401	0.0048	0.0401	0.0048	0.0600	0.0005
+ Δ^3carene	19	81	-	0.0042	0.0036	0.0112	0.0038	0.0117	0.0002
+ β-pinene	2	10	88	0.0154	0.0056	0.0149	0.0054	0.0085	0.0004

σ_{SD} = Standard deviation
b_{avg} = average hygroscopicity parameter determined during nucleation experiments
b_{est} = estimated hygroscopicity parameter, determined at each sequential oxidation stage
b_{exp} = experimental hygroscopicity parameter of pure secondary organic aerosols at each sequential oxidation stage

On comparing estimated hygroscopicity parameter (b_{est}) of the particle to experimentally (b_{exp}) determined we reached following conclusions. Pure isoprene

SOA hygroscopicity parameter (except in experiment 3) at first sequential stage was within the 12% to the estimated that is within the scatter (determined during individual isoprene nucleation experiments).

Adding β-pinene and Δ^3carene oxidation products to the pure isoprene oxidation products have no effect on the overall hygroscopicity of the particle. According to the experimental results (table 3.18) at second sequential stage the water uptake is solely governed by isoprene SOA. At third sequential stage the overall particle hygroscopicity is contributed by isoprene and β-pinene SOA while Δ^3carene SOA has minimal or negligible effect.

The estimated (b_{est}) and experimental (b_{exp}) hygroscopicity parameter matched up within experimental uncertainties.

3.6 Pure organic SOA produced during sequential monodisperse seeded experiments (Section 4.3)

Additional pure organic sequential oxidation products hygroscopicity data collected during sequential monodisperse seeded experiments. Experimental conditions and reactants concentration is given in table 4.1. The HGF of the pure organic along with mixed (AS/SOA) aerosol particles is determined. Figure 3.17 shows the humidograms of pure organic particles produced at three sequential

stages in experiment 6. The humidogram of isoprene oxidation products is presented in green squares. Red diamonds represent the HGF of isoprene + β-pinene oxidation products. Blue circles represent humidograms of oxidation products of isoprene + β-pinene + Δ^3carene.

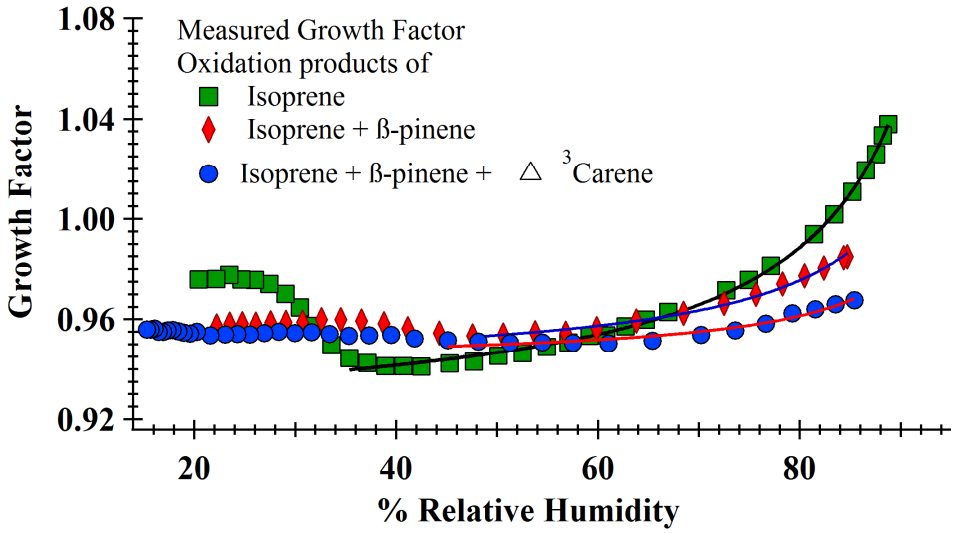

Figure 3.17: Presents typical humidograms of pure organic particles produced at three sequential stages of experiment 6 (chapter 4). Green squares, red diamonds and blue pentagons represent the humidogram of 43, 77 and 114 nm dry diameter particles for the above experiment as in Figures 4.3 through 4.5 (section 4.3). Results are shown for one humidity scan of each size at each stage of the experiment. The data (solid lines) are fitted using equation 3.7.

The humidograms were fitted with equation 3.7 to parameterize the hygroscopicity of the particles. The fitted results are summarized in table 3.19.

Table 3.19: Fitting results of the humidogram of pure organic aerosols produced during monodisperse sequential experiments.

Dry Diameter				
Experiment 6	***b* Scan-I**	***b* Scan-II**	***b* Scan-III**	g
40 nm	0.0494 ± 0.0004	-	-	0.93 ± 0.0004
58 nm	-	0.0240 ± 0.0006	-	0.94 ± 0.0006
76 nm	-	-	0.0133 ± 0.0007	0.94 ± 0.0008
Experiment 7				
32 nm	0.0450 ± 0.0006	-	-	0.95 ± 0.0006
96 nm	-	0.0118 ± 0.0004	-	0.96 ± 0.0005
Experiment 8	-			
60 nm	0.0482 ± 0.0005	-	-	0.96 ± 0.0005
89 nm	0.0194 ± 0.0004	-	-	0.97 ± 0.0004
89 nm	-	0.0191 ± 0.0003	-	0.96 ± 0.0014
Experiment 9				
28 nm	0.0399 ± 0.0006	-	-	0.91 ± 0.0006
93 nm	-	0.0138 ± 0.0005	-	0.96 ± 0.0005

Scan-I, -II and -III are after the first, second and third UV exposure respectively. The g is the offset parameter for each scan.

Apparently the fitted results show that particle hygroscopicity gradually decreased after the second and third sequential stages.

Table 3.20 summarizes HGF results of pure organic SOA from sequential nucleation and sequential monodisperse seeded experiments along with estimated (procedure discussed in section 3.5).

Table 3.20: compares and summarizes the pure organic SOA hygroscopicity parameter, *b* of sequential nucleation, sequential monodisperse seeded experiments and estimated.

Experiment #	**Estimated**	**Sequential Monodisperse seeded experiments**	**Experiment #**	**Estimated**	**Sequential Nucleation Experiments**
SOA'S of		**Pure Organic SOA**	**SOA'S of**		**Pure organic SOA**
6	$b_{est}\pm\sigma_{SD}$	$b_{sexp}\pm\sigma$	**1**	$b_{est}\pm\sigma_{SD}$	$b_{nexp}\pm\sigma$
Isoprene	0.0401±0.0048	0.0494±0.0004	Isoprene	0.0401±0.0048	0.0379±0.0004
+ β-pinene	0.0201±0.0056	0.0240±0.0006	+ β-pinene	0.0241±0.0053	0.0107±0.0002
+ Δ^3carene	0.0093±0.0036	0.0133±0.0007	+ Δ^3carene	0.0077±0.0039	0.0103±0.0002
7			**2**		
Isoprene	0.0401±0.0048	0.0450±0.0006	Isoprene	0.0401±0.0048	0.0378±0.0005
+ β-pinene	0.0159±0.0056	0.0118±0.0004	+ Δ^3carene	0.0133±0.0039	0.0118±0.0002
			+ β-pinene	0.0151±0.0054	0.0087±0.0005
8			**3**		
Isoprene	0.0401±0.0048	0.0482±0.0005	Isoprene	0.0401±0.0048	0.0600±0.0005
+ Δ^3carene	0.0158±0.0034	0.0194±0.0004	+ Δ^3carene	0.0112±0.0038	0.0117±0.0002
	0.0158±0.0034	0.0191±0.0012	+ β-pinene	0.0149±0.0054	0.0085±0.0004
9					
Isoprene	0.0401±0.0048	0.0400±0.0006			
+α-pinene	0.0080±0.0010	0.0138±0.0005			

b_{sexp} = Hygroscopicity parameter of pure organic SOA determined during sequential monodisperse seeded experiments (section 4.3).
b_{nexp} = Experimental hygroscopicity parameter of pure organic aerosols produced during sequential nucleation experiments (section 3.4.2).
b_{est} = Estimated hygroscopicity parameter determined at each sequential stage for both type of experiments discussed in section 3.4.2 and 4.3.
σ_{SD} = Standard deviation.

We compared estimated hygroscopicity parameters *(b_{est})* with experimentally determined *(b_{exp})*. The estimated and experimental hygroscopicity parameters are in close agreement. The results are within (± standard deviation) except in the case of pure isoprene oxidation products (experiments3, 6 and 8). The pure organic aerosols produced during the sequential seeded experiments were in the presence of seed aerosols so the physical and chemical conditions were dissimilar as compared to individual hydrocarbon nucleation and sequential nucleation experiments. The conditions and environment may impact the mechanism of aerosol formation. The various routes and mechanisms of aerosol formation can alter the physical behavior of the particles. The formation mechanism may affect the morphology, shape and structure of aerosols. The difference in hygroscopicity parameter of pure organic from nucleation experiments to the seeded experiments might be might be due to the above-mentioned affects. Table 3.21 summarizes the percentage difference between the hygroscopicity parameter of pure organic from different environment as discussed above.

Table 3.21: compares the average hygroscopicity parameter of various sequential combinations of sequential nucleation experiments to sequential monodisperse seeded experiments.

Experiment	**Sequential Monodisperse seeded experiments**	**Sequential Nucleation Experiments**	
SOA'S of	**Pure Organic SOA**	**Pure organic SOA**	**% difference**
	$b_{sexp}\pm\sigma$	$b_{nexp}\pm\sigma$	$(b_{sexp}- b_{nexp})$
Isoprene	0.0457 ± 0.0005	0.0452 ± 0.0004	1
Isoprene + β-pinene	0.0179 ± 0.0005	0.0107 ± 0.0002	40
Isoprene + Δ^3carene	0.0193 ± 0.0008	0.0118 ± 0.0002	39
Isoprene + β-pinene + Δ^3carene	0.0133 ± 0.0007	0.0103 ± 0.0002	23
Isoprene + Δ^3carene + β-pinene	0.0086 ± 0.0005	-	-
Isoprene + α-pinene	0.0138±0.0005	-	-

b_{sexp} = Average hygroscopicity parameter of pure organic SOA determined during sequential monodisperse seeded experiments (section 4.3).
b_{nexp} = Average hygroscopicity parameter of pure organic aerosols produced during sequential nucleation experiments (section 3.4.2).

We found that isoprene hygroscopicity parameter is almost matching from both sequential systems (seeded and unseeded) however adding β-pinene or Δ^3carene SOA to isoprene oxidation products produces almost 40% difference while adding Δ^3carene SOA to the isoprene + β-pinene SOA produces around 25% difference. The hygroscopicity parameter from both sequential systems (seeded and

unseeded) show significant difference compared to each other however its values remains within the scatter.

3.7 Relation of sample's time of equilibrium with variable RH on growth factor of pure organic aerosol particles

We performed some preliminary experiments to find out if sample (pure organic aerosols) equilibrium time with variable RH in HTDMA is adequate. To perform these experiments instrument was modified from that previously used section 2.6. In the modified instrument; humidified sample can either be directed towards the twenty feet quarter inch stainless steel tube before it reaches to scanning DMA or it can be directly send towards scanning DMA. To maintain laminar flow of humidified sample during the enhanced equilibrium interval coiled stainless steel tubing was used.

To find out effect of extended equilibrium time on HGF of pure organic aerosols, β-pinene was used to produce pure organic aerosol particles. Experimental procedure to produce β-pinene SOA was similar as discussed in section 3.6. After the production of pure organic SOA in the chamber, sample was drawn to the HTDMA system where its growth factor was characterized with

normal and extended equilibrium time. Normal and extended equilibrium times were 2.73 and 14 seconds respectively.

Experimental results of pure organic aerosols with normal and extended equilibrium time showed that there was no significant difference in the hygroscopic growth factor. According to preliminary experimental results time required for sample to equilibrate with variable RH was adequate in our HTDMA system.

4 Mixed (inorganic/organic) particles

4.1 General overview and experimental procedure

Atmospheric aerosols are composed of inorganic and organic compounds. The inorganic portion of the atmospheric particles consists mainly of ammonium sulfate (AS), except in a marine environment. Organic material in the particles is contributed from anthropogenic and biogenic sources. The relative amount of inorganic and organic species in the particles determines the hygroscopic behavior of mixed particles. To parameterize the hygroscopicity of mixed particles, we performed seeded experiments.

To perform the seeded experiments, monodisperse AS seed aerosols were introduced in the clean, particle-free chamber. The hygroscopic growth factor (HGF) of the pure AS seed aerosols was monitored at a fixed RH. We compared calculated values of HGF of seed aerosols (see section 2.4.1) against the experimental values. The results agreed within experimental uncertainties. The HGF measurements of the seed aerosols provided instrument calibration and ensured reliability of the data. After we monitored the HGF of the seed aerosols, a threshold concentration of selected hydrocarbons (isoprene, β-pinene, α-pinene,

Δ^3carene or limonene), along with an excess of isopropyl nitrite (IPN) and nitric oxide (NO) was introduced in the chamber. The reactants were given sufficient time for evaporation and mixing before photochemistry was initiated. Upon photoxidation, the hydrocarbons produced low-volatility oxygenated products. Some of the oxygenated products partitioned from the gas phase to the particle phase (seed aerosols) and condensational growth resulted. The process produced mixed (AS/SOA) particles.

The reactants were briefly exposed to UV for photooxidation. The UV exposures were kept brief to stop photooxidation reactions and as a result particle size distribution remained nearly constant during dark portion of experiments except some minor changes due to wall loss and dilution. Particles composition also stays constant during dark portion of experiment and also if condensable material is unavailable during photooxidation.

The HTDMA was used to measure the hygroscopicity of mixed particles. Humidograms of mixed (AS/SOA) particles were obtained by ramping RH from 20% to 90% in our HTDMA. Humidograms obtained from seeded experiments were fitted using a model created by Kristina Zeromskiene; the model is capable of retrieving particle composition (inorganic and organic volume fractions) and

parameterizing hygroscopicity by analyzing humidograms generated by the HTDMA. One of the benefits of performing monodisperse seeded experiments was to verify our model and to relate particle composition to the hygroscopicity. The experiments were used to evaluate the applicability of the model. The amount of inorganic and organic species in the particle can be calculated by using information on the initial monodisperse seed aerosol size that was introduced in the chamber and the sampled particle size. The hygroscopicity parameter, *b*, of oxidation products of individual hydrocarbons was determined during unseeded experiments. We compared experimental results with the fitted result from the model and found excellent agreement within the experimental uncertainties.

The monodisperse seeded smog chamber experiments are categorized into the following groups.

1. Simple monodisperse seeded experiments (Experiments 1–5)

In these experiments mixed (AS/SOA) particles were produced by depositing oxidation products of β-pinene on monodisperse seed aerosols (AS).

2. Sequential monodisperse seeded experiments (Experiments 6–9)

In these experiments two or three hydrocarbons (isoprene and selected terpenes) were sequentially oxidized to deposit oxidation products on monodisperse seed aerosols (AS) to produce mixed (AS/SOA) particles.

3. Mixed hydrocarbon monodisperse seeded experiments (Experiments 10–11)

In these experiments mixed (AS/SOA) particles were produced by depositing oxidation products of three hydrocarbons at the same time on monodisperse seed aerosols (AS).

Table 4.1 provides an overview of monodisperse seeded experiments of each category. The table summarizes mixing ratios, duration of UV and number of RH scans to measure HGF in each experiment.

Table 4.1: Hydrocarbon combinations, concentrations, IPN and duration of UV exposure in seeded experiments with seed aerosol (NH4)2SO4.

Experiments #	Hydrocarbons (HC)	HC (ppbv)	IPN (ppbv)	No. of RH Scans	UV Duration (minutes)[1]	Comments
1	β-pinene	17	73	3	7	Simple
2	β-pinene	36	73	3	8	Simple
3	β-pinene	36	123	3	10	Simple
4	β-pinene	53	123	3	22	Simple
5	β-pinene	72	147	3	15	Simple
6	Isoprene	210	1226	2	44	Sequential[2]
	β-pinene	53	613	2	15	
	Δ^3carene	89		2	11	
7	Isoprene	210	1840	2	50	Sequential[2]
	β-pinene	53		2	11	
8	Isoprene	210	613	2	41	Sequential[2]
	Δ^3carene	89	490	2	16	
9	Isoprene	210	1717	2	29	Sequential[2]
	α-pinene	88		2	24	
10	β-pinene	26	1226	2	5	Mixed HC
	Δ^3carene	23				
	α-pinene	39				
11	β-pinene	26	1226	2	5	Mixed HC
	Δ^3carene	23				
	α-pinene	39				

[1] UV exposures were prior to RH scan in HTDMA in all experiments.
[2] The sequential experiments with more than 1HC, the HCs are listed in the order of injection.

4.2 Simple monodisperse seeded experiments

In simple monodisperse seeded experiments β-pinene was oxidized in the chamber to produce condensable material. After initiating photochemistry, the seed aerosols underwent condensational growth as oxidation products of β-pinene partitioned from the gas phase to the particle phase and produced mixed (AS/ β-pinene SOA) particles as shown by dotted red lines in figure 4.1. During these experiments only mixed (AS/ β-pinene SOA) particles were produced because there was no nucleation.

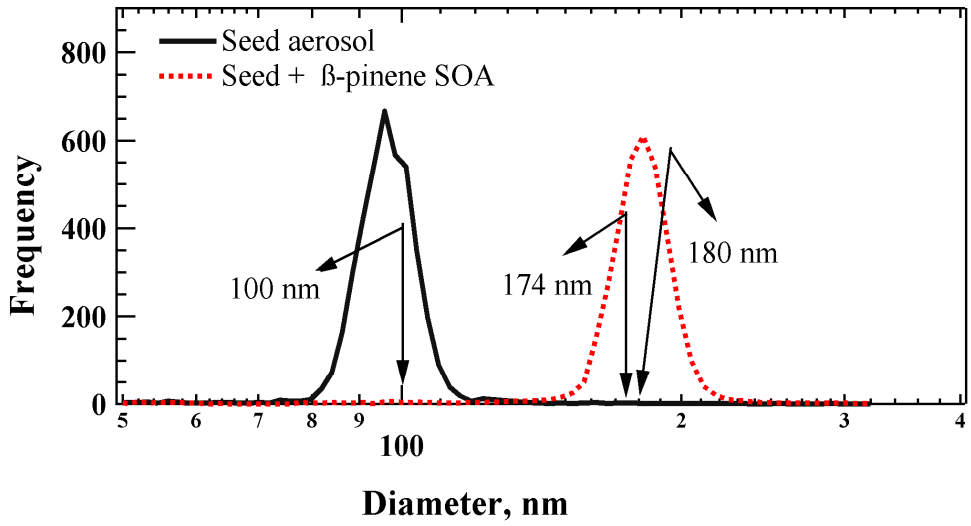

Figure 4.1: Particle size distribution in simple monodisperse seeded chamber experiment. The black line shows the particle size distribution of monodisperse seed particles ((NH4)2SO4). The red line shows the particle size distribution after the condensation of oxidation products of ß-pinene on the monodisperse seed aerosols. Particle sizes sampled for the HTDMA are indicated.

The UV exposure was varied from 5 to 25 minutes from experiment to experiment. The relative humidity was ramped twice with the UV off to investigate particle hygroscopicity and to determine if the hygroscopicity changed as the particles aged. Condensation of the oxidation products onto seed aerosols altered the growth factor, also reported by previous researchers [Sjogren et al., 2007; Hallquist et al., 2009]; an example is shown in Figure 4.2.

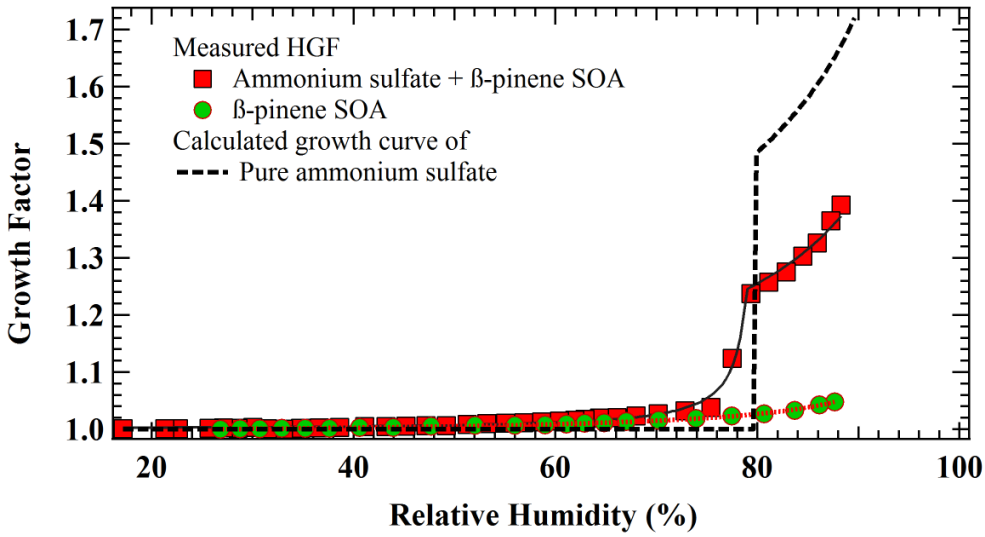

Figure 4.2: Typical humidogram for a seeded experiment. The sampled particle size was 180 nm in diameter and the seed particle size was 100 nm. The curve is fit using the model described in the section 4.2.1. Green circles are typical humidogram of ß-pinene SOA. The red dotted line is fit to the data using equation 3.7. Black broken line is calculated [I. N. Tang and Munkelwitz, 1994] HGF of pure ammonium sulfate. Pure organic (ß-pinene SOA) HGF and calculated ammonium sulfate curves are given for comparison.

There is both gradual uptake of water below 70% RH, as observed for the pure organic particles, and a gradual deliquescence beginning somewhat below the deliquescence point (80% RH) of $(NH_4)_2SO_4$. At higher RH, there is good agreement with the volume additivity (ZSR) approximation. A more detailed analysis requires a model for water uptake in the region in which $(NH_4)_2SO_4$ gradually dissolves.

To parameterize the HGF and particle composition of mixed organic and inorganic species, the following model was developed.

4.2.1 Model for water uptake

The model was developed by Kristina Zeromeskiene (PDF Mozurkewich group) and presented here for completeness. It was developed to obtain an equation to fit growth factors as a function of relative humidity. The model assumes three components: organic material, AS and water. The key assumption is volume additivity; thus the dry particle volume, V_D, is given by

$$V_D = n_{AS}\,\bar{\nu}_{AS} + n_{org}\,\bar{\nu}_{org} \tag{4.1}$$

where n is moles, $\bar{\nu}$ is molar volume, and the subscripts indicate ammonium sulfate and organic material. The total wet particle volume, V_T, is the sum of three volumes: undissolved AS, AS solution, and organic material, including the water associated with it. Thus,

$$V_T = \underbrace{(1 - f_d)\,n_{AS}\,\bar{\nu}_{AS}}_{\text{Undissolved AS}} + \underbrace{f_d n_{AS}\,\bar{\nu}_{AS}\,GF_{AS}^3}_{\text{AS Solution}} + \underbrace{n_{org}\,\bar{\nu}_{org}\,GF_{org}^3}_{\text{Org + Water}} \tag{4.2}$$

where f_d (which must be in the range of 0 to 1) is the fraction of dissolved AS, GF_{AS} is the diameter growth factor of AS (obtained from the empirical pure AS growth curve [I. N. Tang and Munkelwitz, 1994], and GF_{org} is the diameter growth factor of pure organic material from equation 3.7.

We replace moles with the organic dry volume fraction, ε_{org}, defined by

$$\varepsilon_{org} = n_{org}\,\bar{\nabla}_{org}/V_D \tag{4.3}$$

and the dry volume fraction of AS, ε_{AS}, defined by

$$\varepsilon_{AS} = n_{AS}\,\bar{\nabla}_{AS}/V_D \tag{4.4}$$

From equation 4.1, these two fractions clearly add to unity. Dividing equation 4.2 by V_D (equation 4.1) and using these quantities yields an expression for the diameter growth factor:

$$GF_{tot}^3 = \frac{V_T}{V_D} = \frac{(1-f_d)n_{AS}\bar{\nabla}_{AS}+f_d n_{AS}\bar{\nabla}_{AS}GF_{AS}^3+n_{org}\bar{\nabla}_{org}GF_{org}^3}{V_D} \tag{4.5}$$

Replacing quantities in equation 4.5 from equations 4.3 and 4.4 yields:

$$GF_{tot}^3 = \frac{V_T}{V_D} = (1 - f_d)\varepsilon_{AS} + f_d\varepsilon_{AS}GF_{AS}^3 + \varepsilon_{org}GF_{org}^3 \quad (4.6)$$

Then using $\varepsilon_{AS} = 1 - \varepsilon_{org}$ and rearranging terms gives,

$$GF_{tot}^3 = \frac{V_T}{V_D} = \left(1 - \varepsilon_{org}\right)(1 - f_d + f_d GF_{AS}^3) + \varepsilon_{org}GF_{org}^3 \quad (4.7)$$

The value of GF_{org} is replaced using equation 3.1:

$$GF_{tot}^3 = \frac{V_T}{V_D} = f_d\left(1 - \varepsilon_{org}\right)(GF_{AS}^3 - 1) + (1 - \frac{\varepsilon_{org}b}{ln(a_w)}) \quad (4.8)$$

Equation 4.8 is used to fit the humidograms, with ε_{org} and b (equation 3.7) as the fit parameters while a_w is the water activity explained in section 1.7 (Chapter 1).

For pure AS, f_d changes abruptly from zero to unity at the deliquescence point. When organic material is present, it takes up water at low RH; this allows some AS to dissolve so that f_d increases gradually, reaching unity at a RH below the deliquescence point of the pure salt. The major challenge in the model is to calculate f_d as a function of RH.

To do this, we determine the concentration of AS in the solution from the equilibrium expression when solid AS is present. The equilibrium between solid and dissolved AS is described by

$$[NH_4^+]^2\,[SO_4^{2-}] = K \tag{4.9}$$

where activities are indicated by the square brackets and K is an equilibrium constant. We assume that the activity coefficients are the same as in the saturated binary solution so that the activities can be replaced with concentrations; this, along with equation 4.9, amounts to taking the standard state for the ions to be the saturated solution.

The concentrations in equation 4.9 are taken to be moles per unit volume of aqueous solution; the aqueous volume is assumed to be the volume of solution associated with the dissolved AS ($f_d n_{AS}\,\bar{\nu}_{AS}\,GF_{AS}^3$) plus the volume of water associated with the organic material ($n_{org}\,\bar{\nu}_{org}\left(GF_{org}^3 - 1\right)$. Thus,

$$\frac{1}{2}\,[NH_4^+] = [SO_4^{2-}] = \frac{f_d \varepsilon_{AS}}{\bar{\nu}_{AS}\left(f_d(1-\varepsilon_{org})GF_{AS}^3 + \varepsilon_{org}\left(GF_{org}^3 - 1\right)\right)} \tag{4.10}$$

The equilibrium constant, K, is evaluated to give the observed growth factor for pure AS at its deliquescence RH. Using n_{org}=0, f_d=1, GF_{AS}=1.48 [I. N. Tang and

Munkelwitz, 1994; I. N. Tang, 1996], and $\bar{v}_{AS}$= 0.0747 $L\ mol^{-1}$ yields $[SO_4^{2-}] = 4.13\ mol\ L^{-1}$ in the saturated solution. Substituting this into equation 4.9 yields $K = 282\ mol^3 L^{-3}$. Equations 4.9 and 4.10 are used to iteratively calculate the fraction dissolved at a given RH, with the constraint that $f_d \leq 1$. Then equation 4.8 is used to calculate the growth factor.

The model successfully fits the gradual deliquescence, as shown in Figure 4.2. Since the time allowed for particles to equilibrate at the higher RH was short, about 0.26 seconds, the data indicate that depositing a less hygroscopic organic phase onto inorganic particles did not significantly inhibit the mass transport of water to the inorganic material. One possible explanation for this would be that the organic material might not "wet" the salt surface; in that case it would not be uniformly distributed over the surface so that some of the salt was always exposed to the air. A second possibility is that the organic coating may be permeable so that even if it uniformly coats the particle it does not prevent water molecules from reaching the more hygroscopic AS core. This would be consistent with part of the organic phase being a liquid or porous solid.

4.2.2 Comparison of fitted and calculated results of simple monodisperse seeded experiments

Since the seeded chamber experiments began with monodisperse particles of a known size, we know the volume of inorganic material in each of the sampled particle sizes; therefore, the amount of inorganic and organic species in the particle can be calculated from the initial monodisperse seed aerosol size that was introduced in the chamber, along with the sampled particle size. The calculated results along with the fitted results for the humidograms (mixed particles) are presented in Table 4.2 for single HC experiments. There is excellent agreement between the fitted and calculated organic fractions. The hygroscopicity parameters as given in Table 4.2 give an average value of 0.0165 with a standard error of 0.0018. This is in good agreement with the value of 0.0154 obtained from the nucleation experiments. The uncertainty in the calculated ε_{org} is propagated from estimated systematic error of ±3% in the particle size determinations. The model successfully fit the gradual deliquescence and retrieved organic volume fractions and hygroscopicity parameters in keeping with the independently determined values. This supports both the validity of the volume additivity approximation and

the use of the HTDMA data for estimating organic and inorganic volume fractions in the particle.

Table 4.2: Comparison of calculated and fitted results of mixed (AS/SOA) particles in simple monodisperse seeded experiments.

Exp. #	Scan #	DD nm	Calculated		Fitted Results					
			ε_{org}	±σ	$\acute{\varepsilon}_{org}$	±σ	*b*	±σ	*g*	±σ
1	I	180	0.83	0.022	0.84	0.002	0.017	0.001	0.96	0.0010
	II	180	0.83	0.022	0.86	0.002	0.012	0.001	0.94	0.0006
2	I	209	0.89	0.014	0.89	0.004	0.018	0.003	0.97	0.0026
	II	209	0.89	0.014	0.89	0.002	0.010	0.001	0.96	0.0008
3	I	180	0.85	0.019	0.84	0.002	0.017	0.001	0.96	0.0010
	II	180	0.85	0.019	0.86	0.002	0.012	0.001	0.94	0.0006
4	I	151	0.82	0.023	0.85	0.004	0.021	0.002	0.99	0.0021
	II	151	0.82	0.023	0.82	0.004	0.025	0.002	0.97	0.0015
5	I	121	0.44	0.072	0.52	0.001	0.015	0.002	1.00	0.0090
	I	127	0.51	0.062	0.56	0.013	0.020	0.000	0.99	0.0040
	II	127	0.51	0.062	0.57	0.001	0.017	0.007	0.98	0.0030
	I	140	0.64	0.046	0.62	0.006	0.016	0.006	0.96	0.0020

DD is the dry diameter of the particle. ε_{org} and $\acute{\varepsilon}_{org}$ are the calculated and fitted organic volume fraction respectively in the particle, and *b* is the hygroscopicity parameter. The uncertainty in the calculated ε_{org} is propagated from estimated systematic error of ±3% in the particle size determinations. Calculated values are from size measurements, while fitted values are from the model.

4.3 Sequential monodisperse seeded experiments

In these experiments mixed (AS/SOA) particles were produced by sequentially depositing oxidation products of selected hydrocarbons on monodisperse seed aerosols. For this purpose, hydrocarbons at the threshold mixing ratio were sequentially introduced and oxidized in the chamber. Low-volatility organic oxidation products were produced during each sequential oxidation process. The low-volatility oxidation products on partitioning from the gas phase to the particle phase resulted in condensational growth. The process produced mixed (AS/SOA) particles. The subsequent sequential photoxidation of selected hydrocarbons gradually increased the organic volume fraction in the mixed particles. Each photoxidation process involved different hydrocarbons, so along with the composition of the particles, their physical and chemical nature also changed. We studied the impact of gradual change in the particles by examining their hygroscopicity using HTDMA data collected throughout the experiment. The HTDMA data collected during the dark were used to determine hygroscopicity of the aerosol particles. The HGF data collected between consecutive sequential photooxidation stages provided a relevance and close glimpse into complex systems such as ambient particles.

We used isoprene as the starting hydrocarbon in all of the sequential experiments. The main reason behind the choice was its capability of producing a large number of tiny particles on rapid oxidation. The oxidation products of isoprene produced a thin layer on the surface of monodisperse seed aerosols. The thickness of the layer depends on various variables in any particular experiments, e.g., duration and amount of UV exposure, mixing ratio of OH radicals produced and chamber conditions. The organic volume fraction in the mixed (AS/isoprene SOA) particles varied between 35% and 60% in these experiments at the first sequential stage. The subsequent sequential oxidation of hydrocarbons raised the organic volume fraction of the particles to 85%. Experiments were performed under controlled conditions and parameters (reactants and hydrocarbon mixing ratios, and UV duration, etc.). The appropriate use of the parameters enabled us to control the condensational growth of the particles and to keep them within the HTDMA sampling range.

In both phases of the sequential monodisperse seeded experiments, pure organic and mixed (AS/SOA) particles were produced at the same time. This was observed when isoprene was used as the starting hydrocarbon in sequential

experiments. The two modes – pure organic and mixed (AS/SOA) particles – each undergo condensational growth during sequential oxidation stages.

Experiment 6 is a typical example of sequential experiments. In the experiment three hydrocarbons (isoprene, β-pinene and Δ^3carene) were sequentially introduced and oxidized to coat seed aerosols. The concentration of hydrocarbons, IPN and duration of sequential UV exposures are given in table 4.2. In Figure 4.3 brown dotted lines indicate the particle size distribution of monodisperse AS seed aerosols, while green broken lines indicate the particle size distribution after the first UV exposure. The two modes – pure organic (isoprene SOA) and mixed (AS/isoprene SOA) particles – are distinctly evident and separated from each other. Upward arrows are labeled with the sampled particle sizes from each mode. Here the organic mode consists of pure organic oxidation products of isoprene, while mixed particles are of AS and the oxidation products of isoprene.

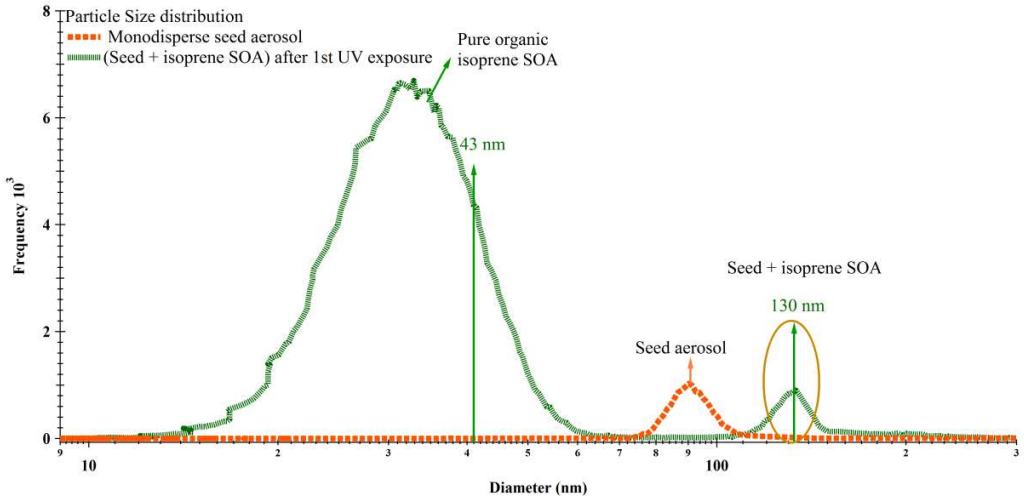

Figure 4.3: Step I and II. Particle size distributions during a typical sequential monodisperse seeded experiment. The brown dotted line represents monodisperse seed aerosols. The green line represents the particles after the first photoxidation. Two particle modes are produced as a result of photoxidation: Pure organic (isoprene SOA) and Mixed (AS/ isoprene SOA). The particles sampled from each mode are indicated.

Figure 4.4 presents the particle size distribution following the second UV exposure and sequential oxidation step. Here red broken lines represent the entire particle size distribution, which has two distinct modes: pure organic (isoprene SOA + β-pinene SOA) and mixed particles (AS/isoprene SOA + β-pinene SOA). Pure organic particles are oxidation products of isoprene and β-pinene, while mixed particles are ammonium sulfate + oxidation products of isoprene and β-pinene,

respectively. In Figure 4.4 the upward arrows indicate sampled particle sizes from each mode.

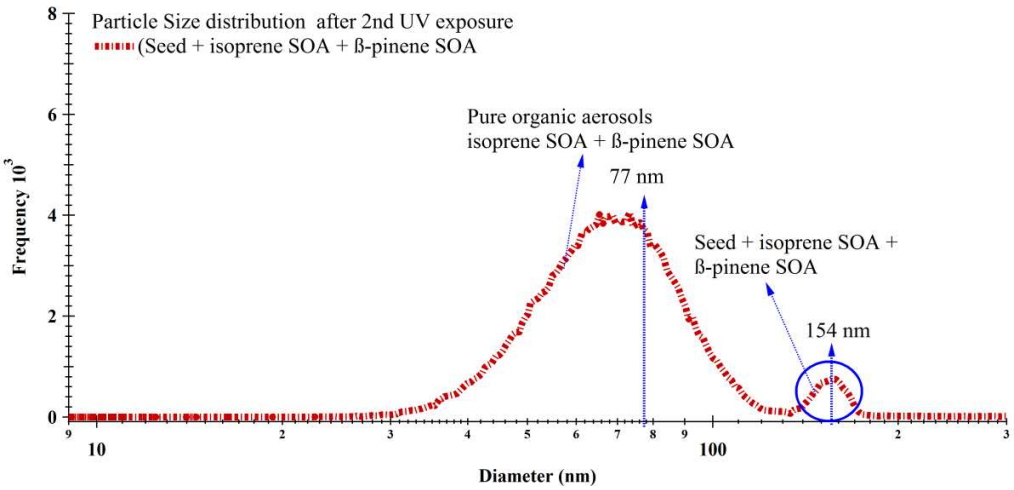

Figure 4.4: Step III. The red dotted line represents the particle size distribution after the 2nd UV exposure. The two particle modes are still evident: pure organic (isoprene SOA + β-pinene SOA) and mixed (AS/isoprene SOA + β-pinene SOA) particles. The particles sampled from each mode are indicated. Seed = ammonium sulfate $(NH_4)_2SO_4$.

The particle size distribution after third UV exposure is presented in figure 4.5. The blue broken lines represent the entire particle size distributions, which have two distinct modes: pure organic (isoprene SOA + β-pinene SOA + Δ^3carene SOA) and mixed (AS/ isoprene SOA + β-pinene SOA + Δ^3carene SOA) particles separately. Both modes increased in their organic loading after condensational

growth due to the third sequential photoxidation process. The pure organic particles are contributed by oxidation products of isoprene + β-pinene + Δ^3carene, while mixed particles contain ammonium sulfate + isoprene + β-pinene + Δ^3carene oxidation products. Upward arrows indicate the sampled particle sizes from each mode.

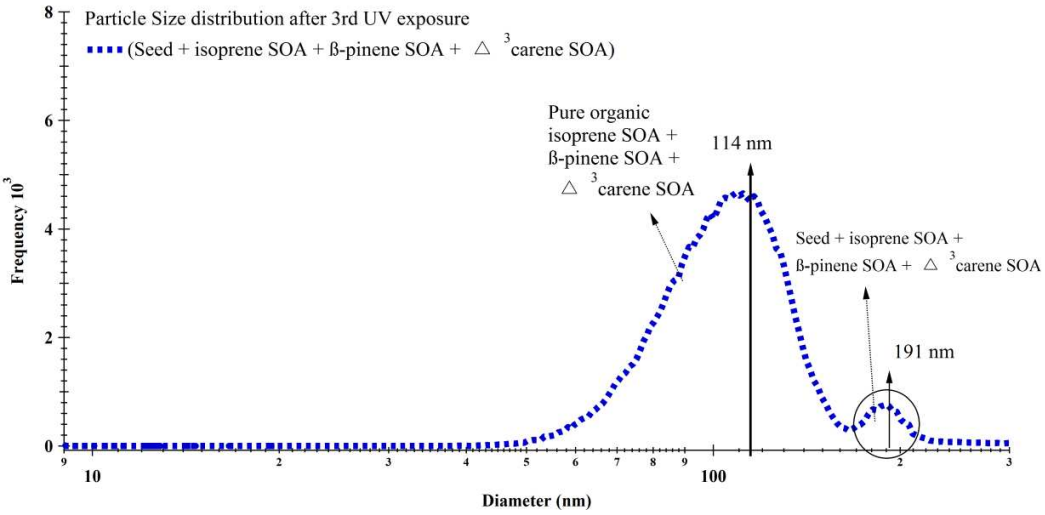

Figure 4.5: Step IV. The blue dotted line represents particle size distribution after the 3rd UV exposure. The two particle modes are again evident, pure organic (isoprene SOA + β-pinene SOA + Δ^3carene SOA) and mixed (AS/ isoprene SOA + β-pinene SOA + Δ^3carene SOA) particles. The particles sampled from each mode are indicated.
Seed = ammonium sulfate $(NH_4)_2SO_4$.

The production of pure organic particles along with mixed (AS/SOA) particles might be due to unavailability of enough seed aerosol surface or of the relatively clean chamber. At the second and third sequential oxidation stage of the experiment, both modes had undergone condensational growth. The hygroscopicity of sampled particle sizes (indicated in figures 4.3 through 4.5) was measured at each sequential stage from both modes (pure organic and mixed).

Mixed particles were produced by sequentially depositing the oxidation products of isoprene, β-pinene and Δ^3carene on monodisperse seed particles of ammonium sulfate (AS). Figure 4.6 shows the humidogram of mixed (AS/SOA) particles. The HGF of the pure seed particles substantially decreased on depositing the oxidation products of hydrocarbons. The HGF of the mixed particles decreased, with a gradual increase in the organic volume fraction in the particles as shown by three humidograms in figure 4.6 after three sequential oxidation stages.

In Figure 4.6 humidogram of mixed (AS/isoprene SOA) particles presented in green squares are observed after the first sequential oxidation stage while in red diamonds and blue circles are of (AS/isoprene + β-Pinene SOA mixed) and (AS/ isoprene + β-Pinene SOA + Δ^3carene SOA) after the second and third sequential photooxidation stages respectively. The humidogram after first sequential stage

shows shrinking behavior below 40% RH and smooth pick-up of water and deliquescence above 40% RH. The humidogram after second sequential stage also show shrinking behavior with much-diminished features however the shrinking behavior of the particles after third sequential stage is almost leveled off below 40% RH compared to the humidograms after first sequential stage. The humidograms (all sequential stages) show both gradual uptake of water at and below 74% RH and a gradual deliquescence beginning around 75% RH, which is much below the deliquescence point (80% RH) of ammonium sulfate

The mixed particles gradual uptake of water and deliquescence (at all sequential stages) means that the organic coating didn't hinder or block water from reaching the inorganic core or it didn't wet the inorganic particles completely or may have a preference for attachment on the surface of seed aerosol.

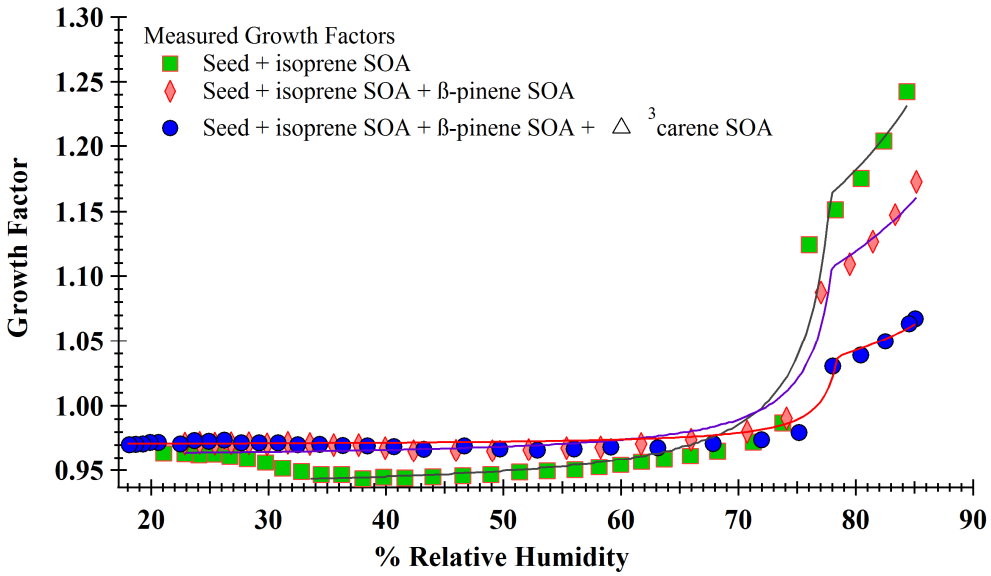

Figure 4.6: Typical humidograms of a sequential monodisperse seeded experiment. The sampled particle size was 130 nm (green squares), 154 nm (red diamonds) and 191 nm (blue circles) in diameter at three different stages of the experiment, and the seed particle size was 100 nm. The curve is fitted using the model (Section 4.2.1).

The humidograms of mixed (AS/SOA) particles were fitted by using the numerical model from Section 4.2.1, and the results are summarized in Table 4.3.

Table 4.3: Comparison of calculated and fitted results of mixed (AS/SOA) particles of sequential monodisperse seeded experiments.

Experiment #	DD nm	Calculated		Fitted Results					
		ε_{org}	±σ	$\acute{\varepsilon}_{org}$	±σ	b	±σ	g	±σ
6	130	0.55	0.057	0.59	0.040	0.037	0.001	0.94	0.007
	150	0.71	0.037	0.77	0.018	0.017	0.002	0.96	0.005
	190	0.85	0.019	0.89	0.003	0.005	0.001	0.97	0.002
7	133	0.58	0.054	0.51	0.021	0.037	0.002	0.97	0.004
	185	0.84	0.020	0.84	0.013	0.014	0.003	1.00	0.005
8	117	0.38	0.079	0.49	0.045	0.045	0.004	0.95	0.009
	124	0.47	0.067	0.49	0.021	0.043	0.003	0.91	0.004
	152	0.71	0.037	0.76	0.009	0.019	0.001	0.99	0.003
	157	0.74	0.032	0.77	0.026	0.016	0.001	0.99	0.008
9	130	0.55	0.058	0.48	0.030	0.036	0.002	0.90	0.004
	183	0.84	0.021	0.82	0.008	0.008	0.004	1.00	0.001

DD is the dry diameter of the particle. ε_{org} and $\acute{\varepsilon}_{org}$ are the calculated and fitted organic volume fraction respectively in the particle, and b is the hygroscopicity parameter. The uncertainty in the calculated ε_{org} is propagated from the estimated systematic error of ±3% in the particle size determinations. Calculated values are from size measurements, while fitted values are from the model.

The model can predict the volume fraction of inorganic and organic species in the particle. When the calculated and fitted results were compared, we found that they were in close agreement. The humidograms' model-estimated results of all experiments gave averages of hygroscopicity parameters ($b \pm \sigma_{SD}$) of 0.0396 ± 0.0024 for AS + isoprene SOA, 0.0155 ± 0.0025 for AS + isoprene + β-pinene SOA, 0.0175 ± 0.0010 for AS + isoprene + Δ^3carene SOA, 0.008 ± 0.0040 for AS

+ isoprene + α-pinene SOA and 0.0050 ± 0.001 for AS + isoprene + β-pinene + Δ^3carene SOA.

The model-estimated hygroscopicity parameter of mixed (AS/SOA) particles and pure organic particles (results from section 3.6) of the same sequential experiments are compared to the estimated parameter and to the SOA of single HCs in table 4.4.

Table 4.4: Compares and summarizes the hygroscopicity parameter b, determined in individual HC nucleation experiments with the estimated and experimental hygroscopicity parameter (pure organic and mixed (AS/SOA) particles) determined in sequential experiments.

Experiment #	% Volume Fraction (V_f)			Simple Nucleation Experiments	Estimated	Seeded Experiments	
SOA'S of						Pure Organic SOA	Mixed (AS/SOA)
				$b_{avg}\pm\sigma_{SD}$	$b_{est}\pm\sigma_{SD}$	$b_{org}\pm\sigma$	$b_{model}\pm\sigma$
6							
Isoprene	100	-	-	0.0401±0.0048	0.0401±0.0048	0.0494±0.0004	0.037±0.001
+ β-pinene	19	83	-	0.0154±0.0056	0.0201±0.0056	0.0240±0.0006	0.017±0.002
+ Δ^3carene	6	26	68	0.0042±0.0027	0.0093±0.0036	0.0133±0.0007	0.005±0.001
7							
Isoprene	100	-	-	0.0401±0.0048	0.0401±0.0048	0.0450±0.0006	0.037±0.002
+ β-pinene	2	98	-	0.0154±0.0056	0.0159±0.0056	0.0118±0.0004	0.014±0.003
8							
Isoprene	100	-	-	0.0401±0.0048	0.0401±0.0048	0.0482±0.0005	0.044±0.004
+ Δ^3carene	32	68	-	0.0042±0.0027	0.0158±0.0034	0.0194±0.0004	0.019±0.001
	32	68	-	0.0042±0.0027	0.0158±0.0034	0.0191±0.0012	0.016±0.001
9							
Isoprene	100	-	-	0.0401±0.0048	0.0401±0.0048	0.0400±0.0006	0.036±0.002
+α-pinene	2	98	-	0.0033±0.0009	0.0080±0.0010	0.0138±0.0005	0.008±0.001

σ_{SD} = Standard deviation

b_{avg} = Average hygroscopicity parameter determined during nucleation experiments.

b_{est} = Estimated hygroscopicity parameter of organics determined at each sequential stage.

b_{org} = Experimental hygroscopicity parameter of pure organic aerosols produced during sequential monodisperse seeded experiment.

b_{model} = Experimental model-estimated hygroscopicity parameter of organics in mixed (AS/SOA) particles during sequential monodisperse seeded experiment.

The hygroscopicity parameters of pure organic and mixed (AS/SOA) particles show significant differences compared to each other and to the estimated values. To understand the effect of sequential addition of individual HCs' SOA to the isoprene SOA we further simplified experimental results to table 4.5.

Table 4.5: compares the average hygroscopicity parameter, *b*, of pure organics and mixed organics produced during sequential seeded experiments with the estimated values.

	Seeded Experiments		
SOA'S of	**Pure Organic SOA**	**Mixed (AS/SOA)**	**Estimated**
	$\boldsymbol{b_{org} \pm \sigma}$	$b_{model} \pm \sigma$	$\boldsymbol{b_{est} \pm \sigma_{SD}}$
Isoprene	0.0457 ± 0.0005	0.0385 ± 0.002	0.0401 ± 0.0048
Isoprene + β-pinene	0.0179 ± 0.0005	0.0155 ± 0.003	0.0180 ± 0.0056
Isoprene + Δ^3carene	0.0193 ± 0.0008	0.0175 ± 0.001	0.0158 ± 0.0034
Isoprene + β-pinene + Δ^3carene	0.0133 ± 0.0007	0.0050 ± 0.001	0.0093 ± 0.0036
Isoprene + α-pinene	0.0138 ± 0.0005	0.0080 ± 0.001	0.0080 ± 0.0010

b_{org} = Average hygroscopicity parameter of pure organic SOA produced during seeded experiments.
b_{model} = Average hygroscopicity parameter of organics evaluated using model during monodisperse seeded sequential experiments.
b_{est} = Estimated hygroscopicity parameter calculated on the basis of volume fraction and individual HC hygroscopicity.
σ_{SD} = Standard deviation

On comparing the average hygroscopicity parameter of isoprene SOA in the pure organic state and in mixed (AS/SOA) states we found almost 16% differences.

Adding β-pinene or Δ^3carene SOA to isoprene SOA in the pure organic state and in the mixed (AS/SOA) state reduces the difference to 10%. The addition of α-pinene SOA to isoprene SOA and Δ^3carene SOA to isoprene + β-pinene SOA in both pure organic and mixed state increases the difference in the hygroscopicity parameter to 40% and 60% respectively. Despite the difference, the hygroscopicity parameter in both states is within the scatter around the estimated value. The results are given in table 4.5. The difference in hygroscopicity parameter in both states might be due to dissimilarity in physical and chemical conditions in the particles. Pure organic particles possess only organic-organic interaction, while mixed (AS/SOA) particles may have organic-organic and organic-inorganic interactions. The physical and chemical difference as discussed above may have impacted the morphology [Woods III et al., 2007]; hence the interaction with water that may lead to a significant difference in hygroscopicity between the two phases. Inorganic material might act as a catalyst to facilitate oligomerization or co-oligomerization [Reinhardt et al., 2007] and as a result fewer sites would be available for water interaction.

The overall hygroscopicity parameter of pure organic and mixed (AS/SOA) particles at each sequential stage is within experimental scatter. Overall we found

that the model can retrieve particles' composition and hygroscopicity successfully by using a humidogram obtained from the HTDMA data.

4.4 Mixed (hydrocarbon) monodisperse seeded experiments

In mixed hydrocarbon monodisperse seeded experiments three hydrocarbons were oxidized at the same time in the chamber to produce mixed (AS/SOA) particles. Experiments 10 and 11 are typical examples of such experiments. The mixing ratio of individual hydrocarbons and other reactants is given in table 4.1.

The mixed particles were produced by depositing oxidation products of β-pinene, Δ^3carene, and α-pinene at the same time on the seed aerosols. Figure 4.7 shows the particle size distributions before and after UV exposure in experiment 11. The red and blue broken lines show particle size distributions of seed aerosols and of mixed (AS/ β-pinene + Δ^3carene + α-pinene SOA) particles respectively. The upward arrows in the figure are labeled with sampled particle sizes.

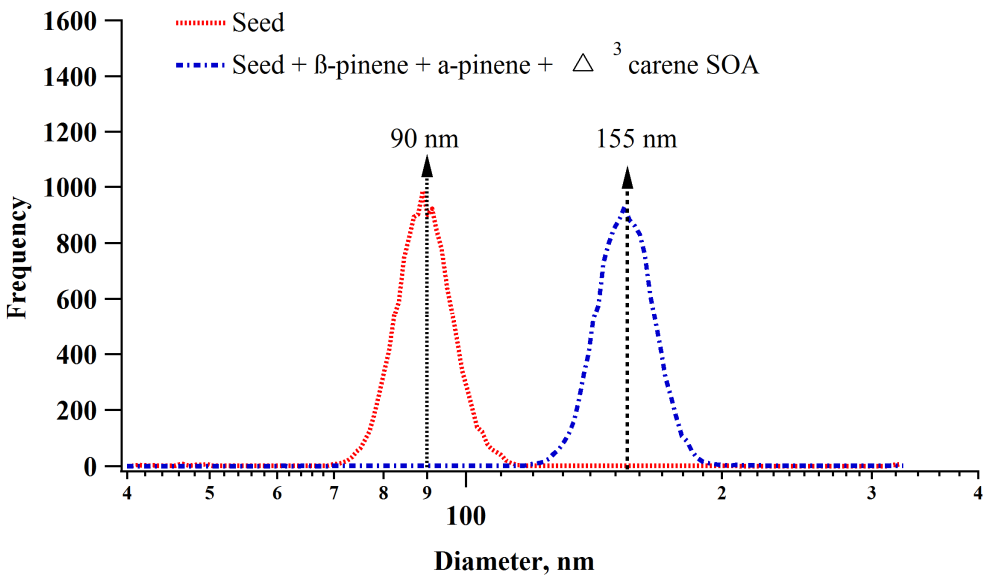

Figure 4.7: Particle size distributions in a typical mixed seeded experiment, experiment 11. Red lines indicate the particle size distribution of monodisperse seeded particles, while blue lines are AS/mixed SOA. The particle sizes sampled by the HTDMA are indicated.

The relative humidity was ramped twice with the UV off to investigate particle hygroscopicity. Figure 4.8 shows a typical example of a humidogram obtained on ramping RH.

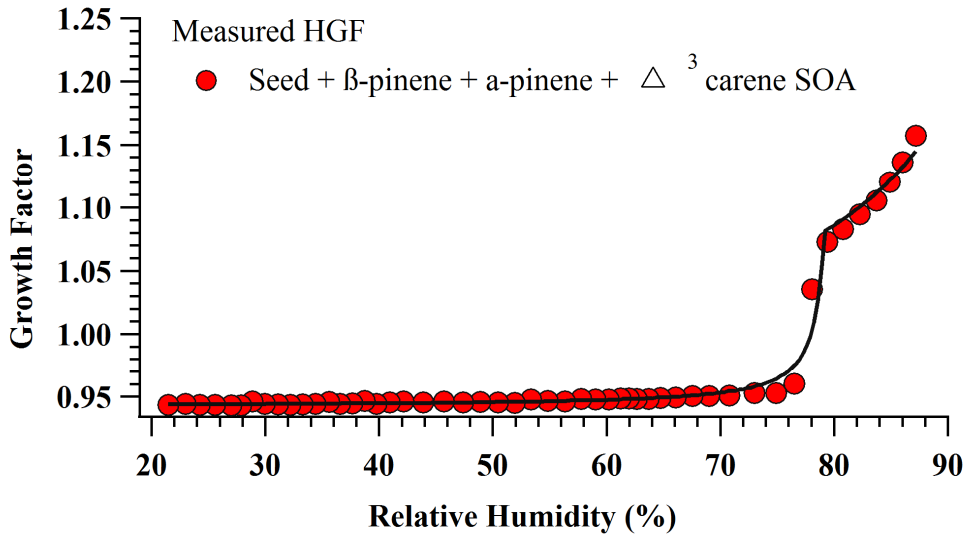

Figure 4.8: A typical humidogram of mixed monodisperse seeded experiment. The sampled particle diameter was 155 nm. The curve is fitted using the model (Section 4.2.1).

The humidogram shows both a gradual but slight uptake of water at and below 76% RH, similar to that of the pure organic particles, and a gradual deliquescence beginning around 77% RH, which is below the deliquescence point (80% RH) of pure ammonium sulfate. We compared humidogram of mixed (AS/mixed HC SOA) SOA with pure ammonium sulfate to see any resemblance because pure ammonium sulfate humidogram (figure 2.9) shows pre-deliquescence due to evaporation of ammonia from ammonium sulfate salt during calibration of HTDMA. We found that both humidograms are quite different from each other as

shown in figure 4.9 and expected there is no interference in the fitted results due to pre-deliquescence of ammonium sulfate salt.

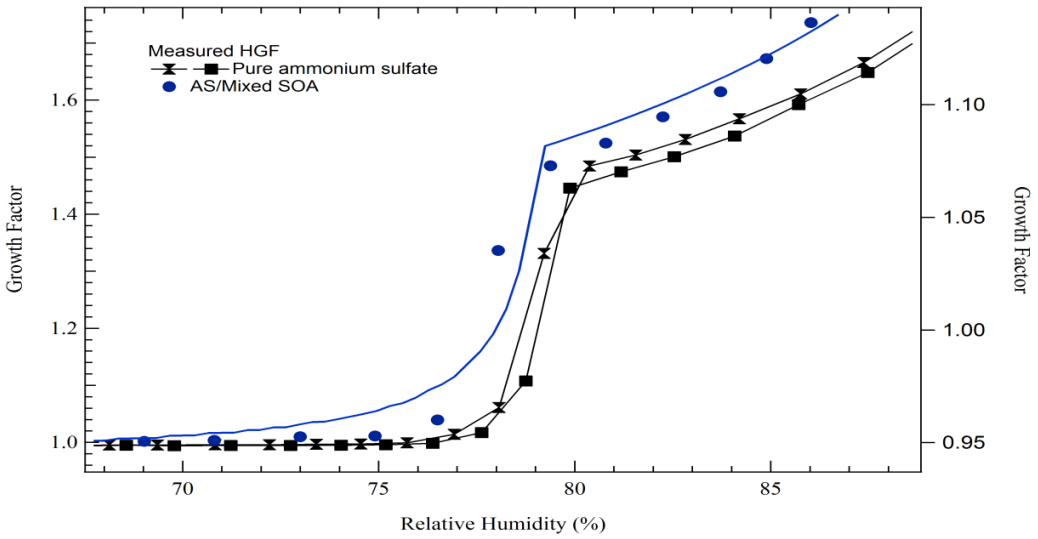

Figure 4.9: Comparison of pure ammonium sulfate humidogram with mixed (AS/*Mixed SOA)

*Mixed SOA = (AS/ β-pinene + Δ^3carene + α-pinene SOA)

The humidograms of mixed (AS/mixed HC SOA) were fitted using the model (section 4.2.1).

The modeled and calculated results are summarized in Table 4.6.

Table 4.6: Comparison of calculated and fitted results of mixed (AS/SOA) particles of Mixed HC monodisperse seeded experiments.

Experiment #	Dry Diameter nm	Calculated		Fitted Results					
		ε_{org}	±σ	$\acute{\varepsilon}_{org}$	±σ	b	±σ	g	±σ
10	227	0.94	0.008	0.93	0.004	0.005	0.002	0.99	0.001
	227	0.94	0.008	0.93	0.002	0.005	0.002	0.98	0.001
11	155	0.78	0.028	0.78	0.007	0.008	0.003	0.94	0.002
	155	0.78	0.028	0.78	0.013	0.009	0.003	0.95	0.003

ε_{org} and $\acute{\varepsilon}_{org}$ are the calculated and fitted organic volume fraction respectively in the particle, and b is the hygroscopicity parameter. The uncertainty in the calculated ε_{org} is propagated from the estimated systematic error of ± 3% in the particle size determinations. Calculated values are from size measurements, while fitted values are from the model.

The humidograms' model-estimated results of all experiments gave averaged hygroscopicity parameter ($b \pm \sigma_{SD}$) of 0.0068 ± 0.0021 for seeded mixed hydrocarbon SOA. The average hygroscopicity parameter of unseeded mixed hydrocarbon SOA (section 3.3) gave an averaged value of 0.0013 ± σ_{SD} 0.0004. The averaged value of the hygroscopicity parameter of seeded mixed hydrocarbon SOA is low compared to that of unseeded mixed hydrocarbon SOA. The reason behind the lower water uptake by seeded SOA of mixed hydrocarbon may be linked to multiple and enhanced organic-organic and organic-inorganic interactions. The interactions may affect the morphology of the particles [Woods III et al., 2007]. Morphology, shape and physical state in combination play an

important role in water uptake properties of the particle. The other possibility of reduced hygroscopicity might be due to formation of dimers, trimers and oligomerization [Reinhardt et al., 2007].

The deliquescence point of mixed (AS/SOA of mixed HCs) aerosol particles was slightly shifted to lower RH compared to pure AS because mixed hydrocarbons oxidation products are very slightly hygroscopic. The less hygroscopic organic coating may not be helpful in efficient gradual dissolution of AS and produces a slight shift of the AS deliquescence point. The hygroscopicity, physical state and relative volume fractions (inorganic/organic) of organic material in combination play important roles in determining the behavior and pattern of the particles' water uptake properties.

The model retrieved particles' composition and hygroscopicity successfully by using a humidogram obtained from the HTDMA data. The estimated and fitted results for the organic volume fraction matched up closely within experimental uncertainties. A less hygroscopic organic coating may not be helpful in partial dissolution of AS at lower RH. The partial dissolution of AS at lower RH may contribute to water uptake, and the modeled fitted results may have discrepancies in estimating organic volume fractions and the hygroscopicity parameter.

5 Summary, Conclusions and Future Directions

5.1 Summary and Conclusions

Hygroscopic properties of pure organic and mixed (AS/SOA) particles were measured using the HTDMA. To produce pure organic SOA and mixed (AS/SOA) particles, isoprene and selected terpenes (β-pinene, α-pinene, Δ^3carene and limonene) were photo-oxidation under controlled conditions. The aerosol particles produced with or without ammonium sulfate seed aerosols are categorized into two groups:

i) pure organic aerosol particles (nucleation [unseeded] experiments)

ii) mixed particles (AS/SOA) (seeded experiments).

The nucleation and seeded experiments are subdivided into three main groups:

a) unseeded/seeded SOA from single HCs

b) unseeded/seeded SOA from mixed HCs (two or three HCs)

c) unseeded/seeded SOA from sequential oxidation of individual HCs (two or three HCs)

The humidograms of pure organic SOA were obtained on ramping RH from 10% to 90% in the HTDMA. The humidograms of pure SOA of individual HCs

were evaluated against an empirical equation, 3.7, and gave an average hygroscopicity parameter (± one standard error) of 0.0401 ± 0.0011 for isoprene, 0.0154 ± 0.0014 for β-pinene, 0.0033 ± 0.0002 for α-pinene, 0.0042 ± 0.0005 for Δ^3carene and 0.0077 ± 0.0002 for limonene. According to experimental results, isoprene SOA are almost three times more hygroscopic than β-pinene SOA while five to ten times more hygroscopic than SOA of α-pinene, Δ^3carene and limonene. β-pinene SOA are almost 50% more hygroscopic than the limonene SOA and 70% to 80% more than SOA of Δ^3carene and α-pinene. The hygroscopicity parameters of designated terpenes SOA are dissimilar, so it is probable that their chemical and physical characteristics are also dissimilar. Oxidation products may form dimers, trimers, oligomers and polymers, which may lead to the formation of glass, rubber or aggregates of amorphous solids. The physical state of an SOA and its hygroscopicity parameter are interrelated. The physical state of the major portion may be solid or a mixture of liquid and hydrophobic solids at room temperature. The major portion of the particle may be resistive to interaction with water, and only a small portion may be responsible for the particle's water uptake.

The SOA from mixed (β-pinene, α-pinene, and Δ^3carene) HCs are very slightly hygroscopic (section 3.3). The hygroscopicity parameter of mixed HCs' SOA

doesn't resemble the hygroscopicity of the SOA of single HCs (β-pinene, α-pinene, or Δ^3carene). To interpret the hygroscopicity of mixed hydrocarbon SOA was impracticable because the experiments provided poor control over the condensing species during SOA formation. To have better control of the experimental parameters, the sequential nucleation experiments (section 3.4.2) were performed. For this purpose we sequentially oxidized several HCs to deposit oxidation products of selected HCs (β-pinene, Δ^3carene) on isoprene SOA. We found that sequentially adding oxidation products of designated terpenes to isoprene SOA apparently reduced the overall uptake of water compared to that of pure isoprene SOA. To understand water uptake by such systems, the volume additivity principle (section 3.5) was applied to estimate the growth factor of the particle. With some discrepancies, the expected growth factors and experimental results were found to be within experimental uncertainties.

The humidogram of mixed (AS/SOA) particles (chapter 4) presented two distinct features: gradual pick-up of water and deliquescence. As the RH was increased, gradual pick-up of water appeared to be governed mainly by organics in the particle before the deliquescence RH was reached, and by inorganics afterwards. Organics may be liquid, viscous and solids (amorphous, glass, rubber,

plasticizer, etc.). The liquid organics may help to partially dissolve seed aerosol at lower than deliquescence RH because in the presence of organics the mixed particles pick up water at low RH and also allow some AS to dissolve, so the dissolved fraction increases gradually, and completely dissolves before reaching the deliquescence point of pure salt. The more hygroscopic organics in mixed (AS/SOA) particles may result in much early deliquescence compared to the deliquescence RH of pure inorganics, while less hygroscopic organics may not affect the deliquescence point of inorganics; however, they can reduce water uptake remarkably. The highly hygroscopic organics in the mixed (AS/SOA) aerosol particles may quicken the process of AS dissolution, and particles might show smooth pick-up of water without deliquescence.

The deliquescence of mixed particles (AS/SOA) suggests that organics don't completely hinder or block uptake of water by inorganics. The overall growth factors of mixed (AS/SOA) particles are contributed by inorganics and organics in the particle. The relative contribution to the overall growth factor of mixed (AS/SOA) particles depends on relative volume fractions (inorganic and organic) and their hygroscopicity.

The mixed (AS/SOA) particles' humidograms were evaluated using the model (section 4.2.1). The model uses the ZSR and volume additivity approach to parameterize humidograms. The applicability of ZSR and volume additivity at the scanning range of RHs supports the conjecture that solute-solute interaction is negligible for mixed (AS/SOA) particles. The model successfully fitted the gradual deliquescence and retrieved organic volume fractions and hygroscopicity parameters. The model-estimated organic volume fraction was within experimental uncertainties of the estimated volume fraction (sections 4.2.2 and 4.3), while the hygroscopicity parameter shows some inconsistencies with the independently determined values. The inconsistencies could be due to variation in the morphology of mixed particles. Overall the results (sections 4.2.2 and 4.3) support both the validity of the volume additivity approximation and the use of the HTDMA data for estimating organic and inorganic volume fractions in field data. Also, if full humidograms are measured, it may be possible to obtain hygroscopicity parameters for the unknown organic phase in mixed organic-inorganic atmospheric particles. At a minimum, the model provides a convenient and physically meaningful method for parameterization of water uptake. As such, it may be useful for summarizing field data obtained with HTDMA instruments. The parameterization could also be used in atmospheric models of aerosol life cycles and environmental effects.

5.2 Future Directions

The applicability of the model was tested against laboratory-generated mixed (inorganic/SOA) aerosol particles, the inorganic fraction of which was ammonium sulfate (AS). Ambient particles' inorganic fraction may be contributed by ammonium nitrate, sodium chloride, etc., with or without the contribution of AS, depending on the environment where they are formed. The applicability of the model to such systems has not been tested.

The HTDMA is an established technique that can successfully reproduce the growth factor of well-known inorganic salts as a function of RH. Inorganic salts are capable of equilibrating rapidly at the higher RH. Since the time allowed for particles to equilibrate at the higher RH was modest, about 2.7 seconds (including one half the time spent in the size selection region of the DMA), but this may not be adequate for pure organic and mixed (inorganic/SOA) aerosol particles [Duplissy et al., 2009]. To support that, HTDMA measurements of pure organic and mixed (Inorganic/organic) aerosol particles are made under equilibrium conditions. It is recommended that the numerous sampling equilibrium intervals with RH should be tested to find out if it produces any impact in growth factor of pure organic and mixed (inorganic/organic) aerosol particles.

Almost all of atmospherically important inorganic salts deliquesced around 90% RH. Hygroscopicity measurements of organic species below 90% RH do not necessarily reflect the water content at higher RH (90%–99.6%), or at the point of CCN activation (>99.6%) [Petters et al., 2009]. For a more in-depth study of hygroscopic behavior of pure organic and mixed (inorganic/organic) aerosol particles, it is recommended that if possible the RH scanning range should be extended to saturation.

6 References

Aalto, P., K. Hämeri, E. D. O. Becker, R. Weber, J. Salm, J. M. Mäkelä, C. Hoell, C. D. O'Dowd, H. Karlsson, H. Hansson, M. Väkevä, I. K. Koponen, G. Buzorius, and M. Kulmala (2001), Physical characterization of aerosol particles during nucleation events, *Tellus, Series B: Chemical and Physical Meteorology, 53*(4), 344-358.

Ackerman, T. P. and O. B. Toon (1981), Absorption of visible radiation in atmosphere containing mixtures of absorbing and nonabsorbing particles, *Appl. Opt., 20*(20), 3661-3667.

Aklilu, Y. -. and M. Mozurkewich (2004), Determination of External and Internal Mixing of Organic and Inorganic Aerosol Components from Hygroscopic Properties of Submicrometer Particles during a Field Study in the Lower Fraser Valley, *Aerosol Science and Technology, 38*(2), 140-154.

Aklilu, Y. (2005a), *The hygroscopic properties of atmospheric particles : influence of composition and atmospheric processes*.

Aklilu, Y. (2005b), The hygroscopic properties of atmospheric particles :influence of composition and atmospheric processes,.

Alexander, D. T. L., P. A. Crozier, and J. R. Anderson (2008), Brown carbon spheres in East Asian outflow and their optical properties, *Science, 321*(5890), 833-836.

Alfarra, M. R., H. Coe, J. D. Allan, K. N. Bower, H. Boudries, M. R. Canagaratna, J. L. Jimenez, J. T. Jayne, A. A. Garforth, S. Li, and D. R. Worsnop (2004), Characterization of urban and rural organic particulate in the Lower Fraser Valley using two Aerodyne Aerosol Mass Spectrometers. *Atmos. Environ., 38*(34), 5745-5758.

Allen, M. D. and O. G. Raabe (1982), Re-evaluation of millikan's oil drop data for the motion of small particles in air, *J. Aerosol Sci., 13*(6), 537-547.

Andersson, M. A., R. Mikkola, S. Rasimus, D. Hoornstra, P. Salin, R. Rahkila, M. Heikkinen, S. Mattila, J. Peltola, S. Kalso, and M. Salkinoja-Salonen (2010), Boar spermatozoa as a biosensor for detecting toxic substances in indoor dust and aerosols, *Toxicol. In. Vitro., 24*(7), 2041-2052, doi:10.1016/j.tiv.2010.08.011.

Andreae, M. O. and D. Rosenfeld (2008), Aerosol-cloud-precipitation interactions. Part 1. The nature and sources of cloud-active aerosols, *Earth-Sci. Rev., 89*(1-2), 13-41.

Andrews, E. and S. M. Larson (1993), Effect of surfactant layers on the size changes of aerosol particles as a function of relative humidity, *Environmental Science and Technology, 27*(5), 857-865.

Angell, C. A. (1995), Formation of glasses from liquids and biopolymers, *Science, 267*(5206), 1924-1935.

Atkins, P. (1994), The properties of simple mixture: partial molar properties, in *Physical Chemistry*, , edited by Anonymous , pp. 208-213, New York, W.H Freeman and Company.

Badger, C. L., I. George, P. T. Griffiths, C. F. Braban, R. A. Cox, and J. P. D. Abbatt (2006), Phase transitions and hygroscopic growth of aerosol particles containing humic acid and mixtures of humic acid and ammonium sulphate, *Atmospheric Chemistry and Physics, 6*(3), 755-768.

Bahreini, R., M. D. Keywood, N. L. Ng, V. Varutbangkul, S. Gao, R. C. Flagan, J. H. Seinfeld, D. R. Worsnop, and J. L. Jimenez (2005), Measurements of Secondary Organic Aerosol from Oxidation of Cycloalkenes, Terpenes, and m-Xylene Using an Aerodyne Aerosol Mass Spectrometer. *Environ. Sci. Technol., 39*(15), 5674-5688.

Baltensperger, U., M. Kalberer, J. Dommen, D. Paulsen, M. R. Alfarra, H. Coe, R. Fisseha, A. Gascho, M. Gysel, S. Nyeki, M. Sax, M. Steinbacher, A. S. H. Prevot, S. Sjogren, E. Weingartner, and R. Zenobi (2005), Secondary organic aerosols from anthropogenic and biogenic precursors. *Faraday Discuss., 130*(Atmospheric Chemistry), 265-278.

Berg, O. H., E. Swietlicki, and R. Krejci (1998), Hygroscopic growth of aerosol particles in the marine boundary layer over the Pacific and Southern Oceans during the First Aerosol Characterization Experiment (ACE 1). *J.Geophys.Res., [Atmos.]; Journal of Geophysical Research, [Atmospheres], 103*(D13), 16535-16545.

Bertram, A. K., S. T. Martin, S. J. Hanna, M. L. Smith, A. Bodsworth, Q. Chen, M. Kuwata, A. Liu, Y. You, and S. R. Zorn (2011), Predicting the relative humidities of liquid-liquid phase separation, efflorescence, and deliquescence of mixed particles of ammonium sulfate, organic material, and water using the organic-to-sulfate mass ratio of the particle and the oxygen-to-carbon elemental ratio of the organic component, *Atmospheric Chemistry and Physics, 11*(21), 10995-11006.

BGI, Collision Nebulizer Instructions, *2001 BGI incorporated 58 Guinan Street Waltham, MA 02451*.

Birmili, W. and A. Wiedensohler (2000), New particle formation in the continental boundary layer: Meteorological and gas phase parameter influence, *Geophys. Res. Lett., 27*(20), 3325-3328, doi:10.1029/1999GL011221.

Bones, D. L., J. P. Reid, D. M. Lienhard, and U. K. Krieger (2012), Comparing the mechanism of water condensation and evaporation in glassy aerosol, *Proc. Natl. Acad. Sci. U. S. A., 109*(29), 11613-11618.

Bonn, B. and G. K. Moortgat (2002), New particle formation during α- and β-pinene oxidation by O 3, OH and NO 3, and the influence of water vapour:

Particle size distribution studies, *Atmospheric Chemistry and Physics, 2*(3), 183-196.

Braban, C. F. and J. P. D. Abbatt (2004), A study of the phase transition behavior of internally mixed ammonium sulfate - Malonic acid aerosols, *Atmospheric Chemistry and Physics, 4*(5), 1451-1459.

Brooks, S. D., M. E. Wise, M. Cushing, and M. A. Tolbert (2002), Deliquescence behavior of organic/ammonium sulfate aerosol, *Geophys. Res. Lett., 29*(19), 23-1.

Buzorius, G. (2001), Cut-off sizes and time constants of the CPC TSI 3010 operating at 1-3 lpm flow rates, *Aerosol Science and Technology, 35*(1), 577-585.

Chakrabarti, H. S., S. Das, and S. Gupta-Bhattacharya (2012), Outdoor airborne fungal spora load in a suburb of Kolkata, India: its variation, meteorological determinants and health impact, *Int. J. Environ. Health Res.*, *22*(1), 37-50, doi:10.1080/09603123.2011.588323.

Chan, C. K., R. C. Flagan, and J. H. Seinfeld (1992), Water activities of NH4NO3/(NH4)2SO4 solutions, *Atmospheric Environment - Part A General Topics, 26 A*(9), 1661-1673.

Chan, M. N. and C. K. Chan (2003), Hygroscopic Properties of Two Model Humic-like Substances and Their Mixtures with Inorganics of Atmospheric Importance, *Environmental Science and Technology, 37*(22), 5109-5115.

Chan, M. N., M. Y. Choi, N. L. Ng, and C. K. Chan (2005), Hygroscopicity of water-soluble organic compounds in atmospheric aerosols: Amino acids and biomass burning derived organic species, *Environmental Science and Technology, 39*(6), 1555-1562.

Chan, T. W. (2005), *Application of principal component analysis to atmospheric aerosol size distribution measurements*.

Charlson, R. J. and J. Heintzenberg (1995), Aerosols as a cause of uncertainty in climate forecasts. *Environ.Sci.Res.Rep.; Environmental Sciences Research Report, 17*(Aerosol Forcing of Climate), 1-10.

Choi, M. Y. and C. K. Chan (2002a), Continuous measurements of the water activities of aqueous droplets of water-soluble organic compounds, *Journal of Physical Chemistry A, 106*(18), 4566-4572.

Choi, M. Y. and C. K. Chan (2002b), The effects of organic species on the hygroscopic behaviors of inorganic aerosols, *Environmental Science and Technology, 36*(11), 2422-2428.

Clarke, A. D., V. N. Kapustin, F. L. Eisele, R. J. Weber, and P. H. McMurry (1999), Particle production near marine clouds: Sulfuric acid and predictions from classical binary nucleation, *Geophys. Res. Lett., 26*(16), 2425-2428.

Cocker, D. R.,III, S. L. Clegg, R. C. Flagan, and J. H. Seinfeld (2001), The effect of water on gas-particle partitioning of secondary organic aerosol. Part I: Î±-pinene/ozone system. *Atmos. Environ., 35*(35), 6049-6072.

Cohen, M. D., R. C. Flagan, and J. H. Seinfeld (1987), Studies of concentrated electrolyte solutions using the electrodynamic balance. 2. Water activities for mixed-electrolyte solutions, *J. Phys. Chem., 91*(17), 4575-4582.

Cooney, C. M. (1998), California moves ahead on diesel exhaust study, *Environ. Sci. Technol., 32*(11), 250.

CRC (2003), *CRC Handbook of chemistry and physics*, vol. 84th ed;, .

Cruz, C. N. and S. N. Pandis (2000a), Deliquescence and hygroscopic growth of mixed inorganic - Organic atmospheric aerosol, *Environmental Science and Technology, 34*(20), 4313-4319.

Cruz, C. N. and S. N. Pandis (2000b), Deliquescence and Hygroscopic Growth of Mixed Inorganic-Organic Atmospheric Aerosol. *Environ. Sci. Technol., 34*(20), 4313-4319.

Curjuric, I., M. Imboden, R. Nadif, A. Kumar, C. Schindler, M. Haun, F. Kronenberg, N. Kunzli, H. Phuleria, D. S. Postma, E. W. Russi, T. Rochat, F. Demenais, and N. M. Probst-Hensch (2012), Different genes interact with particulate matter and tobacco smoke exposure in affecting lung function decline in the general population, *PLoS One, 7*(7), 40175, doi:10.1371/journal.pone.0040175.

Dal, M., M., M. Kulmala, J. M. Makela, P. Aalto, and C. D. O'Dowd (2000), Analysis of the formation and growth of atmospheric aerosols using DMPS data, *AIP Conf. Proc., 534*, 815-818.

Davidson, C. I., R. F. Phalen, and P. A. Solomon (2005), Airborne particulate matter and human health: A review, *Aerosol Science and Technology, 39*(8), 737-749.

Deng, J., T. Wang, Z. Jiang, M. Xie, R. Zhang, X. Huang, and J. Zhu (2011), Characterization of visibility and its affecting factors over Nanjing, China, *Atmos. Res., 101*(3), 681-691, doi:10.1016/j.atmosres.2011.04.016.

Dick, W. D., P. Saxena, and P. H. McMurry (2000), Estimation of water uptake by organic compounds in submicron aerosols measured during the Southeastern Aerosol and Visibility Study, *Journal of Geophysical Research D: Atmospheres, 105*(D1), 1471-1479.

Dinar, E., A. Abo Riziq, C. Spindler, C. Erlick, G. Kiss, and Y. Rudich (2007), The complex refractive index of atmospheric and model humic-like substances (HULIS) retrieved by a cavity ring down aerosol spectrometer (CRD-AS), *Faraday Discuss., 137*, 279-295.

Dockery, D. W., C. A. Pope III, X. Xu, J. D. Spengler, J. H. Ware, M. E. Fay, B. G. Ferris Jr., and F. E. Speizer (1993), An association between air pollution and mortality in six U.S. cities, *N. Engl. J. Med.*, *329*(24), 1753-1759.

Duplissy, J., P. F. De Carlo, J. Dommen, M. R. Alfarra, A. Metzger, I. Barmpadimos, A. S. H. Prevot, E. Weingartner, T. Tritscher, M. Gysel, A. C. Aiken, J. L. Jimenez, M. R. Canagaratna, D. R. Worsnop, D. R. Collins, J. Tomlinson, and U. Baltensperger (2011), Relating hygroscopicity and composition of organic aerosol particulate matter, *Atmospheric Chemistry and Physics*, *11*(3), 1155-1165.

Duplissy, J., M. Gysel, S. Sjogren, N. Meyer, N. Good, L. Kammermann, V. Michaud, R. Weigel, S. Martins Dos Santos, C. Gruening, P. Villani, P. Laj, K. Sellegri, A. Metzger, G. McFiggans, G. Wehrle, R. Richter, J. Dommen, Z. Ristovski, U. Baltensperger, and E. Weingartner (2009), Intercomparison study of six HTDMAs: Results and general recommendations for HTDMA operation, *Atmos.Meas.Techniques*, *2*, 363-378.

Dutkiewicz, J., E. Cisak, J. Sroka, A. Wojcik-Fatla, and V. Zajac (2011), Biological agents as occupational hazards - selected issues, *Ann. Agric. Environ. Med.*, *18*(2), 286-293.

Ferron, G. A., E. Karg, and J. E. Peter (1993), Estimation of deposition of polydisperse hygroscopic aerosols in the human respiratory tract, *J. Aerosol Sci.*, *24*(5), 655-70, doi:10.1016/0021-8502(93)90022-2.

Finlayson-Pitts, B.J. and Pitts, J.N. (2000b), Particles in the troposphere, in *Upper and Lower Atmosphere,* , edited by Anonymous , pp. 349-435pp, San Diego, Academic Press.

Forster, P. (2007) *Changes in Atmospheric Constituents and in Radiative Forcing, in Climate Change 2007: The Physical Science Basis*, 131-234.

Franze, T., M. G. Weller, R. Niessner, and U. Pöschl (2005), Protein nitration by polluted air, *Environmental Science and Technology, 39*(6), 1673-1678.

Gamble, J. F., M. J. Nicolich, and P. Boffetta (2012), Lung cancer and diesel exhaust: an updated critical review of the occupational epidemiology literature, *Crit. Rev. Toxicol., 42*(7), 549-598, doi:10.3109/10408444.2012.690725.

Goldstein, A. H. and I. E. Galbally (2007), Known and unexplored organic constituents in the earth's atmosphere, *Environmental Science and Technology, 41*(5), 1514-1521.

Guenther, A., C. N. Hewitt, D. Erickson, R. Fall, C. Geron, T. Graedel, P. Harley, L. Klinger, M. Lerdau, and et al (1995), A global model of natural volatile organic compound emissions. *J.Geophys.Res., [Atmos.]; Journal of Geophysical Research, [Atmospheres], 100*(D5), 8873-8892.

Gysel, M., S. Nyeki, E. Weingartner, U. Baltensperger, H. Giebl, R. Hitzenberger, A. Petzold, and C. W. Wilson (2003), Properties of jet engine combustion particles during the PartEmis experiment: Hygroscopicity at subsaturated conditions, *Geophys. Res. Lett., 30*(11), 20-1.

Gysel, M., E. Weingartner, and U. Baltensperger (2002), Hygroscopicity of aerosol particles at low temperatures. 2. Theoretical and experimental hygroscopic properties of laboratory generated aerosols, *Environmental Science and Technology, 36*(1), 63-68.

Gysel, M., E. Weingartner, S. Nyeki, D. Paulsen, U. Baltensperger, I. Galambos, and G. Kiss (2004), Hygroscopic properties of water-soluble matter and humic-like organics in atmospheric fine aerosol, *Atmospheric Chemistry and Physics, 4*(1), 35-50.

Haag, W. and B. Kärcher (2004), The impact of aerosols and gravity waves on cirrus clouds at midlatitudes, *Journal of Geophysical Research D: Atmospheres, 109*(12), D12202 1-18.

Hallquist, M., J. C. Wenger, U. Baltensperger, Y. Rudich, D. Simpson, M. Claeys, J. Dommen, N. M. Donahue, C. George, A. H. Goldstein, J. F. Hamilton, H. Herrmann, T. Hoffmann, Y. Iinuma, M. Jang, M. E. Jenkin, J. L. Jimenez, A. Kiendler-Scharr, W. Maenhaut, G. McFiggans, T. F. Mentel, A. Monod, A. S. H. Prévôt, J. H. Seinfeld, J. D. Surratt, R. Szmigielski, and J. Wildt (2009), The formation, properties and impact of secondary organic aerosol: Current and emerging issues, *Atmospheric Chemistry and Physics, 9*(14), 5155-5236.

Hämeri, K., R. Charlson, and H. -. Hansson (2002), Hygroscopic properties of mixed ammonium sulfate and carboxylic acids particles, *AICHE J., 48*(6), 1309-1316.

Hameri, K., M. Kulmala, E. Krissinel', and G. Kodenyov (1996), Homogeneous nucleation in a laminar flow diffusion chamber: The operation principles and possibilities for quantitative rate measurements, *J. Chem. Phys., 105*(17), 7683-7695.

Hämeri, K., M. Rood, and H. -. Hansson (1992), Hygroscopic properties of a NaCl aerosol coated with organic compounds, *J. Aerosol Sci., 23*(SUPPL. 1), 437-440.

Hämeri, K. and M. Väkevä (2000), Ultrafine aerosol particle hygroscopicity and volatility in boreal forest, *Rep.Ser.Aerosol Sci., 47*, 47-59.

Han, S., H. Bian, Y. Zhang, J. Wu, Y. Wang, X. Tie, Y. Li, X. Li, and Q. Yao (2012), Effect of aerosols on visibility and radiation in spring 2009 in Tianjin, China, *Aerosol and Air Quality Research, 12*(2), 211-217.

Haywood, J. D., F. L. Harris, H. E. Grelen, and H. A. Pearson (2001), Vegetative response to 37 years of seasonal burning on a Louisiana longleaf pine site, *South. J. Appl. For., 25*(3), 122-130.

Heintzenberg, J. (1982), Size-segregated measurements of particulate elemental carbon and aerosol light absorption at remote Arctic locations, *Atmos. Environ.*, *16*(10), 2461-2469.

Heintzenberg, J. and R. J. Charlson (2009) *Clouds in the Perturbed Climate System-Their Relationship to Energy Balance*.

Hoffmann, T., J. R. Odum, F. Bowman, D. Collins, D. Klockow, R. C. Flagan, and J. H. Seinfeld (1997), Formation of organic aerosols from the oxidation of biogenic hydrocarbons, *J. Atmos. Chem.*, *26*(2), 189-222.

Holzinger, R., A. Lee, K. T. Paw U, and A. H. Goldstein (2005), Observations of oxidation products above a forest imply biogenic emissions of very reactive compounds. *Atmos.Chem.Phys.; Atmospheric Chemistry and Physics, 5*(1), 67-75.

Hong, P., X. Li, X. Yang, T. Shinkai, Y. Zhang, X. Wang, and R. I. Mackie (2012), Monitoring airborne biotic contaminants in the indoor environment of pig and poultry confinement buildings, *Environ. Microbiol.*, *14*(6), 1420-1431, doi:10.1111/j.1462-2920.2012.02726.x.

Hong, T. and P. L. Gurian (2012), Characterizing Bioaerosol Risk from Environmental Sampling, *Environ. Sci. Technol.*, *46*(12), 6714-6722, doi:10.1021/es300197n.

Horvath, H. (1993), Atmospheric light absorption - A review, *Atmospheric Environment - Part A General Topics, 27 A*(3), 293-317.

Horvath, H. (1995a), Estimation of the average visibility in central Europe, *Atmos. Environ.*, *29*(2), 241-246.

Horvath, H. (1995b), Size segregated light absorption coefficient of the atmospheric aerosol, *Atmos. Environ.*, *29*(8), 875-883.

Huang, W., J. Tan, H. Kan, N. Zhao, W. Song, G. Song, G. Chen, L. Jiang, C. Jiang, R. Chen, and B. Chen (2009), Visibility, air quality and daily mortality in Shanghai, China, *Sci. Total Environ.*, *407*(10), 3295-3300, doi:10.1016/j.scitotenv.2009.02.019.

Huff Hartz, K. E., T. Rosenørn, S. R. Ferchak, T. M. Raymond, M. Bilde, N. M. Donahue, and S. N. Pandis (2005), Cloud condensation nuclei activation of monoterpene and sesquiterpene secondary organic aerosol, *Journal of Geophysical Research D: Atmospheres*, *110*(14), 1-8.

Hyslop, N. P. (2008), Impaired visibility: the air pollution people see, *Atmos. Environ.*, *43*(1), 182-195, doi:10.1016/j.atmosenv.2008.09.067.

IPCC (2007) *Climate Change 2007: The Physical Science Basis*, 161-177.

Jimenez, J. L., M. R. Canagaratna, N. M. Donahue, A. S. H. Prevot, Q. Zhang, J. H. Kroll, P. F. DeCarlo, J. D. Allan, H. Coe, N. L. Ng, A. C. Aiken, K. S. Docherty, I. M. Ulbrich, A. P. Grieshop, A. L. Robinson, J. Duplissy, J. D. Smith, K. R. Wilson, V. A. Lanz, C. Hueglin, Y. L. Sun, J. Tian, A. Laaksonen, T. Raatikainen, J. Rautiainen, P. Vaattovaara, M. Ehn, M. Kulmala, J. M. Tomlinson, D. R. Collins, M. J. Cubison, E. J. Dunlea, J. A. Huffman, T. B. Onasch, M. R. Alfarra, P. I. Williams, K. Bower, Y. Kondo, J. Schneider, F. Drewnick, S. Borrmann, S. Weimer, K. Demerjian, D. Salcedo, L. Cottrell, R. Griffin, A. Takami, T. Miyoshi, S. Hatakeyama, A. Shimono, J. Y. Sun, Y. M. Zhang, K. Dzepina, J. R. Kimmel, D. Sueper, J. T. Jayne, S. C. Herndon, A. M. Trimborn, L. R. Williams, E. C. Wood, A. M. Middlebrook, C. E. Kolb, U. Baltensperger, and D. R. Worsnop (2009), Evolution of organic aerosols in the atmosphere, *Science*, *326*(5959), 1525-1529.

Jokinen, V. and J. M. Mäkelä (1997), Closed-loop arrangement with critical orifice for DMA sheath/excess flow system, *J. Aerosol Sci.*, *28*(4), 643-648.

Jung, J. H., S. Y. Park, J. E. Lee, B. U. Lee, and G. N. Bae (2012), Distinguishing Biotic and Abiotic Particles Using an Ultraviolet Aerodynamic Particle Sizer

for Real-Time Detection of Bacterial Bioaerosols, *Environ. Eng. Sci., 29*(9), 866-874, doi:10.1089/ees.2011.0276.

Kalberer, M., D. Paulsen, M. Sax, M. Steinbacher, J. Dommen, A. S. H. Prevot, R. Fisseha, E. Weingartner, V. Frankevich, R. Zenobi, and U. Baltensperger (2004), Identification of Polymers as Major Components of Atmospheric Organic Aerosols, *Science, 303*(5664), 1659-1662.

Kalberer, M., M. Sax, and V. Samburova (2006), Molecular size evolution of oligomers in organic aerosols collected in urban atmospheres and generated in a smog chamber, *Environmental Science and Technology, 40*(19), 5917-5922.

Kanakidou, M., J. H. Seinfeld, S. N. Pandis, I. Barnes, F. J. Dentener, M. C. Facchini, R. Van Dingenen, B. Ervens, A. Nenes, C. J. Nielsen, E. Swietlicki, J. P. Putaud, Y. Balkanski, S. Fuzzi, J. Horth, G. K. Moortgat, R. Winterhalter, C. E. L. Myhre, K. Tsigaridis, E. Vignati, E. G. Stephanou, and J. Wilson (2005), Organic aerosol and global climate modelling: A review, *Atmospheric Chemistry and Physics, 5*(4), 1053-1123.

Kavouras, I. G., N. Mihalopoulos, and E. G. Stephanou (1998), Formation of atmospheric particles from organic acids produced by forests, *Nature, 395*(6703), 683-686.

Kinney, P. D., G. E. Mulholland, and N. P. Bryner (1991), Use of the electrostatic classification method size 0.1um SRM particles-A feasibility study, *96*, 147-167.

Klimova, Y. V., I. A. Kuznetsov, M. M. Rasulov, A. V. Demanov, and O. O. Kuraleva (2011), Transregional carrying over of hydrogen sulphide and other pollutants of air - risk factor of development of the tuberculosis of lungs, *Estestv. Tekh. Nauki*(6), 142-143.

Knutson, E. O. and K. T. Whitby (1975), Anomalous unipolar diffusion charging of polystyrene latex aerosols, *J. Colloid Interface Sci., 53*(3), 493-495.

Koehler, K. A., S. M. Kreidenweis, P. J. DeMott, A. J. Prenni, C. M. Carrico, B. Ervens, and G. Feingold (2006), Water activity and activation diameters from hygroscopicity data - Part II: application to organic species. *Atmos. Chem. Phys.*, *6*(3), 795-809.

Kostenidou, E., R. K. Pathak, and S. N. Pandis (2007), An Algorithm for the Calculation of Secondary Organic Aerosol Density Combining AMS and SMPS Data. *Aerosol. Sci. Technol., 41*(11), 1002-1010.

Kulmala, M., H. Vehkamäki, T. Petäjä, M. Dal Maso, A. Lauri, V. -. Kerminen, W. Birmili, and P. H. McMurry (2004), Formation and growth rates of ultrafine atmospheric particles: A review of observations, *J. Aerosol Sci., 35*(2), 143-176.

Kulmala, M., P. Korhonen, T. Vesala, H. Hansson, K. Noone, and B. Svenningsson (1996), The effect of hygroscopicity on cloud droplet formation. *Tellus, Ser.B; Tellus, Series B: Chemical and Physical Meteorology, 48B*(3), 347-360.

Lawrence, M. G. (2005), The relationship between relative humidity and the dewpoint temperature in moist air: A simple conversion and applications. *Bull. Am. Meteorol. Soc., 86,* 225-233.

Leaitch, W. R., J. W. Bottenheim, T. A. Biesenthal, S. -. Li, P. S. K. Liu, K. Asalian, H. Dryfhout-Clark, F. Hopper, and F. Brechtel (1999), A case study of gas-to-particle conversion in an eastern Canadian forest, *Journal of Geophysical Research D: Atmospheres, 104*(D7), 8095-8111.

Lesins, G., P. Chylek, and U. Lohmann (2002), A study of internal and external mixing scenarios and its effect on aerosol optical properties and direct radiative forcing, *Journal of Geophysical Research D: Atmospheres, 107*(9-10), 5-1.

Liu, B. Y. H., D. Y. H. Pui, and K. T. Whitby (1978), The aerosol mobility chromatograph: a new detector for sulfuric acid aerosols, *Atmos. Environ., 12*(1-3), 99-104.

Lu, C., S. Niu, L. Tang, J. Lv, L. Zhao, and B. Zhu (2010), Chemical composition of fog water in Nanjing area of China and its related fog microphysics, *Atmos. Res., 97*(1-2), 47-69, doi:10.1016/j.atmosres.2010.03.007.

Lu, J. and F. M. Bowman (2010), A detailed aerosol mixing state model for investigating interactions between mixing state, semivolatile partitioning, and coagulation, *Atmospheric Chemistry and Physics, 10*(8), 4033-4046.

Marcolli, C. and U. K. Krieger (2006), Phase changes during hygroscopic cycles of mixed organic/inorganic model systems of tropospheric aerosols, *Journal of Physical Chemistry A, 110*(5), 1881-1893.

Marcolli, C., B. Luo, and T. Peter (2004), Mixing of the Organic Aerosol Fractions: Liquids as the Thermodynamically Stable Phases, *Journal of Physical Chemistry A, 108*(12), 2216-2224.

May, K. R. (1973), The collison nebulizer: Description, performance and application, *J. Aerosol Sci., 4*(3), 235-238,IN1,239-243.

McMurry, P. H. (2000), The history of condensation nucleus counters, *Aerosol Science and Technology, 33*(4), 297-322.

Metzger, S., B. Steil, L. Xu, J. E. Penner, and J. Lelieveld (2011), Aerosol hygroscopic growth parameterization based on a solute specific coefficient, *Atmospheric Chemistry and Physics Discussions, 11*(9), 24813-24855.

Meyer, N. K., J. Duplissy, M. Gysel, A. Metzger, J. Dommen, E. Weingartner, M. R. Alfarra, A. S. H. Prevot, C. Fletcher, N. Good, G. McFiggans, Ã M. Jonsson, M. Hallquist, U. Baltensperger, and Z. D. Ristovski (2009a), Analysis of the hygroscopic and volatile properties of ammonium sulphate seeded and unseeded SOA particles, *Atmos. Chem. Phys., 9*(2), 721-732.

Meyer, N. K., J. Duplissy, M. Gysel, A. Metzger, J. Dommen, E. Weingartner, M. R. Alfarra, A. S. H. Prevot, C. Fletcher, N. Good, G. McFiggans, A. M. Jonsson, M. Hallquist, U. Baltensperger, and Z. D. Ristovski (2009b), Analysis of the hygroscopic and volatile properties of ammonium sulphate seeded and unseeded SOA particles, *Atmospheric Chemistry and Physics, 9*(2), 721-732.

Mikhailov, E., S. Vlasenko, S. T. Martin, T. Koop, and U. Pöschl (2009), Amorphous and crystalline aerosol particles interacting with water vapor: Conceptual framework and experimental evidence for restructuring, phase transitions and kinetic limitations, *Atmospheric Chemistry and Physics, 9*(24), 9491-9522.

Mortimer, R. G. (2000), *Determination of activity coefficients of electrolytes*, A harcourt science and technology company, San Diego.

Mozurkewich, M., T. -. Chan, Y. -. Aklilu, and B. Verheggen (2004), Aerosol particle size distributions in the lower Fraser Valley: Evidence for particle nucleation and growth, *Atmospheric Chemistry and Physics, 4*(4), 1047-1062.

Murray, L. C. and R. J. Farber (1988), Statistical and empirical relationships between visibility and particulates in the southwestern United States, *Proc. - APCA Annu. Meet., 81st*(3), 88.

Noll, K. E., P. K. Mueller, and M. Imada (1968), Visibility and aerosol concentration in urban air, *Atmospheric Environment (1967), 2*(5), 465-475.

Nriagu, J. O. and J. M. Pacyna (1988), Quantitative assessment of worldwide contamination of air, water and soils by trace metals, *Nature, 333*(6169), 134-139.

O'Dowd, C., G. McFiggans, D. J. Creasey, L. Pirjola, C. Hoell, M. H. Smith, B. J. Allan, J. M. C. Plane, D. E. Heard, J. D. Lee, M. J. Pilling, and M. Kulmala (1999), On the photochemical production of new particles in the coastal boundary layer, *Geophys. Res. Lett., 26*(12), 1707-1710.

Pandithurai, G., S. Dipu, T. V. Prabha, R. S. Maheskumar, J. R. Kulkarni, and B. N. Goswami (2012), Aerosol effect on droplet spectral dispersion in warm continental cumuli, *Journal of Geophysical Research D: Atmospheres, 117*(16).

Pant, A., A. Fok, M. T. Parsons, J. Mak, and A. K. Bertram (2004), Deliquescence and crystallization of ammonium sulfate-glutaric acid and sodium chloride-glutaric acid particles, *Geophys. Res. Lett., 31*(12), L12111 1-4.

Parsons, M. T., D. A. Knopf, and A. K. Bertram (2004), Deliquescence and crystallization of ammonium sulfate particles internally mixed with water-soluble organic compounds, *Journal of Physical Chemistry A, 108*(52), 11600-11608.

Peckhaus, A., S. Grass, L. Treuel, and R. Zellner (2012), Deliquescence and efflorescence behavior of ternary inorganic/organic/water aerosol particles, *Journal of Physical Chemistry A, 116*(24), 6199-6210.

Peng, C., M. N. Chan, and C. K. Chan (2001), The hygroscopic properties of dicarboxylic and multifunctional acids: Measurements and UNIFAC predictions, *Environmental Science and Technology, 35*(22), 4495-4501.

Pepper, I. L. and S. E. Dowd (2009), Aeromicrobiology, Elsevier Inc.

Peters, A., D. W. Dockery, J. Heinrich, and H. E. Wichmann (1997), Short-term effects of particulate air pollution on respiratory morbidity in asthmatic children. *Eur. Respir. J., 10*(4), 872-879.

Peters, A., H. E. Wichmann, T. Tuch, J. Heinrich, and J. Heyder (1997), Respiratory effects are associated with the number of ultrafine particles, *Am. J. Respir. Crit. Care Med., 155*(4), 1376-1383.

Petters, M. D. and S. M. Kreidenweis (2007), A single parameter representation of hygroscopic growth and cloud condensation nucleus activity. *Atmos. Chem. Phys., 7*(8), 1961-1971.

Petters, M. D., H. Wex, C. M. Carrico, E. Hallbauer, A. Massling, G. R. McMeeking, L. Poulain, Z. Wu, S. M. Kreidenweis, and F. Stratmann (2009), Towards closing the gap between hygroscopic growth and activation for secondary organic aerosol-Part 2: Theoretical approaches, *Atmospheric Chemistry and Physics, 9*(12), 3999-4009.

Pierce, J. R., I. Riipinen, M. Kulmala, M. Ehn, T. Petäjä, H. Junninen, D. R. Worsnop, and N. M. Donahue (2011), Quantification of the volatility of secondary organic compounds in ultrafine particles during nucleation events, *Atmospheric Chemistry and Physics, 11*(17), 9019-9036.

Plummer, L. E., S. Smiley-Jewell, and K. E. Pinkerton (2012), Impact of air pollution on lung inflammation and the role of Toll-like receptors, *Int. J. Interferon, Cytokine Mediator Res., 4*, 43-57, doi:10.2147/IJICMR.S29352.

Pope III, C. A. and D. W. Dockery (2006), Health effects of fine particulate air pollution: Lines that connect, *Journal of the Air and Waste Management Association, 56*(6), 709-742.

Pope III, C. A., M. Ezzati, and D. W. Dockery (2009), Fine-particulate air pollution and life expectancy in the United States, *N. Engl. J. Med., 360*(4), 376-386.

Pope, C. A., III. (2000a), Epidemiology of fine particulate air pollution and human health: Biologic mechanisms and who's at risk, *Environ. Health Perspect. Suppl., 108*(4), 713-723.

Pope, C. A., III. (2000b), Review: epidemiological basis for particulate air pollution health standards, *Aerosol. Sci. Technol., 32*(1), 4-14, doi:10.1080/027868200303885.

Pope, C. A., III, D. J. Eatough, D. R. Gold, Y. Pang, K. R. Nielsen, P. Nath, R. L. Verrier, and R. E. Kanner (2001), Acute exposure to environmental tobacco smoke and heart rate variability, *Environ. Health Perspect., 109*(7), 711-716, doi:10.1289/ehp.01109711.

Pope, C. A.,III, R. T. Burnett, M. J. Thun, E. E. Calle, D. Krewski, K. Ito, and G. D. Thurston (2002), Lung cancer, cardiopulmonary mortality, and long-term exposure to fine particulate air pollution. *JAMA, J.Am.Med.Assoc., 287*(9), 1132-1141.

Pope, F. D., B. J. Dennis-Smither, P. T. Griffiths, S. L. Clegg, and R. A. Cox (2010), Studies of single aerosol particles containing malonic acid, glutaric acid, and their mixtures with sodium chloride. I. Hygroscopic growth, *Journal of Physical Chemistry A, 114*(16), 5335-5341.

Prather, K. A., C. D. Hatch, and V. H. Grassian (2008), Analysis of atmospheric aerosols, *Annu. Rev. Anal. Chem., 1*, 485-514, doi:10.1146/annurev.anchem.1.031207.113030.

Prenni, A. J., P. J. DeMott, S. M. Kreidenweis, D. E. Sherman, L. M. Russell, and Y. Ming (2001), The effects of low molecular weight dicarboxylic acids on cloud formation, *Journal of Physical Chemistry A, 105*(50), 11240-11248.

Prenni, A. J., P. J. DeMott, and S. M. Kreidenweis (2003), Water uptake of internally mixed particles containing ammonium sulfate and dicarboxylic acids. *Atmos. Environ., 37*(30), 4243-4251.

Rader, D. J. and P. H. McMurry (1986), Application of the tandem differential mobility analyzer to studies of droplet growth or evaporation. *J. Aerosol Sci., 17*(5), 771-787.

Reinhardt, A., C. Emmenegger, B. Gerrits, C. Panse, J. Dommen, U. Baltensperger, R. Zenobi, and M. Kalberer (2007), Ultrahigh mass resolution and accurate mass measurements as a tool to characterize oligomers in secondary organic aerosols, *Anal. Chem., 79*(11), 4074-4082.

Rose, D., S. S. Gunthe, E. Mikhailov, G. P. Frank, U. Dusek, M. O. Andreae, and U. Pöschl (2008), Calibration and measurement uncertainties of a continuous-flow cloud condensation nuclei counter (DMT-CCNC): CCN activation of

ammonium sulfate and sodium chloride aerosol particles in theory and experiment, *Atmospheric Chemistry and Physics, 8*(5), 1153-1179.

Saathoff, H., K. -. Naumann, M. Schnaiter, W. Schock, O. Mohler, U. Schurath, E. Weingartner, M. Gysel, and U. Baltensperger (2003), Coating of soot and (NH4)2SO4 particles by ozonolysis products of Î±-pinene. *J. Aerosol Sci., 34*(10), 1297-1321.

Salma, I., R. Ocskay, and G. G. Láng (2008), Properties of atmospheric humic-like substances – Water system, *Atmospheric Chemistry and Physics, 8*(8), 2243-2254.

Saxena, P. and L. M. Hildemann (1996), Water-soluble organics in atmospheric particles: A critical review of the literature and application of thermodynamics to identify candidate compounds, *J. Atmos. Chem., 24*(1), 57-109.

Seinfeld, J. H. and Pandis, S.N. (2006), *Atmospheric chemistry and physics*, J. Wiley & Sons, New York.

Seinfeld, J. H. and S. N. Pandis (1998) *Atmospheric Chemistry and Physics*.

Sekigawa, K., Estimation of the Volume Fraction of Water Soluble Material in Submicron Aerosols in the Atmosphere, *1983 J. Meteor. Soc. Japan 61*(3), 359-366.

Shi, Q., Y. Q. Li, P. Davidovits, J. T. Jayne, D. R. Worsnop, M. Mozurkewich, and C. E. Kolb (1999), Isotope exchange for gas-phase acetic acid and ethanol at aqueous interfaces: A study of surface reactions, *J Phys Chem B, 103*(13), 2417-2430.

Sjogren, S., M. Gysel, E. Weingartner, M. R. Alfarra, J. Duplissy, J. Cozic, J. Crosier, H. Coe, and U. Baltensperger (2007), Hygroscopicity of the submicrometer aerosol at the high-alpine site Jungfraujoch, 3580m a.s.l., Switzerland, *Atmospheric Chemistry and Physics Discussions, 7*(5), 13699-13732.

Smith, M. L., M. Kuwata, and S. T. Martin (2011), Secondary organic material produced by the dark ozonolysis of-pinene minimally affects the deliquescence and efflorescence of ammonium sulfate, *Aerosol Science and Technology, 45*(2), 244-261.

Stanier, C. O., A. Y. Khlystov, and S. N. Pandis (2004), Nucleation events during the Pittsburgh Air Quality Study: Description and relation to key meteorological, gas phase, and aerosol parameters, *Aerosol Science and Technology, 38*(SUPPL. 1), 253-264.

Stjern, C. W., A. Stohl, and J. E. Kristjánsson (2011), Have aerosols affected trends in visibility and precipitation in Europe? *Journal of Geophysical Research D: Atmospheres, 116*(2).

Stolzenberg, M.R. and McMurray, P.H., (1988), TDMAFIT user's manual, *Publication No 653 Dept. of Mech. Eng. Univ. of Minnesota, Minneapolis, MN*.

Swietlicki, E., H. -. Hansson, K. Hämeri, B. Svenningsson, A. Massling, G. Mcfiggans, P. H. Mcmurry, T. Petäjä, P. Tunved, M. Gysel, D. Topping, E. Weingartner, U. Baltensperger, J. Rissler, A. Wiedensohler, and M. Kulmala (2008), Hygroscopic properties of submicrometer atmospheric aerosol particles measured with H-TDMA instruments in various environments - A review, *Tellus, Series B: Chemical and Physical Meteorology, 60 B*(3), 432-469.

Takahama, S., R. K. Pathak, and S. N. Pandis (2007), Efflorescence transitions of ammonium sulfate particles coated with secondary organic aerosol, *Environmental Science and Technology, 41*(7), 2289-2295.

Tang, I. N. and H. R. Munkelwitz (1994), Water activities, densities, and refractive indices of aqueous sulfates and sodium nitrate droplets of atmospheric importance. *J.Geophys.Res., 99*(D9), 18,801-8.

Tang, I. N. (1980), Deliquescence properties and particle size change of hygroscopic aerosols. *Gener.Aerosols Facil.Exposure Exp., [Tech.Pap.Symp.]*, 153-167.

Tang, I. N. (1996), Chemical and size effects of hygroscopic aerosols on light scattering coefficients. *J.Geophys.Res., [Atmos.]; Journal of Geophysical Research, [Atmospheres], 101*(D14), 19245-19250.

Tang, I. N. (1997), Thermodynamic and optical properties of mixed-salt aerosols of atmospheric importance. *J.Geophys.Res., [Atmos.]; Journal of Geophysical Research, [Atmospheres], 102*(D2), 1883-1893.

Titos, G., I. Foyo-Moreno, H. Lyamani, X. Querol, A. Alastuey, and L. Alados-Arboledas (2012), Optical properties and chemical composition of aerosol particles at an urban location: An estimation of the aerosol mass scattering and absorption efficiencies, *Journal of Geophysical Research D: Atmospheres, 117*(4).

Tritscher, T., J. Dommen, P. F. Decarlo, M. Gysel, P. B. Barmet, A. P. Praplan, E. Weingartner, A. S. H. Prévt, I. Riipinen, N. M. Donahue, and U. Baltensperger (2011), Volatility and hygroscopicity of aging secondary organic aerosol in a smog chamber, *Atmospheric Chemistry and Physics, 11*(22), 11477-11496.

Tsay.S.C, Stephens. G.L, and Greenwald.T.J. (1991), An investigation of aerosol microstructure on visual air quality, *Atmos. Environ., 25A*, 1039-1053.

Twomey, S. (1974), Pollution and the planetary albedo, *Atmos. Environ., 8*(12), 1251-1256.

VanReken, T. M., N. L. Ng, R. C. Flagan, and J. H. Seinfeld (2005), Cloud condensation nucleus activation properties of biogenic secondary organic aerosol, *Journal of Geophysical Research D: Atmospheres, 110*(7), 1-9.

Varutbangkul, V., F. J. Brechtel, R. Bahreini, N. L. Ng, M. D. Keywood, J. H. Kroll, R. C. Flagan, J. H. Seinfeld, A. Lee, and A. H. Goldstein (2006),

Hygroscopicity of secondary organic aerosols formed by oxidation of cycloalkenes, monoterpenes, sesquiterpenes, and related compounds. *Atmos.Chem.Phys.*, *6*(9), 2367-2388.

Verheggen, B. and M. Mozurkewich (2002), Determination of nucleation and growth rates from observation of a SO2 induced atmospheric nucleation event, *Journal of Geophysical Research D: Atmospheres*, *107*(11), AAC 5-1 - AAC 5-12.

Virkkula, A., R. Van Dingenen, F. Raes, and J. Hjorth (1999), Hygroscopic properties of aerosol formed by oxidation of limonene, α-pinene, and β-pinene, *Journal of Geophysical Research D: Atmospheres*, *104*(D3), 3569-3579.

Virtanen, A., J. Joutsensaari, T. Koop, J. Kannosto, P. Yli-Pirilä, J. Leskinen, J. M. Mäkelä, J. K. Holopainen, U. Pöschl, M. Kulmala, D. R. Worsnop, and A. Laaksonen (2010), An amorphous solid state of biogenic secondary organic aerosol particles, *Nature*, *467*(7317), 824-827.

Waggoner, A. P., R. E. Weiss, and N. C. Ahlquist (1981), Optical characteristics of atmospheric aerosols, *Atmospheric Environment - Part A General Topics*, *15*(10-11), 1891-1909.

Wang, J., A. A. Hoffmann, R. J. Park, D. J. Jacob, and S. T. Martin (2008), Global distribution of solid and aqueous sulfafte aerosols: Effect of the hysteresis of particle phase transitions, *Journal of Geophysical Research D: Atmospheres*, *113*(11).

Wen, C. and H. Yeh (2010), Comparative influences of airborne pollutants and meteorological parameters on atmospheric visibility and turbidity, *Atmos. Res.*, *96*(4), 496-509, doi:10.1016/j.atmosres.2009.12.005.

Whitby, K. T., R. B. Husar, and B. Y. H. Liu (1972), Aerosol size distribution of Los Angeles smog, *J. Colloid Interface Sci.*, *39*(1), 177-204, doi:10.1016/0021-9797(72)90153-1.

Whitby, K. T. (1978), The physical characteristics of sulfur aerosols, *Atmos. Environ., 12*(1-3), 135-159.

Winkler, P. and C. Junge (1972), The growth of atmospheric aerosol particles as a function of relative humidity Part I: method and measurements at different locations, *Journal de Recherches Atmospheriques - ISSN 0021-7972*, *6*, 617-638.

Wise, M. E., J. D. Surratt, D. B. Curtis, J. E. Shilling, and M. A. Tolbert (2003), Hygroscopic growth of ammonium sulfate/dicarboxylic acids, *J.Geophys.Res., 108*(D20), 4638-4642.

Woo, K. S., D. R. Chen, D. Y. H. Pui, and P. H. McMurry (2001), Measurement of Atlanta aerosol size distributions: observations of ultrafine particle events, *Aerosol. Sci. Technol., 34*(1), 75-87, doi:10.1080/02786820120056.

Woods III, E., H. S. Kim, C. N. Wivagg, S. J. Dotson, K. E. Broekhuizen, and E. F. Frohardt (2007), Phase transitions and surface morphology of surfactant-coated aerosol particles, *Journal of Physical Chemistry A, 111*(43), 11013-11020.

Yu, F., G. Luo, and X. Ma (2012), Regional and global modeling of aerosol optical properties with a size, composition, and mixing state resolved particle microphysics model, *Atmospheric Chemistry and Physics, 12*(13), 5719-5736.

Zelenyuk, A., J. Yang, C. Song, R. A. Zaveri, and D. Imre (2008), A new real-time method for determining particles' sphericity and density: Application to secondary organic aerosol formed by ozonolysis of α-pinene, *Environmental Science and Technology, 42*(21), 8033-8038.

Zobrist, B., C. Marcolli, D. A. Pedernera, and T. Koop (2008), Do atmospheric aerosols form glasses? *Atmospheric Chemistry and Physics, 8*(17), 5221-5244.